Alma Mater Studiorum - Universita' di Bologna

DOTTORATO DI RICERCA IN SCIENZE AMBIENTALI:
TUTELA E GESTIONE DELLE RISORSE NATURALI
CICLO XXII

Settore scientifico-disciplinare
GEO12

Towards Rapid Environmental Assessment and Coastal Forecasting in the Northern Adriatic Sea

Presentata dalla
Dott.ssa Simona Simoncelli

Coordinatore Dottorato
Prof.ssa Elena Fabbri

Relatore
Prof.ssa Nadia Pinardi

Correlatori
Dr. Paolo Oddo
Prof. Arthur J. Mariano
Dott. Giuseppe Montanari

Esame finale anno 2010

To my son Giacomo

Acknowledgment

I'd like to thank my advisor Prof. Nadia Pinardi which guided me during these years of study and research, sharing her deep knowledge in Oceanography, and initiating me to this subject.
Many thanks to Dr. Paolo Oddo for his help, advices and support.
I am pleased to acknowledge Prof. Arthur J. Mariano for his fruitful collaboration and teaching, and Edward Ryan for his efficient support during my period of study at RSMAS, University of Miami. A sincere gratitude to all MPO division at RSMAS for guesting me, allowing me to use all the facilities and to attend lectures and seminars. I really enjoyed the classes of Prof William Johns and the possibility he gave me to participate to a scientific cruise. Many thanks in particular to Guilherme Castelao, Marcello Magaldi, Annalisa Griffa and my office mate Angelique Haza.
I am grateful to Dott. Giuseppe Montanari and Dott. Attilio Rinaldi from ARPA Daphne that provided most of the data used in this thesis and for their collaboration during these years.
Thanks to Marco Deserti, Jacopo Chiggiato and Enrico Minguzzi from ARPA - SIM (Servizio Idrometeorologico) of Emilia Romagna that provided LAMI data and Reno River data.
Thanks to Simone Colella from GOS ISAC CNR Roma for the collaboration and for providing satellite data.
Thanks to Giulio Notarstefano from OGS Trieste that provided satellite SST data.
All the work has been carried out at SINCEM laboratory and I express my gratitude to Dott. Luca Giacomelli that manage very efficiently all the computing facilities. I'd like to acknowledge Antonio Guarnieri and Claudia Fratianni from INGV for their help.
Last but not least, I am grateful to all my family that supported and encouraged me during these years to fulfill this objective, in particular my husband Donato.

Contents

1 Introduction **1**

1.1 The Area of Study . . . 1

1.1.1 The Adriatic Sea . . . 1

1.1.2 The Northern Adriatic Basin . . . 3

1.1.3 Environmental Criticality . . . 6

1.2 Towards an Integrated Observing and Prediction System . . . 8

1.2.1 The Adriatic Coastal Monitoring Network . . . 8

1.2.2 The Adriatic Forecasting System . . . 9

1.3 Objectives and Methodology . . . 10

1.4 Structure of the Thesis . . . 11

2 Climatological Data Analysis in the Emilia Romagna Coastal Area **13**

2.1 Introduction . . . 13

2.2 Observational Data Sets . . . 17

2.2.1 Historical Observations and Quality Control Procedure 17

2.2.2 High Resolution Data Collection . . . 22

2.3 Mapping Methodology . . . 24

2.3.1 Spatial Correlations . . . 27

2.4 Climatological Fields . . . 32

2.4.1 Temperature . . . 32

2.4.2 Salinity . . . 34

2.4.3 Current Field . . . 36

2.5 Discussion . . . 38

2.6 Conclusions . . . 42

3 Coastal Modeling in The Northern Adriatic Sea **43**

3.1 Introduction . . . 43

3.2 The Adriatic Shelf Model . . . 44

3.2.1 Topography . . . 46

3.2.2 Nesting and Open Boundary Conditions . . . 46

3.2.3 River Runoff . . . 48
3.2.4 Simulation Experiments . . . 52
3.2.5 Atmospheric Forcing . . . 52
3.2.6 Initial Conditions . . . 53
3.3 Observations . . . 54
3.3.1 Satellite SST Observations . . . 54
3.3.2 ADRIA03 Observations . . . 54
3.3.3 Coastal Observations . . . 55
3.4 Model Validation . . . 56
3.5 Results . . . 58
3.5.1 Comparison with Satellite SST Observations . . . 58
3.5.2 Comparison with ADRIA03 . . . 61
3.5.3 Comparison with Coastal CTDs . . . 61
3.6 Summary and Conclusions . . . 69

4 Rapid Environmental Assessment in The Northern Adriatic 73
4.1 Introduction . . . 73
4.2 The Adriatic Shelf Model . . . 76
4.2.1 River Runoff . . . 77
4.2.2 Atmospheric Forcing . . . 77
4.3 Coastal Observations . . . 80
4.4 Initialization Methods . . . 81
4.4.1 Interpolation-Extrapolation Procedure . . . 81
4.4.2 Blending Large Scale Fields and Coastal Observations . 85
4.5 Coastal REA Experimental Design . . . 91
4.5.1 Spin Up . . . 92
4.6 Results . . . 96
4.6.1 Spring CREA Experiment . . . 98
4.6.2 Summer CREA Experiment . . . 100
4.7 Summary and Conclusions . . . 103

5 Conclusions 105
5.1 Future Developments . . . 107

A Northern Adriatic River Data 109

B Satellite SST Data Validation 113

Bibliography 117

List of Tables

3.1 ASHELF and AFS sets up. 45
3.2 Po River runoff repartition percentages between its main delta arms as function of the total discharge in m^3/sec at Pontelagoscuro station. 48
3.3 CTD data available from ADRICOSM observing system during the Spring Experiment time period. 57
3.4 CTD data available from ADRICOSM observing system during the Summer Experiment time period. 57

4.1 CTD data collection periods. 80
4.2 List of blending experiments with homogeneous parameter matrix and isotropic correlation length scales expressed in degrees. C(2) is the zero crossing scale and C(4) is the e-folding scale. 87
4.3 Heterogeneous Parameter Matrix (PM) defined for BA initial condition estimation. Each area, displayed in figure 4.1a and sorted by bin number, has its own set of correlation parameters. The other bins uses B0 correlation parameters as in table 4.2. 88
4.4 RMSE calculated from AFS and CREA Summer and Spring experiments. AFS and DE have been forced by ECMWF atmospheric data, while the others consider LAMI high resolution forcing. 96

A.1 ASHELF Rivers and monthly climatological outflow in m^3/sec. 111

List of Figures

1.1 Nested modeling system which consists of a hierarchy of three numerical models, the Mediterranean Forecasting System (MFS) in the Mediterranean Sea outer domain, the Adriatic Forecasting System (AFS) in the Adriatic basin and the Adriatic Shelf model (ASHELF) in the Northern Adriatic sea inner domain. . 2

1.2 The Adriatic Sea bathymetry. Red squares enclose the three coastal areas of the Northern Adriatic basin where this study will focus. 3

1.3 Schematic of the Adriatic Sea surface circulation from *Artegiani et al.* (1997b) 4

1.4 Winter and Summer seasonal circulation calculated from climatological simulations in the Northern Adriatic from *Zavatarelli and Pinardi* (2003) 5

1.5 Monthly average of chlorophyll deriverd from SeaWiFS sensor satellite images for the period 1997-2004: a) February distribution; b) August distribution. From *Montanari et al.* (2006). 6

1.6 Schematic of the Adriatic Forecasting System procedure from *Guarnieri et al.* (2009) 10

2.1 a) Adriatic Sea bathymetry and, in the red square, the Emilia Romagna coastal area. b) bathymetry of Emilia Romagna Coastal Area. Black dots stand for monitoring stations, while blue triangles indicate points from ECMWF grid where we calculated monthly wind climatology. 14

2.2 a) Po River mean daily runoff (black line) for the period 1995-2002 and (red line) the corresponding monthly climatology. b) Wind monthly climatology calculated in the 3 points displayed in figure 2.1 from ECMWF analyses. 15

2.3 Data statistics (after *Montanari et al.* (2006)). 18

2.4 a) Monthly area averaged temperature and salinity profiles and b) the relative standard deviations (after *Montanari et al.* (2006)). 20

2.5 Monthly area averaged density profiles. 21
2.6 Sampling schemes for the high resolution surveys and their relative area averaged temperature and salinity profiles (black line) enclosed between ±1 standard deviation profiles. Gray line is the climatological profile enclosed between ±1 standard deviation profiles. a) August 2003; b) March 2004. 23
2.7 As in figure 2.6: a) November 2004; b) May 2005. 24
2.8 a) Temperature and b) salinity isotropic correlation functions calculated at 1m, 5m and 8m depth. 28
2.9 a) Temperature and salinity two dimensional correlation functions, calculated from March 2004 survey at 3m depth, subtracting first order polynomial trends surfaces: c) temperature; d) salinity. Trend explained variance (%) is indicated in the plot title. 29
2.10 a) Temperature and salinity two dimensional correlation functions, calculated from May 2005 survey at 3m depth, subtracting first order polynomial trend surfaces: c) temperature; d) salinity. Trend explained variance (%) is indicated in the plot title. 30
2.11 Temperature climatological maps (after *Montanari et al.* (2006)). Note that the color index varies with the month. 33
2.12 Salinity climatological maps (after *Montanari et al.* (2006)). . 35
2.13 Climatological currents and the underlying density fields. (after *Montanari et al.* (2006)) 37
2.14 Schematic of the climatological coastal circulation (from *Montanari et al.* (2006)). 39
2.15 Vertical section of temperature (top), salinity (middle) and meridional component of geostrophic velocity along the transect off Cesenatico (bottom). 41

3.1 a) AFS topography interpolated on ASHELF grid; b) ASHELF high resolution topography 44
3.2 a) ASHELF original topography; b) blended ASHELF new topography; c) AFS topography interpolated on ASHELF grid. 47
3.3 a) Po River daily mean outflow for the year 2003 and monthly climatology calculated for the years 1995-2002. b) Reno River daily outflow for 2003 and Raicich monthly climatology. c) Po River daily temperature sampled at Canavella station and temperature sampled at station 1002 of Emilia Romagna coastal monitoring network, located just south the Po delta. 51

3.4 Air temperature time series from ECMWF analyses averaged on ASHELF domain: a) during the Spring Experiment; b) during the Summer Experiment. Wind time series from ECMWF analyses averaged on ASHELF domain: c) during the Spring experiment; d) during the Summer Experiment. 53

3.5 CTD data distribution map from ADRIA03 campaign conducted from April 28th to May 4th, 2003. 55

3.6 Coastal monitoring networks in the Northern Adriatic sea considered for ASHELF validation: a) Emilia Romagna; b) Gulf of Trieste; c) Rovinj. 56

3.7 Time averaged SST maps for the simulated time periods. (Left) Spring Expriment results: a) Observed satellite SST; b) AFS SST; c) ASHELF SST. (Right) Summer Experiment results: d) Observed satellite SST; e) AFS SST; f) ASHELF SST. . . . 59

3.8 (Left) SST skill scores time series for the Spring Experiment: a) BIAS; b) RMSE; c) PCC. (Right) SST skill scores time series for the Summer Experiment: d) BIAS; e) RMSE; f) PCC 60

3.9 (Top) Area averaged density, salinity and temperature profiles from CTD observations, ASHELF and AFS models. (Middle) AFS and ASHELF bias profiles of density, salinity and temperature. (Bottom) AFS and ASHELF RMSE profiles of density, salinity and temperature 62

3.10 Temperature hovmoller plots in Emilia Romagna Coastal area during Spring experiment. A) Observations; B) AFS; C) ASHELF. D) Temperature RMSE time series. Salinity hovmoller plots in Emilia Romagna Coastal area during spring experiment. E) Observations; F) AFS; G) ASHELF. H) Salinity RMSE time series. 64

3.11 RMSE temperature and salinity profiles calculated fROM the Spring Experiment: a) Emilia Romagna; b) Gulf of Trieste; c) Rovinj. 65

3.12 Temperature hovmoller plots in Emilia Romagna Coastal area during Summer experiment. A) Observations; B) AFS; C) ASHELF. D) Temperature PCC time series. Salinity hovmoller plots in Emilia Romagna Coastal area during Summer experiment. E) Observations; F) AFS; FG) ASHELF. H) Salinity PCC time series. 66

3.13 Temperature hovmoller plots in Gulf of Trieste during Summer experiment. A) Observations; B) AFS; C) ASHELF. D) Temperature PCC time series. Salinity hovmoller plots in Gulf of Trieste during Summer experiment. E) Observations; F) AFS; G) ASHELF. H) Salinity PCC time series. 67

3.14 Temperature hovmoller plots in Rovinj coastal area during Summer experiment. A) Observations; B) AFS; C) ASHELF. D) Temperature RMSE time series. Salinity hovmoller plots in Rovinj coastal area during Summer experiment. E) Observations; F) AFS; FG) ASHELF. H) Salinity RMSE time series. 68

3.15 RMSE temperature and salinity profiles calculated from the Summer Experiment: a) Emilia Romagna; b) Gulf of Treste; c) Rovinj. 69

4.1 a) ASHELF model domain and topography. ASHELF domain has been divided in squared bins to define an heterogeneous Parameter Matrix for the OA technique; b) Emilia Romagna; c) Gulf of Trieste; d) Rovinj coastal areas and monitoring networks. 75

4.2 Area average air temperature time series from ECMWF (black) and from LAMI (red) calculated on ASHELF domain for 2 periods: a) Apr-May 2003; c) Aug-Sept 2003. Small subplot displays the mean air temperature diurnal cycle. Area average wind velocity time series over ASHELF domain: b) Apr-May 2003; d) Aug-Sept 2003. 79

4.3 Initial condition area averaged profiles on May 5th: a) Emilia Romagna; b) Gulf of Trieste; c) Rovinj. Black solid line represents observations. Dashed black line stands for the synthetic profile from interpolated AFS (IAFS). OAFS is the OA result of AFS field mapped using B0 correlation length scales (see tab.4.2). B0 is OA result from blending AFS with observation using B0 correlation length scales. BA is OA result from blending AFS with coastal CTD using BA correlation length scales (see tab.4.3). 83

4.4 Initial condition area averaged profiles on August 11th. Details in fig.4.3. 84

4.5 SST fields on May 5th for the Rovinj coastal area: a) satellite high resolution SST image; b) IAFS SST field; c) B0 observed SST; d) B0 blended SST; e) BA observed SST; f) BA blended SST. (SST fields have been masked for mapping error greater than 30%) 90

4.6 SST fields on May 5th for the Emilia Romagna coastal area and the Gulf of Trieste. a) Emilia Romagna IAFS SST field; b) BA observed SST; c) BA blended initial condition SST; d) Gulf of Trieste IAFS SST; e) BA observed SST; f) BA blended SST. (SST fields have been masked for mapping error greater than 30%) 91

4.7 CREA initialization and forecast procedure. 92

4.8 Spin Up experiment diagram. 93

4.9 (a) Total Kinetic Energy ratio between ASHELF and AFS calculated on target days, May 5th and August 11th. (b) Temperature RMSE (c) salinity RMSE calculated on day May 5th for the Emilia Romagna area. 95

4.10 SST maps on May 13th: a) Satellite SST image; b) AFS daily mean SST field and currents. ASHELF SST and currents after one week of simulation from the Spring CREA experiment starting May 5th: c) forced by ECMWF (DE); d) forced by LAMI (D). 97

4.11 Model results after one week of simulation from the Summer CREA experiment starting August 11th. a) AFS salinity daily mean field and currents; b) ASHELF salinity daily mean field and currents forced by ECMWF (DE); c)ASHELF salinity field and currents forced by LAMI. 99

4.12 Model results from the Spring CREA experiment starting May 5th. a) Emilia Romagna on May 12th; b) Rovinj coastal area on May 13th. 101

4.13 Model results after one week of simulation from the Summer CREA experiment starting August 11th. a) Emilia Romagna; b) Gulf of Trieste; c) Rovinj. 102

B.1 High resolution satellite SST validation with coastal CTD in the Gulf of Trieste for the year 2003: a) RMSE time series calculated at the CTD monitoring days, considering all the available daily SST images. b) Data from (a) have been divided as function of sampling day time within 3 hours intervals. RMSE have been calculated separately for each time interval. The black triangle on the abscissa indicates the annual average CTD sampling time. c) RMSE time series from SST-CTD cross-validation, considering only SST images closer to the CTD sampling time. 114
B.2 High resolution satellite SST validation with coastal CTD in the Emilia Romagna coastal area. (see fig.B.2 for details) . . . 115

Chapter 1

Introduction

1.1 The Area of Study

This thesis will focus on the Northern Adriatic Basin coastal area which constitutes the continental shelf of the Adriatic Sea. A high resolution numerical model of the Adriatic Shelf (ASHELF) will be presented within the context of a new Rapid Environmental Assessment (REA) strategy (*Robinson*, 1999) which employs opportunity coastal observations and operational forecast products to generate short range data-driven predictions for the coastal area. ASHELF is embedded in a nested modeling system, displayed in figure 1.1, whose outer domain covers the Mediterranean Sea and the intermediate domain incorporates the Adriatic Sea. The nesting approach allows a progressive refinement of the models resolution and consequently the possibility to downscale from basin scale up to coastal processes.
It follows a brief description of the main Adriatic and Northern Adriatic basins characteristics and circulation together with their environmental criticality. *Section 2* introduces the monitoring and forecasting system established in the Adriatic Sea in the framework of ADRICOSM Project which will be exploited in the thesis. *Section 3* describes the methodology applied, the objectives of the thesis and its structure.

1.1.1 The Adriatic Sea

The Adriatic Sea (fig.1.2) is an elongated semi-enclosed basin located in the northern part of the eastern Mediterranean Sea between the Italian Peninsula and the the Balkans. It connects to the Mediterranean Sea through the Otranto channel. The coast is gentle sloping and smooth on the Italian side but irregular and rocky on the eastern side, where many islands and channels are present.

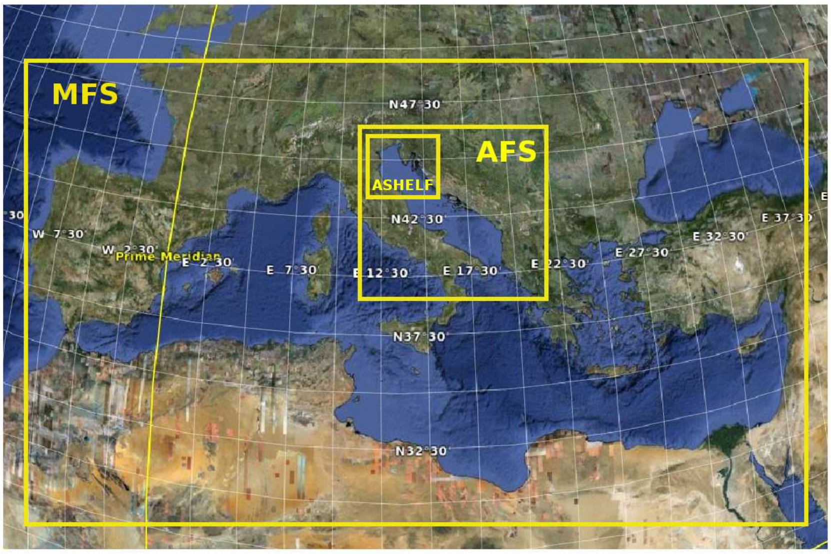

Figure 1.1: Nested modeling system which consists of a hierarchy of three numerical models, the Mediterranean Forecasting System (MFS) in the Mediterranean Sea outer domain, the Adriatic Forecasting System (AFS) in the Adriatic basin and the Adriatic Shelf model (ASHELF) in the Northern Adriatic sea inner domain.

The general circulation of the Adriatic Sea and its seasonal and inter-annual variations have been largely investigated in the past years through both direct observations (*Artegiani et al.* (1997a), *Artegiani et al.* (1997b), *Poulain* (2001)) and numerical simulations (*Zavatarelli et al.* (2002), *Zavatarelli and Pinardi* (2003), *Oddo et al.* (2005)). They depict a general cyclonic circulation with three cyclonic gyres in the northern, central and southern subbasins, an intensified WACC (Western Adriatic Coastal Current) flowing along the italian shoreline exiting the Adriatic through the Otranto Straight and counterbalanced by a northwestward flow of warm and salty water along the eastern side, named EAC (Eastern Adriatic Current). A schematic of the surface Adriatic circulation from *Artegiani et al.* (1997b) has been inserted in figure 1.3.
One principal forcing of the circulation is the wind that divide into two main regimes, Bora northeasterly wind and Scirocco southeasterly wind. The other main forcing is the river freshwater inflow. Adriatic rivers concentrates on

the Albanian coast on the east side and all along the Italian border, sustaining the WACC. The main river is Po, discharging in the Northern Adriatic, which accounts for the 80% of the total freshwater discharge.

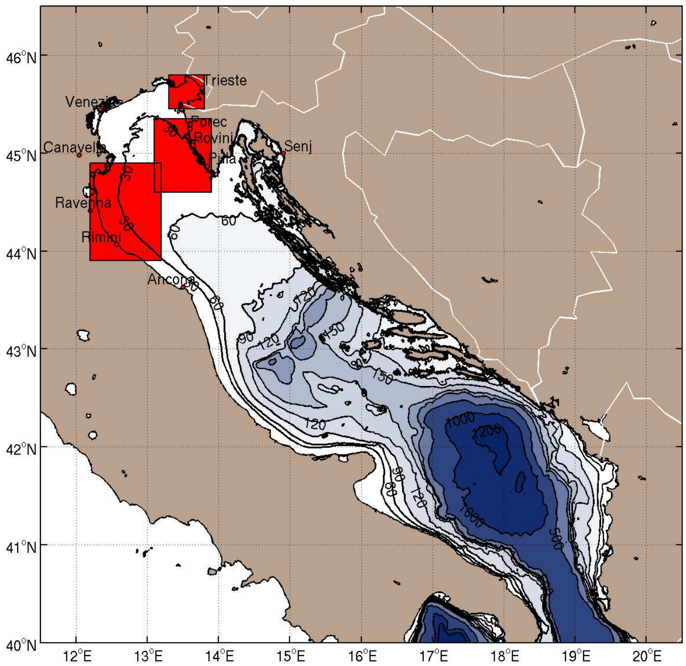

Figure 1.2: The Adriatic Sea bathymetry. Red squares enclose the three coastal areas of the Northern Adriatic basin where this study will focus.

1.1.2 The Northern Adriatic Basin

The Adriatic shelf extends over the whole Northern Adriatic Basin up to the 120m bathymetric which represents the shelf break and its slope is very gentle (0.5 m/km) with 40m of mean depth.
The Adriatic shelf hydrodynamics is controlled by the air-sea fluxes, the river runoff and the inflow of heat and salt at the shelf break. The fluxes of heat and water combine in a buoyancy budget B (m^2s^{-3}), that for the Adriatic basin is nil on average owing to the contrasting effects of heat and freshwater

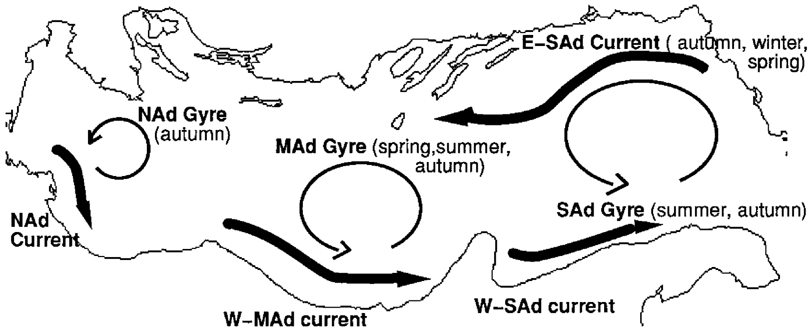

Figure 1.3: Schematic of the Adriatic Sea surface circulation from *Artegiani et al.* (1997b)

fluxes:

$$B = -\frac{\alpha g}{\rho_0 c_p} Q - g\beta(E - P - \frac{R}{A})S \tag{1.1}$$

where Q is the net heat flux (W/m^2), α is the thermal expansion coefficient (K^{-1}), c_p is the specific heat of water ($Jkg^{-1}K^{-1}$), ρ_0 is water density (kg/m^3), g is acceleration due to gravity (m/s^2), E the evaporation rate (m/s), P the precipitation rate (m/s), R is river volume discharge (m^3/s) divided by the river section area (A, m^2), β is the haline expansion coefficient (psu^{-1}) and S the surface salinity (psu).
Supic and Orlic (1999) estimated the seasonal cycle of buoyancy flux from observations (1966-1992) at three nearby locations (Trieste, Rovinj, Mali Losinj) on Northern Adriatic east coast and found that there, it depends primarily on seasonal heating regime. B is positive during winter and negative in summer with annual mean close to zero. Significant spatial variations in buoyancy flux over the shelf establish horizontal density gradients, on account of spatial variations in either bathymetry, buoyancy input and vertical mixing. This has important implications on the dense water formation process that occur on the Adriatic shelf during winter where vertical overturning is not prevented by increased vertical stability due to freshwater inflow. *Supic and Orlic* (1999) did not consider river runoff in the fresh water flux which instead highly affects all the north-western area, mainly due to the Po River, together with others big rivers like Brenta, Adrige, Piave, Tagliamento, Isonzo. River plumes developing on the north-western shelf are deflected to the right (Northern Hemisphere) under the effect of earth rotation and form a coastal current that flows all along the italian coast named WACC.
Zavatarelli and Pinardi (2003) studied for the first time the climatological

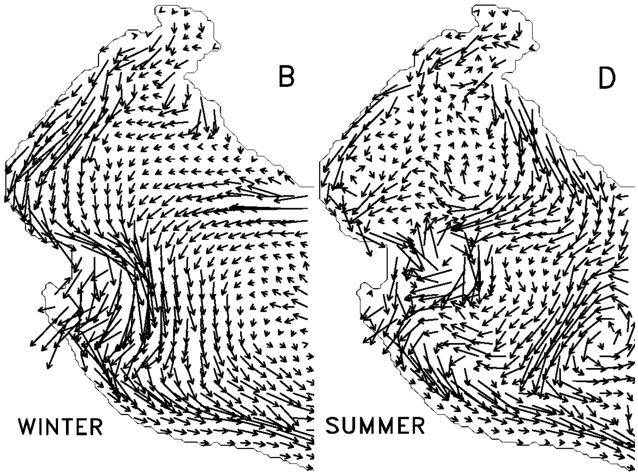

Figure 1.4: Winter and Summer seasonal circulation calculated from climatological simulations in the Northern Adriatic from *Zavatarelli and Pinardi* (2003)

seasonal circulation in the Northern Adriatic at high horizontal resolution (1.5 km) through numerical simulations with a nested approach. Figure 1.4 displays the winter and summer climatological circulation from *Zavatarelli and Pinardi* (2003).
During winter the inflow EAC deflects toward the center of the basin due to the development of an anticyclonic structure located along the northern coast of the Istrian peninsula. The outflow on the western coast is defined by a strong and narrow WACC particularly intense in the Po River delta region where it slightly extend off-shore and turns back to the Emilia Romagna coast flowing perpendicular to the shoreline and then driving south.
During summer, the anticyclonic structure, appearing in winter offshore of the Istrian coast, extends south to form an anticyclonic meander that confines EAC in the meridional part of the basin (along the 40 m bathymetric) and connects with a well developed anti-cyclone in front of the Po River delta. This anti-cyclone pushes waters towards the Emilia Romagna coastal area where the flow deviates back southward along the western coast.
The occurrence of a southward current along the eastern northern Adriatic coast, named Istrian Coastal Countercurrent (ICCC), has been observed by *Supić et al.* (2000) and *Lyons et al.* (2007). From monthly averages of the surface circulation (*Zavatarelli and Pinardi*, 2003) emerges that the ICCC is part of a completely closed anticyclonic gyre.

1.1.3 Environmental Criticality

The Northern Adriatic basin represents one of the most delicate environmental systems of the whole Mediterranean Sea where high economical interests impact. The combined action of high anthropic pressure, meteo-climatic condition, river runoff and topographic characteristics made the Northern Adriatic system highly susceptible.
Due to the significant nutrient load, discharged principally by the Po River, the Adriatic Shelf is affected since late seventies by severe eutrophication phenomena that have important consequences on the marine ecosystem and on the socio-economy of the area.

The Po River catchment embraces an area of approximately $71,000 km^2$

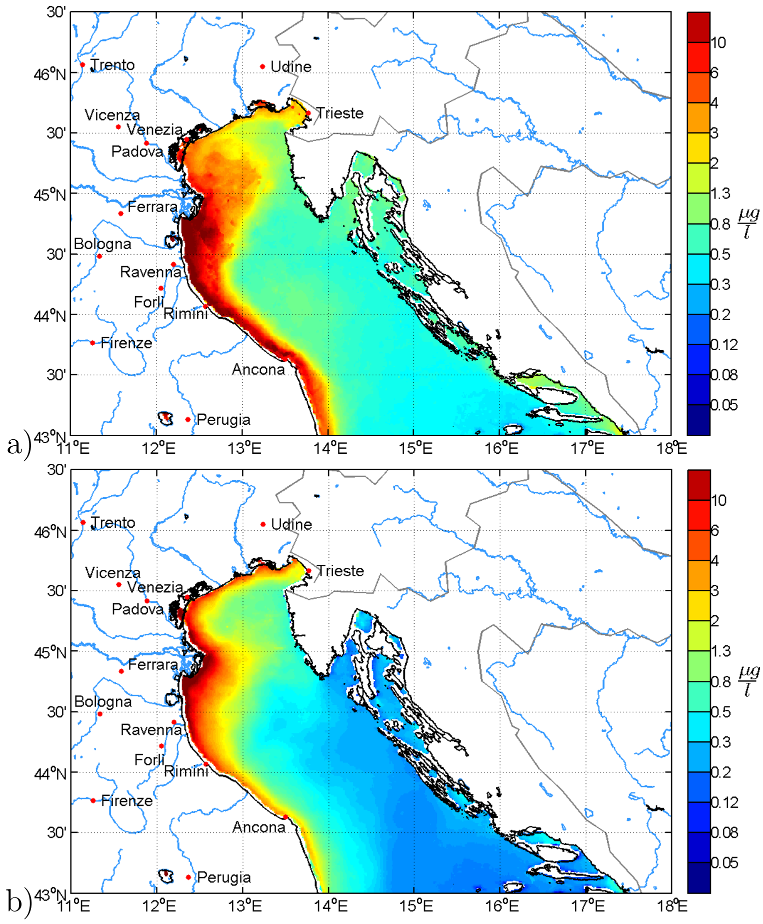

Figure 1.5: Monthly average of chlorophyll deriverd from SeaWiFS sensor satellite images for the period 1997-2004: a) February distribution; b) August distribution. From *Montanari et al.* (2006).

(about a quarter of the whole surface of Italy) where a population of 16 millions of inhabitants (about a quarter of the whole Italian population) lives. Consequently this area has a considerable relevance from the economic point of view: it provides 40% of the national GDP (Gross Domestic Product), 37% of industrial product, 55% of cattle raised as well as 35% of the Italian agricultural production comes from this area (*Artioli et al.*, 2005).
Intensive agricoltural and cattle raising activities produce high emissions of nutrients that are partially collected by the Po River. This trophic load produces intense eutrophication and dystrophic crisis that impact mostly on the Emilia Romagna coastal area owing to the general cyclonic circulation.
Figure 1.5, from *Montanari et al.* (2006), shows February (a) and August (b) chlorophyll climatology calculated from SeaWiFS (Sea Viewing Wide Field of View Sensor) data for the period 1998-2004. These two months represent the extremes of the chlorophyll seasonal cycle. Ocean color products like chlorophyll are considered good proxies of primary production either of local or remote origin and also passive tracers of river freshwater. Areas of maximum chlorophyll concentration delineate the Region Of Freshwater Influence (ROFI, *Hill* (1998)) over the Adriatic shelf. The Northern Adriatic ROFI occupies the shallowest part of the shelf, delimited approximately by the 40m isobath (fig.1.2), and includes all the Emilia Romagna coastal strip, where the highest chlorophyll concentrations are always observed. The eutrophic level caused by extended and frequent algal blooms and the consequent effects on the marine ecosystem, depict in the Adriatic shelf and in the Emilia Romagna coastal area, one of the most critical environmental condition of the whole Mediterranean Sea. The stratifying action of buoyancy input represents a key regulator of primary production and in concomitance with stagnant weather conditions it might isolate bottom water from the exchange with the atmosphere bringing about anoxic conditions, causing massive fish mortality and damaging the benthic ecosystem. Tourism is affected too by colored smelly tides and increased turbidity.
Another phenomena appeared in the 1980s in the Adriatic increasing its environmental criticality: the mucilages. Many efforts have been spent to study and understand this process and its rising factors (*Giani et al.*, 2005).
For these reasons an intense monitoring program was set up by the region Emilia Romagna from the 1980s, that it will be discussed in the next chapter. These socio-economical aspects in fact motivated us to study the coastal hydro-dynamics in this area as fundamental step towards the understanding of the relationship between the physical processes and the ecosystem.

1.2 Towards an Integrated Observing and Prediction System

In this study we exploits the monitoring and forecasting system established in the framework of ADRICOSM (ADRiatic sea integrated COastal areaS and river basin Management system) Pilot Project (*Castellari et al.*, 2006).

1.2.1 The Adriatic Coastal Monitoring Network

ADRICOSM Project intended to implement a near-real time (NRT) operational coastal management system in the Adriatic Basin to answer urgent societal questions such as the sustainable development of coastal areas, the exploitation of coastal resources and the protection of the coastal environment. ADRICOSM co-ordinated a highly complex network of platforms for oceanographic NRT data collection that made available a lot of observations for a long time period (September 2002-December 2003).

The CTD networks considered in this study were upgraded or established in three coastal areas of the Northern Adriatic basin, enclosed in red squares in figure 1.2: Emilia-Romagna, Gulf of Trieste and Rovinj. The responsible institutions for monitoring were: ARPA (Azienda Regionale Prevenzione e Ambiente, regional environmental protection agency) of Emilia Romagna (Italy); LMB (Laboratory of Marine Biology) of Trieste (Italy); MBS (Marine Biological Station) of Piran (Slovenia); CMR (Centre for Marine Research) of Rovinj (Croatia). They performed weekly coastal monitoring campaigns on coincident sampling days, when weather conditions were favorable.

The Emilia-Romagna coastal monitoring network has been established in the late seventies to face the environmental emergency related to eutrophication processes and then maintained from the regional environmental protection agency (ARPA) to control water quality and study the marine ecosystem and coastal hydrodynamics. The monitoring array is made up of 40 stations situated along transects perpendicular to the coastline at distances of 500 m, 3, 6 or 10 km from the coastline sampled on a weekly basis on two consecutive days. Emilia Romagna coastal area is sandy, shallow and gently sloping so the deepest stations reach approximately 20 meters depth. *Montanari et al.* (2006) studied the mean currents in the Emilia-Romagna region from an historical hydrographic data set and elaborated a climatological circulation scheme in good agreement with *Zavatarelli and Pinardi* (2003) simulations. Part of the work in *Montanari et al.* (2006) has been developed during the fist part of this thesis and will be described in detail in chapter 2.

In the Gulf of Trieste bi-weekly (October 2002 - March 2003) and weekly

(April - September 2003) cruises (*Celio et al.*, 2006) were performed over the sampling grid of 19 stations providing an adequate spatial and temporal coverage of the area during one day cruise. The Gulf of Trieste is a semi-enclosed basin of about 30 km diameter characterized by a relatively complex topography. Its main NE-SW axis divides a deeper pool (maximum depths is 26m) in the southern-central part from a slope in the northern area, influenced by the Isonzo River estuary. *Malačič and Petelin* (2009) studied by numerical simulation the climatological circulation inside the Gulf of Trieste and describe a general inflow on the southern part of the Gulf that makes a cyclonic turn during average winter conditions. An outflow at the surface crosses the Gulf diagonally and merges with the fresh water belt originating from the Isonzo River along the northern coastline. This outflow is sustained by the dominant Bora wind which blows along the NE-SW axis. The cyclonic turn enhances during spring and closes in an elongated cyclonic gyres in summer, while an anti-cyclonic gyre forms in the eastern side of the Gulf. In stratified conditions the surface of the Gulf is characterized by an anti-cyclonic gyre due to the inertial plume of the Isonzo River.
The third coastal network off Rovinj is made up of 19 stations mainly arranged on three transects perpendicular to the coast. Here the sea bottom fast descend offshore and reaches 40m of depth at few kilometers from the shore. *Lyons et al.* (2007) present a detailed analysis of all the CTD data collected in this area, providing a description of water masses and geostrophic circulation of the northeastern Adriatic Sea for the period May-September 2003.

1.2.2 The Adriatic Forecasting System

The Adriatic Forecasting System (AFS) has been first implemented by *Oddo et al.* (2005) in the framework of ADRICOSM Project and upgraded by *Guarnieri et al.* (2009). It nests into the Mediterranean Forecasting System (MFS, *Pinardi et al.* (2003), *Tonani et al.* (2008)), which constitutes the modeling system (fig.1.1) in the outer domain.
The MFS produces weekly analyses and daily forecasts at about 6.5 km of horizontal resolution which are published at the web page http://gnoo.bo.ingv.it/mfs/. MFS provide informations at AFS lateral open boundary located in the Ionian Sea along the $39°N$ parallel, south of the Otranto Straight.
AFS is based on the Princeton Ocean Model (POM, *Blumberg and Mellor* (1987)) code solved over 31 terrain following σ layers at a horizontal resolution of 2.2 km. It produces once a week with a daily system, as described in the diagram in figure 1.6, 9 days forecast of the main hydrodynamics state

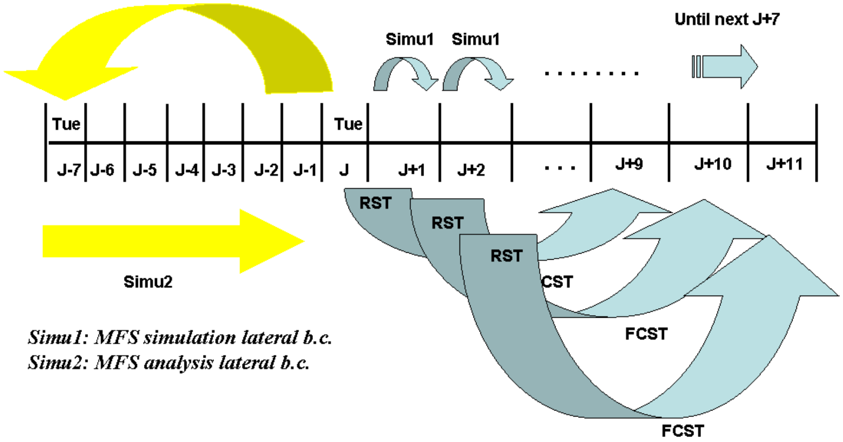

Figure 1.6: Schematic of the Adriatic Forecasting System procedure from *Guarnieri et al.* (2009)

variables (currents, temperature, salinity, sea level and air-sea fluxes). AFS is weekly rewinded back in time of one week, following the assimilation cycle of the nesting MFS, to prevent from a degeneration at the open boundary. AFS products are published at the web page http://gnoo.bo.ingv.it/afs/.

1.3 Objectives and Methodology

Coastal ocean forecast is a challenging task for the oceanographic community stimulated by the international issue of Integrated Coastal Zone Management (ICZM) problems. The sustainable development of the coastal areas depends on the quality of the marine environment and an assessment/forecasting system is necessary to enable policy decisions to be taken in a modern and efficient way. Sustainable coastal zone management requires an efficient and accurate assessment of the state of the coastal environment.
Objective of the thesis is to demonstrate the feasibility of an integrated Coastal Ocean Observing and Prediction System (COOPS) in the Northern Adriatic Sea aimed to support both management of the coastal zone and a rapid response to environmental emergencies. This COOPS builds on an operational regional forecasting system and coastal observational networks of opportunity partially established in the framework of ADRICOSM Project. A data assimilation scheme is the COOPS third major component that allows to produce data-driven simulations closer to reality (*Robinson*, 1999).

The methodology of Rapid Environmental Assessment (REA), conceptualized by *Robinson* (2002) in the nineties, has been adopted in our study to develop a COOPS in the Northern Adriatic and a Coastal REA (CREA) that initializes the coastal high resolution model, ASHELF, nested within the regional forecasting system, AFS, blending the AFS large scale fields with the available opportunity coastal observations to generate the best field estimates.
REA methodology is composed of three main phases that will be developed in three main chaptes of the thesis. Each phase covers a specific task:

1. a *Descriptive Phase* aimed at identifying the relevant circulation structures and the time/space scales of variability in the area under investigation.

2. a *Dynamical Phase* has the goal to implement the numerical prediction system. The numerical model is calibrated, i.e., domain and computational parameters are tuned to the region and its phenomena through sensitivity analyses. The modeling system is validated with observations.

3. a *Predictive phase* is devoted to the forecasting and the initialization by means of blended model and data initial conditions. We call this phase CREA.

1.4 Structure of the Thesis

The thesis is organized into three main chapters that follow the three phases required for COOPS system implementation. Each chapter consists of the content of a manuscript which will be submitted for publication.
Chapter 2 presents a climatological data analysis of Emilia Romagna coastal area partially published in *Montanari et al.* (2006). The analysis is based on the very large data set collected by Struttura Oceanografica Daphne, Operational Oceanographic Unit of the regional environmental protection agency (ARPA, Azienda Regionale Prevenzione e Ambiente), in the period 1995-2002 over Emilia Romagna operational monitoring network. Basic statistical analysis are applied to first quality control the measurements and understand the evolution of the water column structure during the year. Monthly climatologies of temperature and salinity are mapped. Climatological current estimation enables to identify the relevant circulation features and their time/space scales of variability. Four high resolution cruises dedicated to the study of the correlation functions were carried out and discussed.

Chapter 3 is dedicated to the implementation of the high resolution (800m) Adriatic shelf model (ASHELF) nested within the hierarchical modeling system that consists of the Mediterranean Forecasting System (MFS) and the Adriatic Forecasting System (AFS). ASHELF model validation with in situ coastal observations and satellite sea surface temperature data is described. *Chapter 4* contains the design and calibration/validation of the CREA system applied to the Northern Adriatic. An assimilation technique exerts a correction of the ASHELF initial field, provided by AFS model, on the basis of opportunity coastal observations. The blending of the two data sets is carried out through a multi-scale optimal interpolation technique developed by *Mariano and Brown* (1992). ASHELF spin up time is investigated too, through a dedicated experiment, in order to obtain the maximum forecast accuracy and up to 7 days accurate forecast.

Chapter 2

Climatological Data Analysis in the Emilia Romagna Coastal Area

Note that part of the content of this Chapter is a co-authored book with Dott. G. Montanari, Dott. A. Rinaldi from Operational Oceanographic Unit Daphne (ARPA Emilia Romagna) Prof. N. Pinardi and Dott. L. Giacomelli entitled *The Currents of Emilia Romagna Coastal Strip during the Period 1995-2002"* and published within *"I Quaderni di ARPA"* collection.

2.1 Introduction

The Emilia Romagna coastal strip (fig.2.1) is part of the Adriatic Sea continental shelf and is located on the north-western coast, just south the Po River delta. Its shoreline creates a smooth embayment where the isobaths settle parallel to it. The sandy bottom is very shallow and reaches 30m of depth at 30 km far offshore, as depicted in fig. 2.1a.

The coastal processes and the hydrodynamic characteristics depends mainly from the Po River, the winds and their interaction with local topography and ambient stratification.

Po River accounts for about one third of the total riverine freshwater input in the Adriatic Sea (*Kourafalou*, 1999). Its annual average discharge is $1600 m^/ sec$ but it may peak to values of $9000 m^/ sec$ during intense flood events. Figure 2.2a shows Po River daily and monthly averaged runoff for the period 1995-2002, where it is evident a strong seasonal variability, characterized by maximum values in spring and fall. Po river delta consists of 5 main branches that give origin to a broad plume which moves offshore at

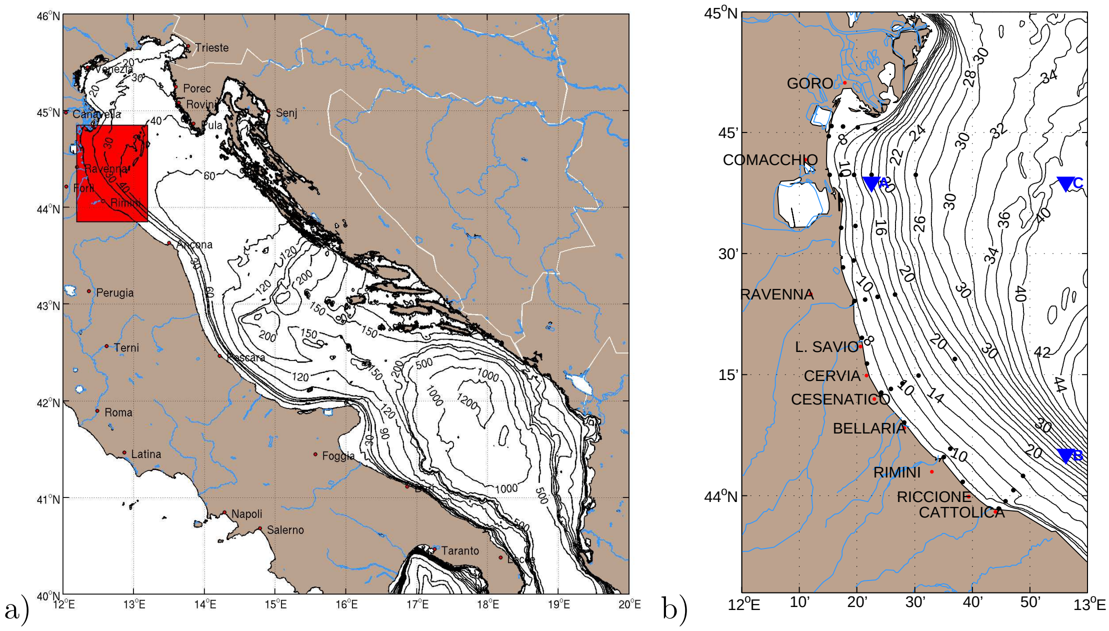

Figure 2.1: a) Adriatic Sea bathymetry and, in the red square, the Emilia Romagna coastal area. b) bathymetry of Emilia Romagna Coastal Area. Black dots stand for monitoring stations, while blue triangles indicate points from ECMWF grid where we calculated monthly wind climatology.

the surface depending on combined effect of inflow velocity, wind regime and ambient stratification, before being deflected southward in a coastal current that reattaches to the Emilia Romagna coast downstream. This coastal current is named WACC. The WACC is part of the general cyclonic circulation that characterizes the Adriatic Sea in conjunction with the Eastern Adriatic Coastal Current (EAC) that brings up north saltier and warmer water coming from the Mediterranean Sea along the eastern coast. The WACC, studied by *Zavatarelli and Pinardi* (2003) through climatological simulations, intensifies and narrows during winter while it detaches from the coast meandering and forming cyclonic and anticyclonic eddies during summer. WACC detachment is a common feature in front of the Po river delta where an anticyclone emerges from the climatology during summer.
Two typical wind regimes characterizes this regions, northeasterly Bora winds and southeasterly Scirocco winds. Figure 2.2b show monthly climatological wind velocity at three nearby location (marked in fig.2.1b) in the Emilia Romagna coastal area estimated from European Centre for Medium-Range Weather Forecasts (ECMWF) operational products for the period 1979-2000. The results show dominating Bora winds during winter months from Decem-

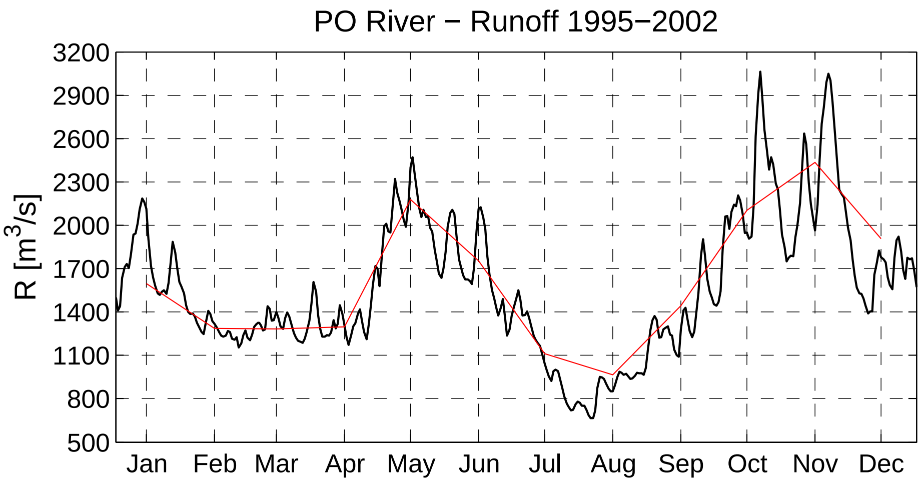

a)

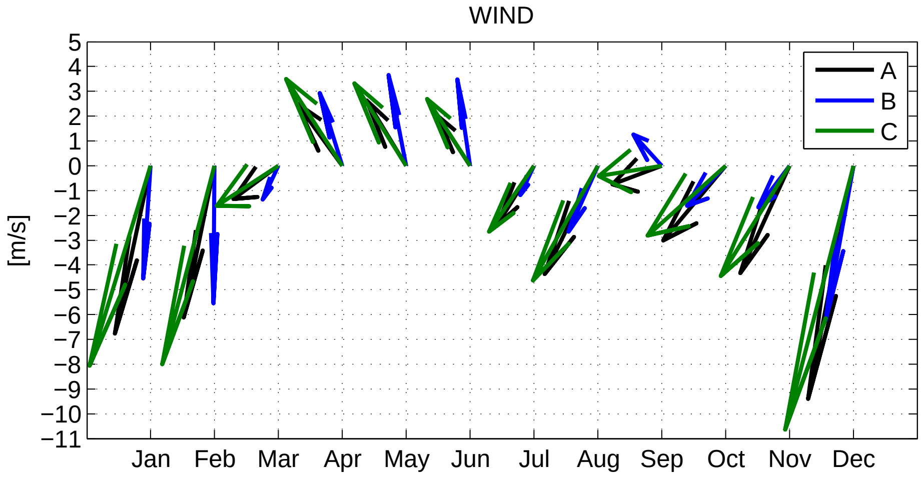

b)

Figure 2.2: a) Po River mean daily runoff (black line) for the period 1995-2002 and (red line) the corresponding monthly climatology. b) Wind monthly climatology calculated in the 3 points displayed in figure 2.1 from ECMWF analyses.

ber to February and dominating Scirocco winds from April to June. During summertime (July-August) and autumn (October-November) a weak north-easterly wind prevails. Minimum wind regime occur in March and September, with a prevailing direction from northeast-east.

Bora restricts the Po plume offshore development and enhances the WACC, confining it towards the coast. The free surface rises up leading to down-welling phenomena. Upwelling favorable wind, Scirocco, advects low-salinity Po waters towards the northern Adriatic shelf and weakens the WACC which

in some cases can reverse as observed by *Poulain et al.* (2004).
Due to the direct influece of Po River and the WACC, the whole Emilia Romagna coastal area is characterized by strong temperature and salinity gradients and a high space/time variability. This variability presents a well defined seasonal periodicity but intense weather events can rapidly change the overall ambient condition, strengthened by the shallow topography.
Emilia Romagna coastal monitoring activity is unique in the overall Mediterranean Sea, since it has been the first one established in the late seventies to face the environmental emergency caused by eutrophication phenomena affecting the Adriatic shelf and determining important consequences on local economy. The Operational Oceanographic Unit Daphne was set up by the regional authority in 1978, as part of the local environmental protection agency (ARPA, Azienda Regionale Prevenzione e Ambiente), together with an extensive monitoring program aimed to survey the coastal environment and its marine resources. The fundamental purpose of this activity is the study and the understanding of the processes occurring within the coastal zone and it originates from the necessity of policy maker to manage such a critical area, where many human, environmental and economical interests impact. This can be considered a first attempt of sustainable coastal management, anticipating the concept of Integrated Coastal Zone Management (ICZM), introduced by the Europe Commission in 1996. The operational observing system allowed to acquire a huge amount of informations about the physical and bio-geo-chemical characteristics of the area, through the sampling of many variable like temperature, salinity, pH, turbidity, chlorophyll concentration, dissolved oxygen, nutrients.
Our objective is to analyze vertical profiles of temperature and salinity collected weekly during the period 1995-2002 and present a climatology to give a first basic description of the hydrological characteristics of the coastal zone and their space/time scales of variability. Moreover, we attempt to describe the climatological density-driven circulation deduced from the mapping of the hydrological data.
Artegiani et al. (1997b) carried out for the first time a seasonal analysis of hydrological parameters in the Adriatic Sea on the basis of seasons defined by the annual cycle of heat storage since the available data set was insufficient to perform a monthly analysis. They also described the baroclinic general circulation of the Adriatic Sea obtained by temperature and salinity seasonal horizontal distributions. *Jeffries and Lee* (2007) presented a new climatology for the Northern Adriatic which characterizes temperature and salinity fields associated with response to dominant forcing (riverine input and wind) acting on variable ambient stratification.
The high variability of coastal environments requires large amounts of obser-

vations to capture its climatological characteristics with enough statistical significance. The large data set collected by ARPA in the Emilia Romagna region is characterized by an exclusive spatial and temporal coverage that makes possible to perform a monthly analysis and produce for the first time a reliable climatology for the coastal area.
The availability of a coastal climatology is very important since it enables to set up an efficient data quality control procedure, to understand the main processes driving the coastal dynamics, to identify the main circulation patterns, to better identify anomalous events and thus to manage more efficiently the coastal environment. Moreover this descriptive phase is a fundamental step towards an accurate prediction of the coastal environment and the assimilation of coastal data in numerical models.
This work initiated and proceeds in collaboration with the regional environmental protection agency (ARPA) that supported also four extraordinary survey experiments aimed to identify the characteristics space scales of temperature and salinity fields through the study of their correlation functions.
Section 2 describes in detail the Emilia Romagna observational network, the measurement data set and the applied preliminary data quality control procedure. The dedicated surveys to the study of the temperature and salinity correlation function are also presented. *Section 3* details the methodology utilized for climatology calculation/mapping, for geostrophic current estimation and correlation function analysis. *Section 4* provides a detailed description of temperature and salinity climatologies and the derived climatological currents. *Section 5* summarizes our findings while *Section 6* draws the conclusions.

2.2 Observational Data Sets

2.2.1 Historical Observations and Quality Control Procedure

The coastal monitoring network of ARPA Daphne covers an area extending 20 km offshore with 34 stations, displayed in figure 2.1b, along 14 transects perpendicular to the coastline. The stations on each transect are situated at distances of 0.5, 3, 6, 10, 20 km from the shoreline. Sampling frequency is weekly with two days survey to cover the entire network. Monitoring is carried out with an oceanographic vessel called Daphne II, equipped to collect measurements for this coastal area. Daphne II is provided with a CTD probe which collects vertical profiles of temperature, salinity, pH, dissolved oxygen and chlorophyll-a together with an on board laboratory for the pre-treatment and refrigeration of the collected samples of both water or sediment. CTD

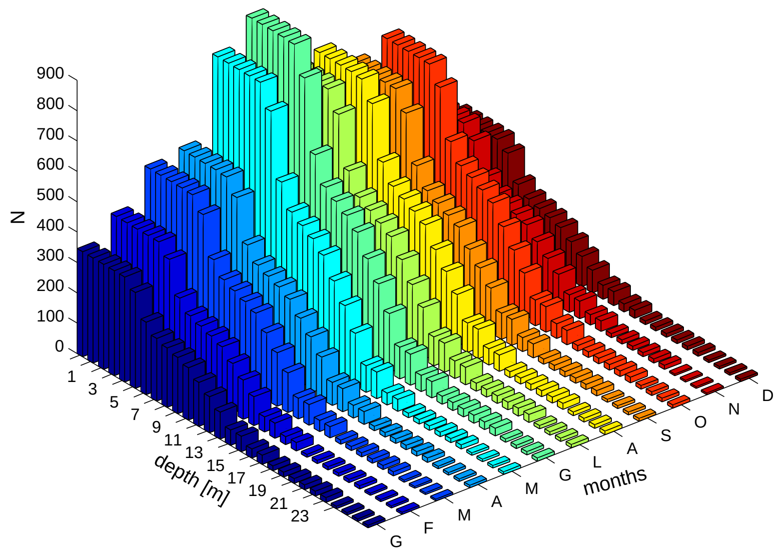

Figure 2.3: Data statistics (after *Montanari et al.* (2006)).

profiles start from 0.5m depth and stop at few centimeters from the bottom, after the sensor has stabilized, while on the water column data record are stored every half a meter of depth.

The data considered in this study are temperature and salinity profiles that cover the period 1995-2002. Data distribution as a function of depth and sampling month is depicted in figure 2.3. Data diminish progressively with depth as a function of local bathymetry, while over the year it diminishes during winter time owing to bad weather condition. This preliminary statistics indicate that next analysis will be highly significant within the first 10 meter of the water column and significant within 20m where more than 30 measurement are present for each month.

Before being able to analyze the available data it has been necessary to carry out a data quality control. This consists in assigning to each profile quality indices in order to exclude data subject to various type of errors (instrumental, operational or statistical significance) from successive investigation. We referred to *Stephens et al.* (2002) and *Boyer et al.* (2002) for the quality check procedure implementation. Quality control is carried out through non exclusive, sequential tests. This means that every observation passes all the checks and that every check has a corresponding quality index. Every profile is checked in the following manner and order:

1. duplicate elimination through station code, positioning and acquisition date check.

2. Monotonic pressure growth with depth and maximum observation depth less than the nominal maximum station depth.

3. Gross range check consisting of a test for the observations to be within a broad range of values considered to be relevant for the region. In particular we consider the temperature interval $4-30C^\circ$ and the salinity interval $16-39psu$.

4. Statistical check.

After the third quality control step, a vertical linear interpolation of the data on standard levels, chosen to be at each meter depth, has been applied. The successive statistical check is based on the estimation of monthly area average profiles and the relative standard deviation. At depth shallower than 15m values which differ from the corresponding monthly average more than three standard deviations were flagged, while below 15m we applied the two standard deviation threshold, since the variability diminish as function of depth. This statistical method is repeated twice in order to exclude in the first phase gross errors that increase the standard deviation estimate, improving the resulting effectiveness of the control. The area average monthly profiles of temperature and salinity used for data quality control and their corresponding standard deviations are shown in figure 2.4a and b.

Temperature profiles show an evident seasonal cycle with $20C^\circ$ of maximum excursion at the surface and $10C^\circ$ on the bottom layer. The thermocline appears in April and establishes in May, as a consequence of atmospheric warming, and lasts for the summer till September. Maximum values reach on average $26C^\circ$ at the surface and $20C^\circ$ on the bottom in August. In September the water column starts to cool down at the surface but still keeping bottom values around $20C^\circ$ till October, when the water column looks quite homogeneous. In November-December the entire water column cools down progressively and presents a vertical gradient with lowest temperatures at the surface which last till February. This temperature inversion is allowed by very low salinity values at the surface. Minimum values occur on January with $7C^\circ$ at the surface and February with $9C^\circ$ on the bottom. From January to March the water column looks homogeneous. Mean bottom values around $10C^\circ$ persist during the winter till April.
Salinity profiles remain consistent during the year with the highest values

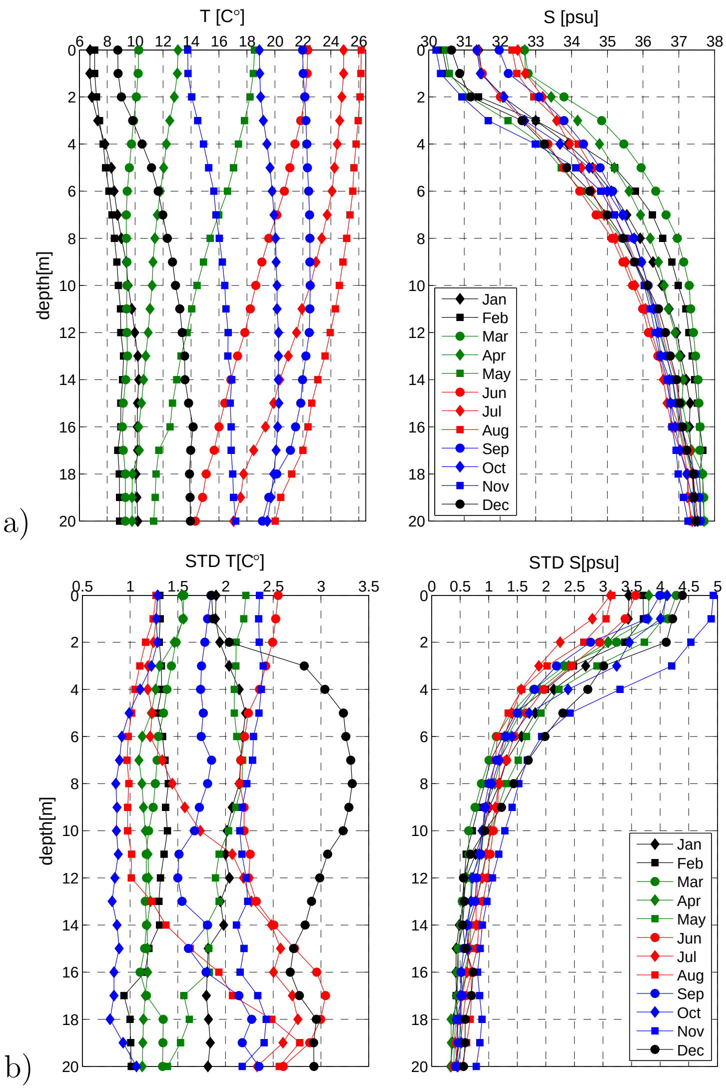

Figure 2.4: a) Monthly area averaged temperature and salinity profiles and b) the relative standard deviations (after *Montanari et al.* (2006)).

on the bottom layer, below 15m depth, between 37-38psu. Minimum values at the surface are below 31 psu in November, December, February and May, while the highest values remain above 32 psu in March-April and July-August, periods of minimum Po river discharge. Figure 2.2 highlights a strong correlation between the peaks of the Po river maximum discharge (May, November) and the minimum of salinity over the coastal area.
Standard deviation profiles (fig.2.4b) present for salinity a common trend all year long with maximum values within the first 5m layer, pointing out

which part of the water column is subject to the strongest variability due to river freshwater influence. The period with maximum salinity variability (November, December) matches with the maximum Po runoff. Temperature variability does not present a particular tendency with depth except for the months of July and August where the standard deviation value increases with depth and December that shows a sub-surface maximum. Again, the months subject to the greatest variability are November-December together with May-June. During these periods the coastal system exhibits a transition ambient conditions, since the water column shifts from homogeneous to stratified conditions and vice versa. This transition depends from the combination of heat flux at the surface, the wind regime and the Po river discharge which might vary from year to year determining a higher variability.

The low salinity values characterizing always the Emilia Romagna costal area, determine a density compensation process that stabilize gravitationally the water column during winter season, when the coldest water is present at the surface. This is confirmed by the estimated monthly density profiles shown in fig.2.5, that indicate a persistent stratification all year long. Density profiles distinguish two regimes, one from December to April (Winter-Spring) and one from June to November (Summer-Autumn). May profile is anomalous and presents the maximum density gradient. We speculate a double effect, diluting and thermal, of water of river origin on the density field since in this period of the year freshwater is warmer than seawater.

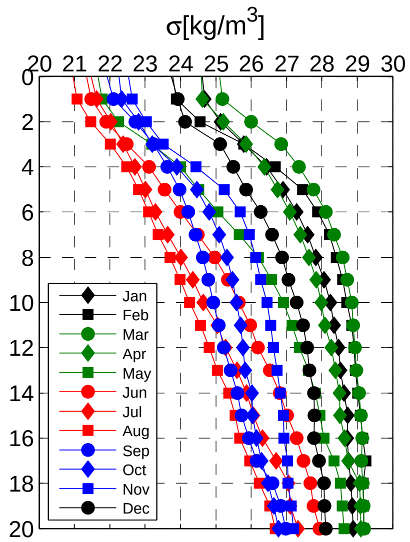

Figure 2.5: Monthly area averaged density profiles.

2.2.2 High Resolution Data Collection

Four high resolution quasi-synoptic monitoring campaigns have been conducted in different periods of the year to study the characteristic correlation length scales of temperature and salinity fields on the coastal zone. This high quality data set obtained by oversampling the area under investigation was meant to improve our objective analysis mapping technique through the definition of correlations scales estimated from data and to design an optimally efficient observational network for future coastal forecast esercizes.
High resolution surveys took place on:

1. 26-27 August 2003, 107 casts;

2. 16-17 March 2004, 100 casts;

3. 23-24 November 2004, 98 casts;

4. 10-12 May 2005, 97 casts;

The sampling strategy adopted is presented in figures 2.6-2.7 and it consists of highly resolved CTD measurement at the nominal distance of 3 km along several transects separated by the same distance. This allowed a fast coverage of the region in two consecutive days to obtain a quasi-synoptic data set. A different sampling scheme has been adopted during May 2005 (fig.2.7b), where we reduced the number of transects along the coast to add stations offshore in the northern zone. Moreover the inshore station on each transect is at 3 km instead of 0.5 km. Our purpose was to increase the coverage in the offshore direction.
All casts have been quality checked, as described in the previous section. We then area averaged temperature and salinity fields between all stations for each survey and calculated the relative standard deviation. The resulting profiles are shown in figures 2.6-2.7 together with their relative climatological profile to have indication if the synoptic data-sets might be representative of the average condition of the coastal area at the corresponding period of the year.
August temperature and salinity profiles (fig.2.6a) describe a quite homogeneous water column, warmer and saltier than its relative climatological profile. Below 10 m depth temperature slightly diminishes, while salinity diminishes at the surface due to river freshwater influence. In March (fig.2.6b) temperature started already to warm up due to atmospheric warming with the maximum gradient located at 3m depth. Subsurface temperature is colder than its climatological value. Salinity profile presents very low values at the surface ($24 psu$) indicating a massive freshwater input. The halocline is

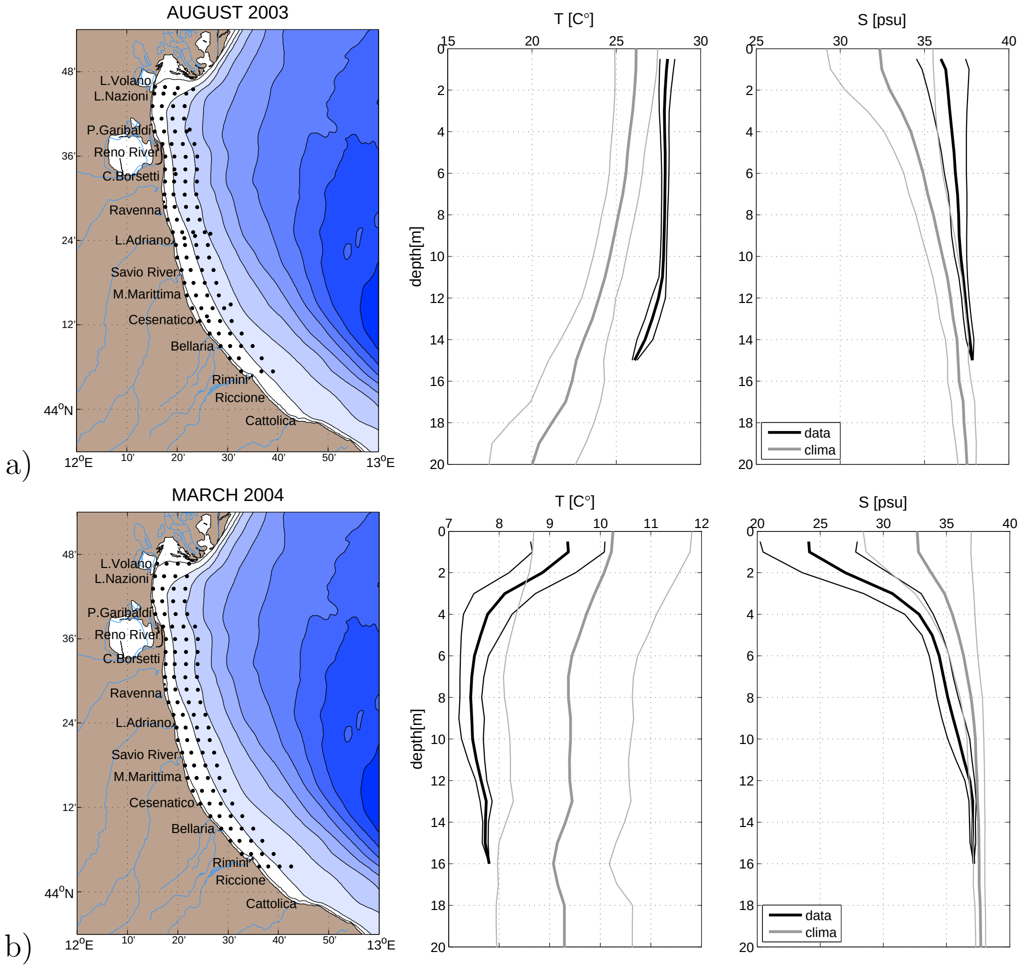

Figure 2.6: Sampling schemes for the high resolution surveys and their relative area averaged temperature and salinity profiles (black line) enclosed between ±1 standard deviation profiles. Gray line is the climatological profile enclosed between ±1 standard deviation profiles. a) August 2003; b) March 2004.

situated at 3m depth. November (fig.2.7a) temperature profile presents the typical winter profile, with a colder layer at the surface, compensated gravitationally from corresponding low salinity values. Both temperature and salinity are in good accordance with the climatological profile. Thermocline and halocline settle at 4m depth. May survey (fig.2.7b) revealed a homogeneous water column up to 8m depth where both temperature and salinity start to vary. Thermocline is situated at 12m depth. May condition is in agreement with its climatology.

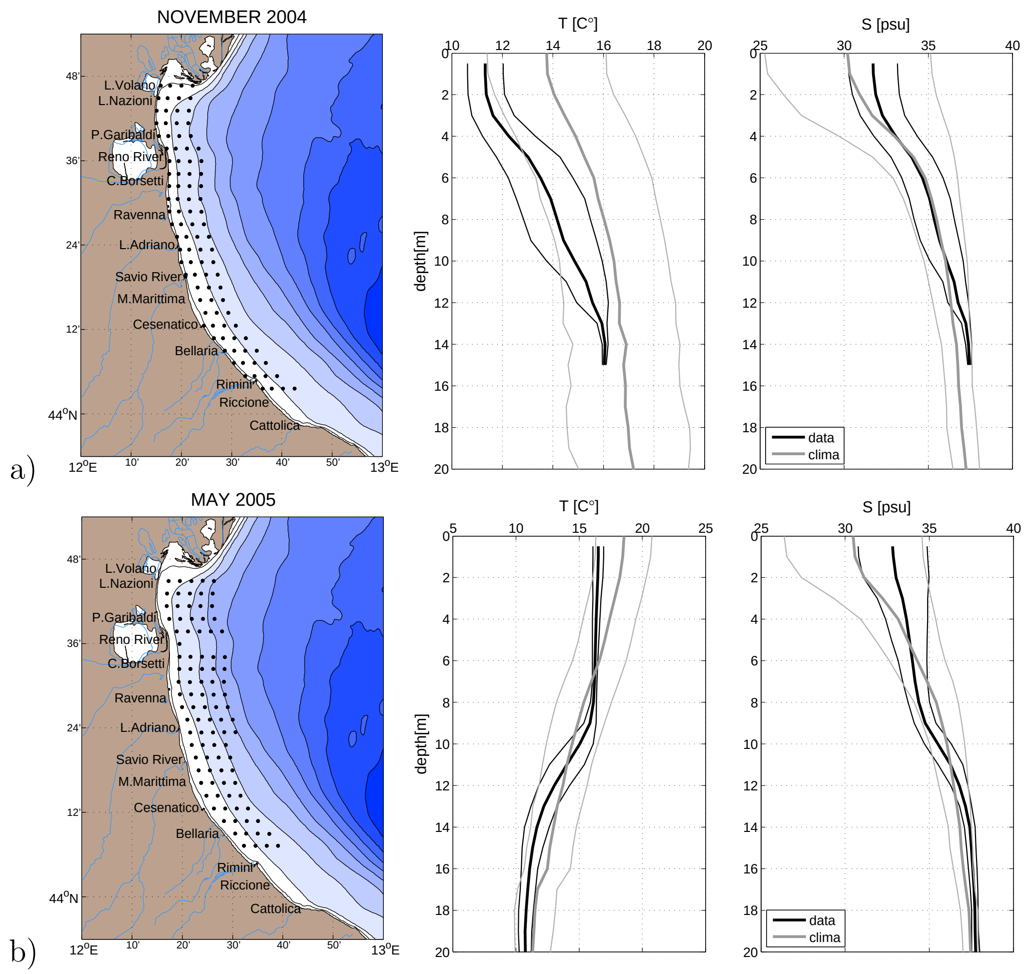

Figure 2.7: As in figure 2.6: a) November 2004; b) May 2005.

2.3 Mapping Methodology

Our analysis focuses on climatology estimation from historical observations for every monitoring station at every pre-set depth level. These climatological values are then analyzed to produce temperature and salinity distributions through the Objective Analysis (OA) technique (*Bretherton et al.* (1976), *Carter and Robinson* (1987)). This is an optimal interpolation technique which allows the evaluation of system state variables on a regular grid (mapping), starting from erroneous observations distributed non-uniformly in space and time. It is in fact supposed that the measured value ϕ is the sum of the true field value $\theta(\vec{r})$ at a certain point and a random error ε:

$$\phi = \theta(\vec{r}) + \varepsilon \tag{2.1}$$

Every type of optimal analysis implies specific assumptions about the characteristics of the field under investigation. Basic assumption is that the field must be stationary and homogeneous, i.e. its statistical characteristics must remain unvaried in the time interval and space domain considered. This implies also that its second order statistics, or correlation function, is homogeneous.
The application of OA requires a priori knowledge of the correlation function which depends on the distance between the observations and not on their location (homogeneity hypothesis). When data are scarce analytical models are assumed but, when sufficient data exists, the correlations can be calculated from observable quantities in terms of time and space lags, treating space and time in equivalent ways. We estimated the correlation matrices from the 4 high resolution surveys data sets, considering each data set as synoptic, with the aim of understanding how correlation field behaves in Emilia Romagna coastal area and to infer which are the characteristic length scales of temperature and salinity mesoscale field for an efficient OA scheme implementation. The analysis of the correlation functions will be presented in details in the next paragraph.
The temperature and salinity climatological data have been objectively analyzed by conventional methods (*Bretherton et al.* (1976), *Carter and Robinson* (1987)) using an isotropic, homogeneous correlation function of the form:

$$R(r) = \Big[1 - \frac{r^2}{a^2}\Big] e^{-\frac{r^2}{2b^2}} \qquad , \qquad r^2 = x^2 + y^2 \qquad , \qquad a > \sqrt{2}b \tag{2.2}$$

where r is the distance, a is the zero-crossing correlation length scale and b is the e-folding scale. This form of the correlation function starts out positive and becomes negative after the zero-crossing ($r = a$). The large negative values ($r > a$) are damped out by the decay scale b of the Gaussian function. First term on the right side of equation 2.2 are the first two terms from a Taylor series expansion of the cosine function which models wave behavior. Thus, a is also equal to 1/4 of the dominant wavelength and must be greater than or equal to $\sqrt{2}b$ so that correlation function is positive semi-definite and represents a physically realizable stochastic process, non negative everywhere.
Although the correlation matrices indicate strong anisotropy in salinity and temperature field, we ended up using an isotropic function. This procedure is common in OA because large trends present in the data are reproduced well in the objective maps, even if an isotropic correlation function is considered. OA technique provides the estimation error field, expressed in percentage of the variance, that represent the OA field error variance normalized by the observed variance. This error is independent from the field value but depends

from the data distribution, noise level and mapping grid resolution, therefore it is used for initial sensitivity experiments, but also to tailor an optimally efficient monitoring scheme. All the maps presented have been masked where estimation error is more than the 30%.
A sensitivity analysis, with the approach used by *Robinson et al.* (1987), was carried out to define the correlation parameters a and b in *Montanari et al.* (2006), taking into account the preliminary investigation on the observed correlation matrices. A zero-crossing distance of 40 km and a decay scale of 20 km slightly overestimate their observed values but they represent a good compromise. Overestimation of correlation parameters leads to smoother interpolated field, instead smaller parameters may produce less realistic features (*Robinson et al.*, 1987).
In estimating the fields at one grid point, not all the observations are taken into consideration, but only those that satisfy the criterion of greatest correlation, and thus defined, influential data. An influential radius of 25 km has been set up within to select the 5 most correlated observation to the estimation grid point that correspond to nearest ones.
The interpolation domain spans between $12.2-13°$ in longitude and $43.9-44.9°$ in latitude with a horizontal grid resolution of 1.5 km, which represents the finest interpolation grid allowed by the Emilia Romagna observational network. The noise level assigned to temperature and salinity observations is equal to the 10% of the field variance.
In ROFI (Region of Freshwater Influence, *Hill* (1998)) coastal and shelf areas where buoyancy input is the major forcing and stratification persists on average all year long, horizontal density gradients sustain a velocity field established by the geostrophic balance between pressure gradient and Coriolis acceleration. We applied this approximation to deduce mean geostrophic velocity fields from temperature and salinity climatology (*Limić and Orlić* (1986), *Paschini et al.* (1993), *Artegiani et al.* (1997b)). We calculated the dynamic height anomaly field from:

$$\Delta D(p_1,p_2) = \int_{p_1}^{p_2} (\alpha - \alpha_{35,0,P})dP \tag{2.3}$$

where $\alpha_{35,0,p}$ is the reference specific volume for a salinity of $35psu$ and temperature of $0C°$ and varying pressure P.
Geostrophic velocity, meridional (v) and zonal (u) components, are function of dynamic height anomaly:

$$f(v_2-v_1) = \frac{\partial}{\partial x}\Delta D(p_1,p_2) \quad , \quad f(u_2-u_1) = -\frac{\partial}{\partial y}\Delta D(p_1,p_2) \tag{2.4}$$

This method allows to estimate geostrophic current velocity from density distribution relative to a reference level p_1, considering the velocity at this level (u_1, v_1) equal to zero. This is a good approximation when the defined reference level is deep but in coastal areas this method has clearly been seldom adopted. However we have evaluated the geostrophic velocity field choosing 10m as reference level to be able to take into account a sufficient number of monitoring locations.

2.3.1 Spatial Correlations

The objective calculation of a correlation function requires data domain subdivision into bin intervals. We chose a bin size of to 3.5 km on the basis of the data distribution. Observations have been first coupled according to their distance. Then for each bin a single correlation estimate has been computed from all data pairs whose spatial separation fell within its increment.
Usual methods involve also the removal of the mean field to subtract the large scale trend and make the correlation estimate more isotropic. We computed different trend surfaces, from first to third order polynomial fitting functions. In this preliminary study of correlation functions, we estimated first the isotropic correlation $R(k)$, which is function of the space lag k, not depending from the direction:

$$R(k) = \frac{\sum_{i=1}^{n-k} Z(i)Z(i+k)}{\sqrt{\sum_{i=1}^{n-k} Z^2(i)Z^2(i+k)}} \tag{2.5}$$

Then, two-dimensional correlation matrix $R(k, l)$ has been computed, as function of k, space lag perpendicular to the coastline, and l, parallel to the coastline, through the formula:

$$R(k,l) = \frac{\sum Z(i,j)Z(i+k,j+l)}{\sqrt{\sum Z^2(i,j)X^2(i+k,j+l)}} \tag{2.6}$$

The isotropic binned correlation functions for temperature and salinity, calculated for the 4 cruises, are shown in figure 2.8. Three levels were selected, at 1, 5 and 8m as the most representative to describe the variability of the correlation fields at different depth. The area average at each depth has been subtracted from both temperature and salinity fields, since all the polynomial trends tested were capturing too much of the field variability, compromising the correlation estimation. This is reasonable in a small domain like the Emilia Romagna coastal area.
Temperature correlation (fig.2.8a) shows for August a Gaussian shape curve with zero crossing scale reducing with depth, from 25 at 1m, to 18 km at 8m. March correlation presents a Gaussian shape with a zero crossing scale of about 20 km at the surface and at 8m depth, while at 5m, it seems noisy

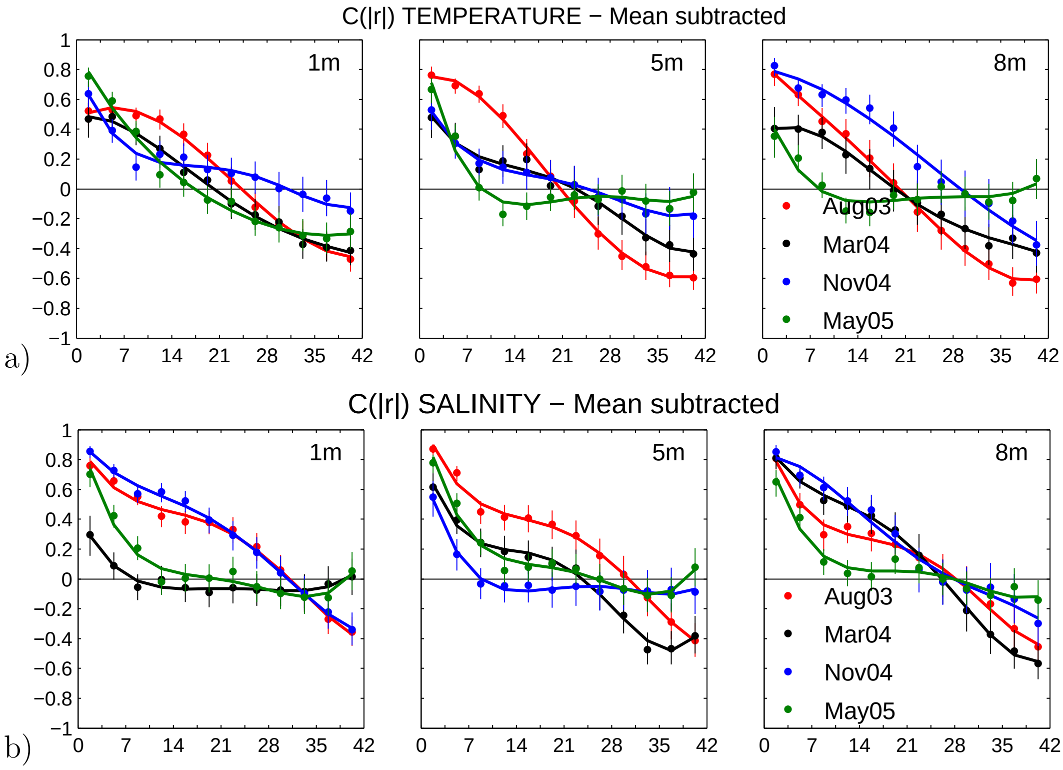

Figure 2.8: a) Temperature and b) salinity isotropic correlation functions calculated at 1m, 5m and 8m depth.

with a little longer correlation length scale. November binned correlation is noisy at 1 and 5m but is smooth at 8m depth, where it exhibits a zero-crossing scale of about 30km, thus longer than August and March ones. May correlation is captured at the surface, while at increasing depth it looks noisy with a second maximum which might indicate that the average subtracted is not enough to detrend the data properly. May's length scale is the shortest one (15km).

In salinity correlations (fig.2.8b) a multiple scale signal emerges, with the only exception of November's one at 8m. At this depth all zero-crossing length scales overlap at 27km. August and November correlations both exhibit at the surface a 30km zero-crossing scale, which is longer than temperature one.

Two dimensional correlation functions for March and May surveys at 3m depth are shown in figures 2.9a and 2.10a. They have been estimated subtracting from each data-set a first order polynomial trend (i.e. first order plane fit in longitude and latitude, see fig.2.9b-c and fig.2.10b-c. The explained variance (ratio between the observed variance and the variance ex-

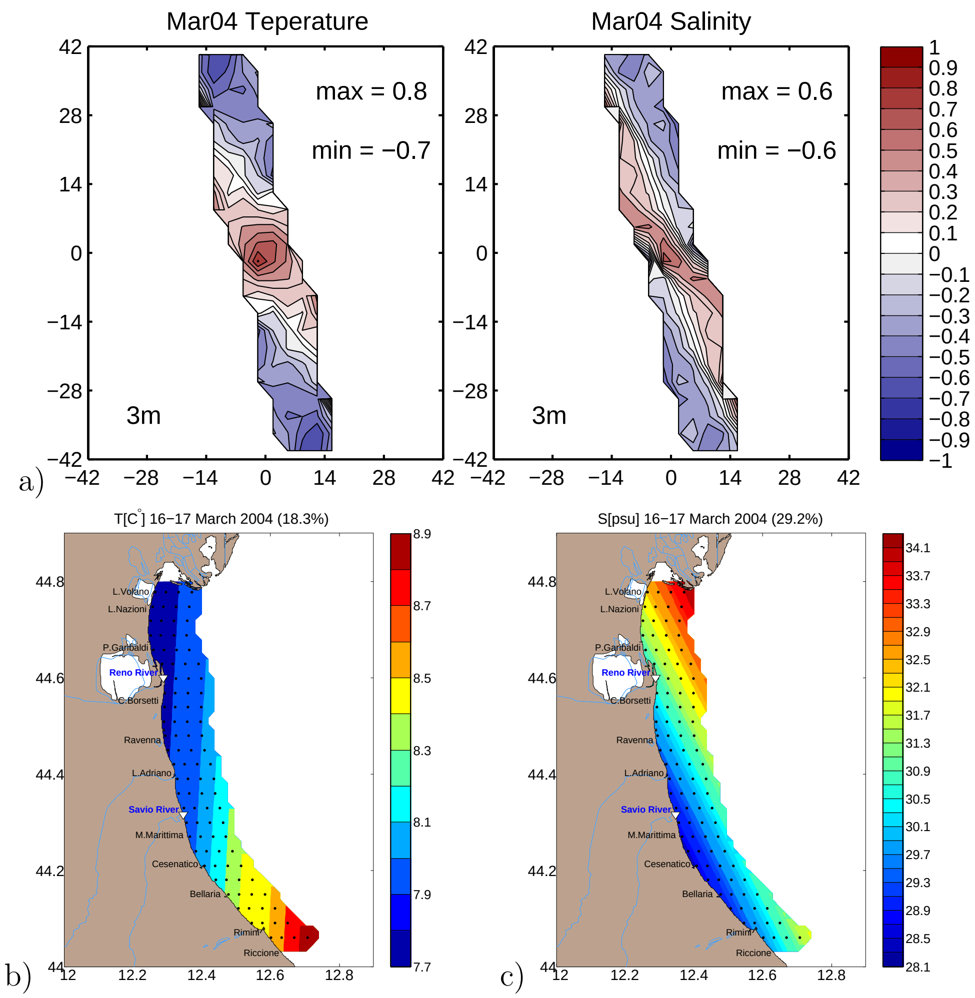

Figure 2.9: a) Temperature and salinity two dimensional correlation functions, calculated from March 2004 survey at 3m depth, subtracting first order polynomial trends surfaces: c) temperature; d) salinity. Trend explained variance (%) is indicated in the plot title.

plained by the linear regression model) has been computed to measure how much of the data signal is captured from the relative trend surface.
March temperature correlation shape is an ellipse with its main axes aligned in the along-shore direction, meaning that the de-trending was not efficient in capturing all the large scale signal, in fact its explained variance is 18.3%. Temperature trend (fig. 2.9b) represents a zonal gradient with increasing temperature from northwestern stations to southeastern ones. Salinity correlation exhibits the same shape but with much longer length scales in the along-shore direction. Salinity trend (fig. 2.9c) presents a gradient in the

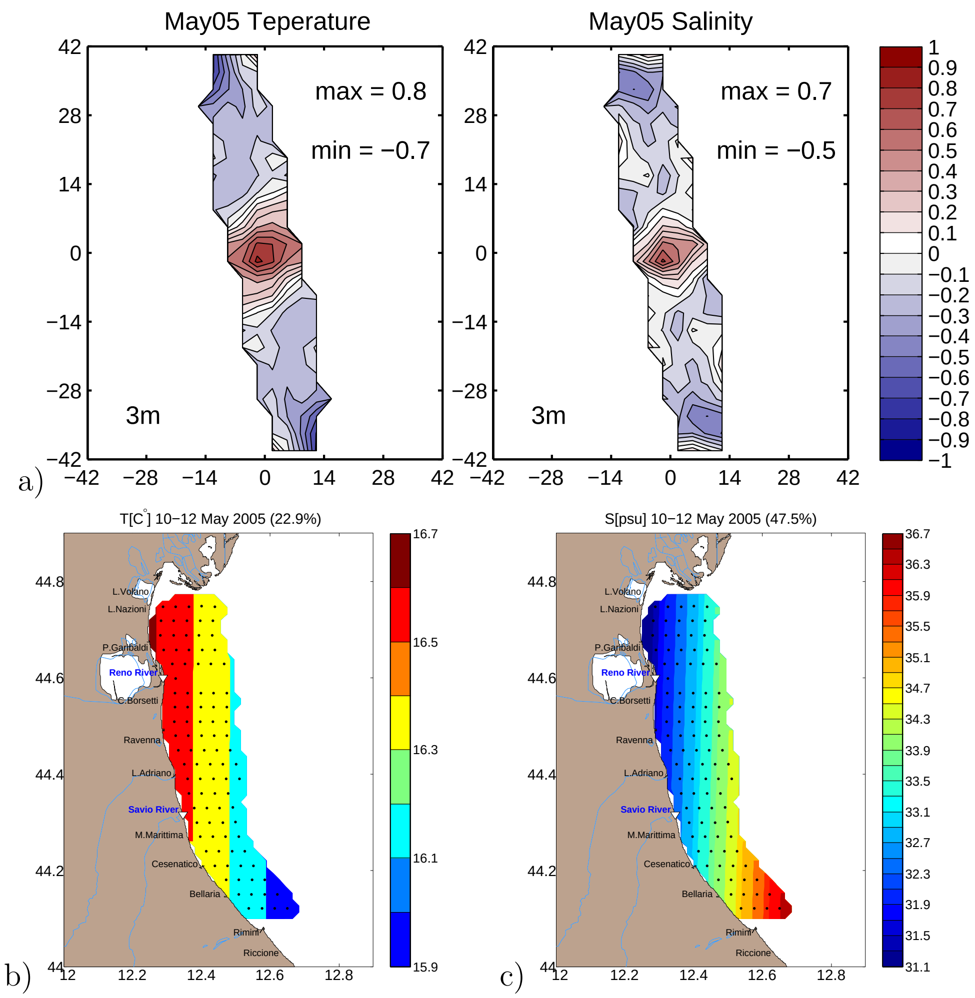

Figure 2.10: a) Temperature and salinity two dimensional correlation functions, calculated from May 2005 survey at 3m depth, subtracting first order polynomial trend surfaces: c) temperature; d) salinity. Trend explained variance (%) is indicated in the plot title.

cross-shore direction with minimum salinity in front of Cesenatico and maximum value in the northwestern area. The explained variance is small and equal to 29.2%. May correlation ellipse (fig.2.10a) is rotated with its main axes in the cross-shore direction. The ellipse keeps the same orientation but slightly reduces with depth, where smaller scale features appear. Temperature trend (fig.2.10b) reproduces again a zonal gradient, but reversed with respect to March case, since maximum temperature values are now in the northwestern area. The explained variance is 22.9%. Salinity correlation field (fig.2.10a) looks quite homogeneous and characterized by smaller scales

than the temperature ones. Salinity correlation is dominated by smaller scales features as depth increases. Salinity trend (fig.2.10c) resembles the temperature one, where minimum salinity values correspond to the highest temperature values indicating a freshwater input warmer than ambient seawater, typical of spring season. In this case de-trending procedure was very efficient, as confirmed by the highest explained variance value(47.5%).
Correlation function analysis proves the difficulty in capturing the signal of the true correlation from observations and in separating it from the large scale trend which might characterize the whole coastal area. Dedicated surveys conducted in different seasons represented effectively different ambient conditions and the consequent range of variability of de-correlation length scales, but the sampling strategy was not successful to fully resolve the true correlation field in the cross-shore direction. The sampling scheme applied in May 2005 was designed with this purpose but it was still not enough.
Let us summarize on general basis our findings. Salinity correlation field looks more anisotropic and characterized by larger space scales than temperature ones. A general tendency is the reduction of correlation scale with depth, as observed also by *Bergamasco et al.* (1996) in the Northern Adriatic and by *Nittis et al.* (1993) but for a much deeper data set in the Ionian Sea. Temperature isotropic correlations display a de-correlation length scale which vary seasonally from a minimum value of about 15 km in May to a maximum value of 30 km in November, but we cannot assert a clear relationship with ambient stratification, as done in *Jeffries and Lee* (2007) for the whole Northern Adriatic sea.
In March and May cases a linear trend was partially efficient in capturing the large scale signal and correlation ellipses appear neat, still affected by anisotropy but not fully resolved. Trend removal was not fully efficient, because in Emilia Romagna coastal area it appears in multiple scales and orientations.
These results do not allow to fit a functional form to the estimated correlation, but they help in the tuning process of analytical correlation parameters.

2.4 Climatological Fields

2.4.1 Temperature

Figure 2.11 presents temperature monthly climatology fields. January shows the coldest temperature of the year with minimum values close to the shoreline. Two maxima are present, one just south the Po River delta and one in front of Cesenatico, where the strong gradient perpendicular to the coast might indicate the presence of a coastal current flowing parallel to it. In February temperature gradient is less intense, with minimum values offshore in the area north of Ravenna and maximum values offshore in the southernmost area. In March an area of high temperature develops between the Po delta and Ravenna, with a general tendency of warmer waters inshore and colder offshore. This warm water pool persists until August. In April the highest temperature zone extends in the northernmost area from the coast to the open sea and off Ravenna there forms another high temperature area. May is characterized by the intensification of the temperature gradient that settles perpendicular to the coast with minimum values close to it, with the exception of the near delta area, where the warm water pool is still present. Minimum temperature values are off P.Garibaldi and south of Riccione. In June the temperature pattern resembles May's one but it is characterized by a weaker gradient, with a minimum of temperature off P.Garibaldi at 20 km from the shore.

The most radical change in temperature distribution comes in July, when the maximum gradient aligns itself with the coast instead of being perpendicular to it, furthermore three well defined areas with distinct temperature are noted: the first is to the north of the Reno River; the second is centered off Ravenna; the third lies south of Cesenatico. This situation persists in August when the three zones become even more well-defined. A low temperature pool off P.Garibaldi emerges again like in February, March, May and June.

A change occurs in September when all the area inshore and north of Cesenatico cools down, with minimum values off the Reno river mouth. Gradient direction turns gradually and sets perpendicular to the coast from October to December, when it reaches its maximum intensity.

Temperature fields show: a clear division into three distinct areas along the coast during summer month (July, August); a homogeneous distribution along the coast during the winter months (December, January) and a subdivision into two areas in spring (March, April) and autumn (September, October).

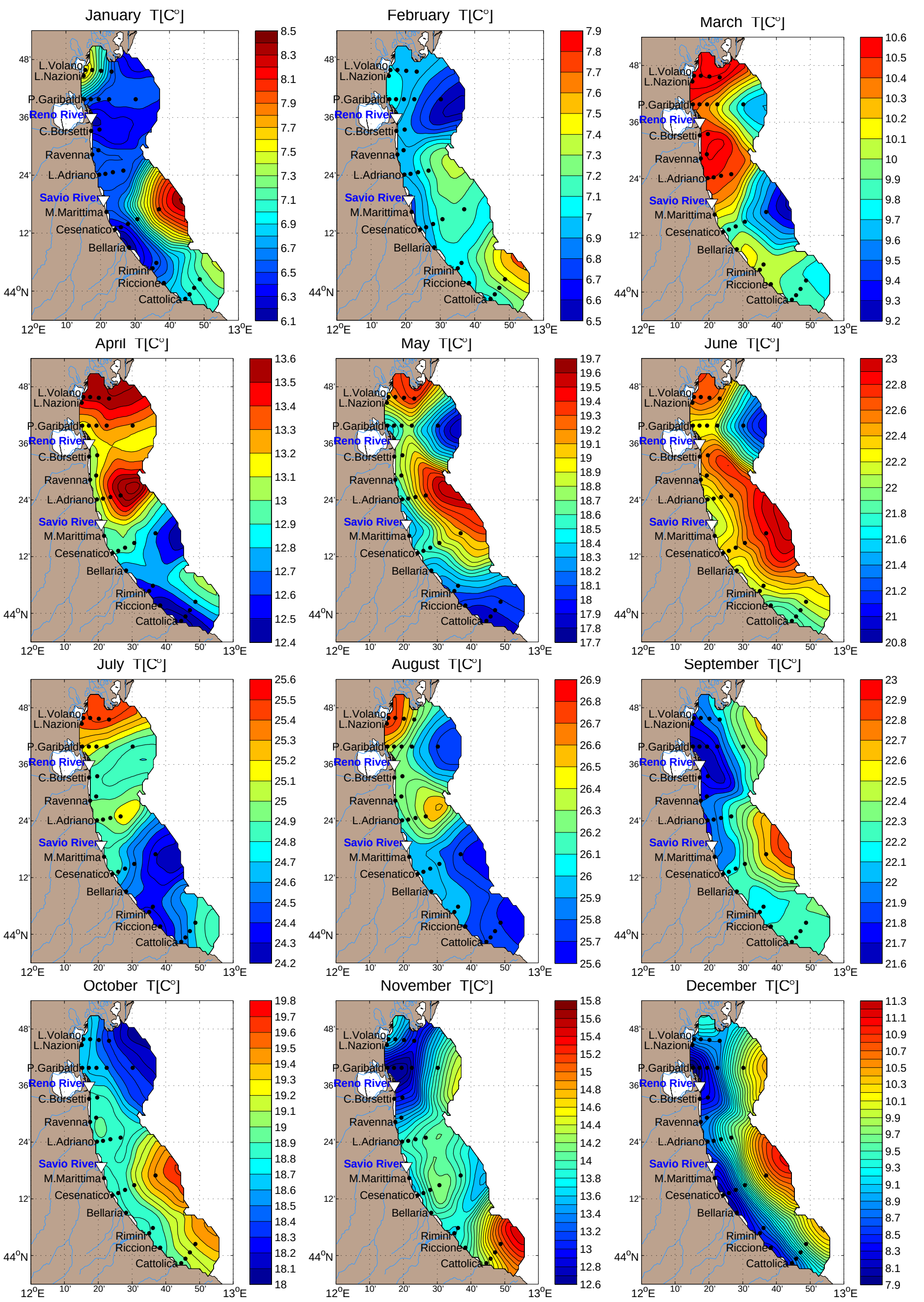

Figure 2.11: Temperature climatological maps (after *Montanari et al.* (2006)). Note that the color index varies with the month.

2.4.2 Salinity

Figure 2.12 presents salinity monthly climatology fields. Surface salinity ranges on average between $26 - 36psu$. A threshold of $31psu$ delineates the switch from blue to red color helping in the identification of the ROFI in blue.
Salinity distribution presents a clear distinction between the northernmost region, under the direct influence of river freshwater, and the southernmost one characterized by saltier water. A transition zone with intermediate salinity characteristics is located between Ravenna and Lido Adriano, where the gradient disposes parallel to the coast all year long. The Po delta area, south of the Goro Lagoon, shows the lowest salinity values, except during winter months, December and January, when a pool of salty water appears, pointing out that river freshwater is not present.
From November to February minimum values of salinity appear off the Reno river outlet and extend down south till Savio river outlet probably due to their combined local freshwater influence. In these months the southernmost area is characterized by a gradient perpendicular to the shore, with saltier water offshore. March, September, October display a similar pattern with a tight gradient aligned to coast in the northernmost area that gradually rotates to settle perpendicular to it in the southernmost area. In March-April and August-September-October, the southernmost area exhibits the highest salinities. In May, when Po River discharge peaks, the whole coastal area is characterized by low salinity with minimum values surrounding the Po River delta. We must stress out that in the northernmost area low salinity values coincide with warm temperature values and vice versa owing to the heating effect of river freshwater at the surface starting in spring (April,May) and lasting for the summertime. From June to September the salinity gradient persists on direction parallel to cast, with a gradual increase of salinity from north to south.
Salinity distributions suggest the coastal strip subdivision into three main zones: the northernmost ROFI; the southernmost zone presenting saltier waters, influenced by open water coming from offshore, with a predominant cross-shore gradient from October to February; a central transition zone with intermediate salinity characteristics, where the gradient keeps on parallel to coast. Two opposing general pattern emerge: in autumn-winter a cross-shore gradient prevails which prevents exchanges between the coast and the open sea, while in spring-summer, an along-shore gradient establishes that isolates the northernmost zone of the coast from the southernmost one. Moreover surface salinity field is characterized in general by larger amplitude gradients than temperature field, as indicated also from correlation function analysis.

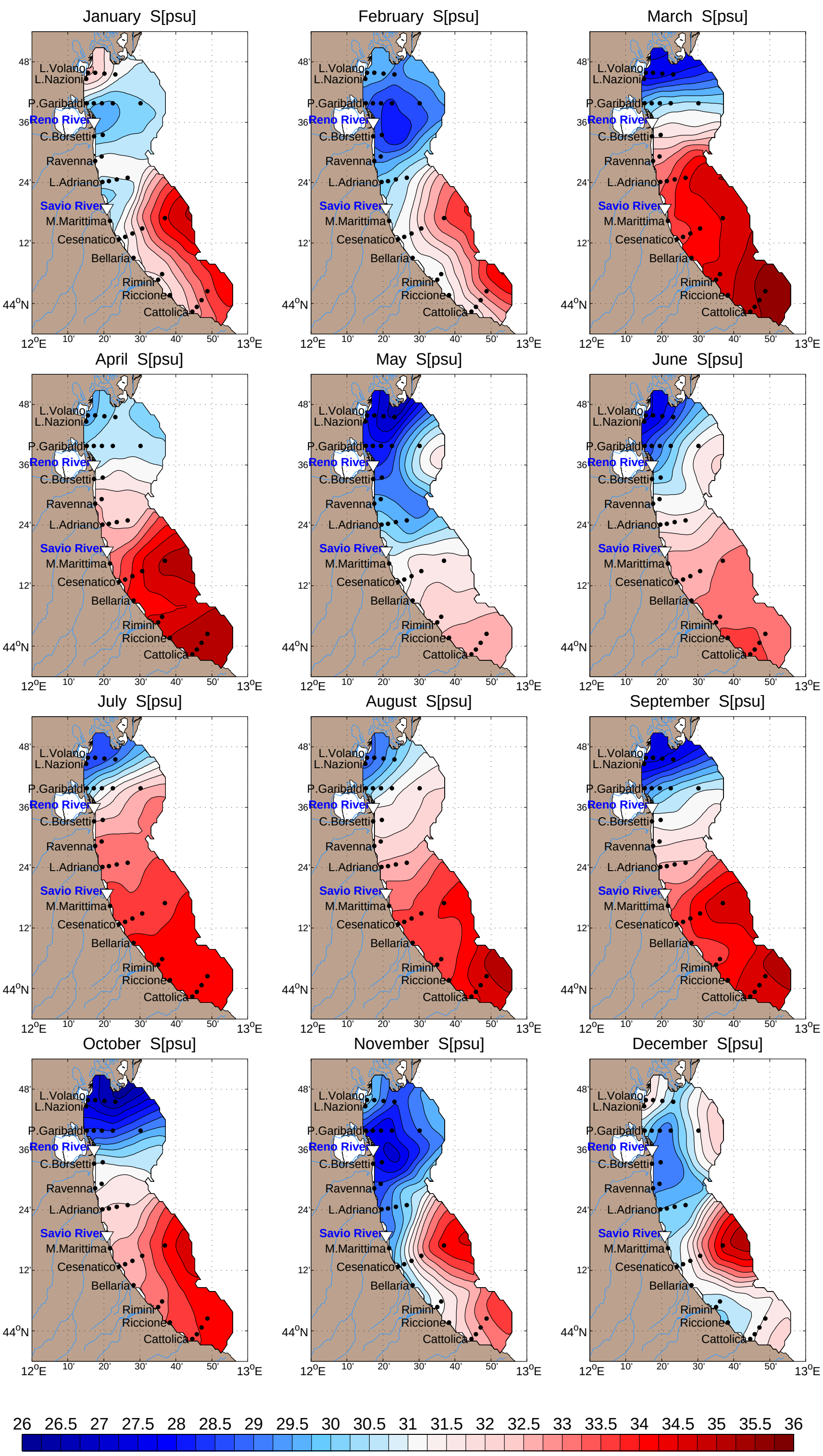

Figure 2.12: Salinity climatological maps (after *Montanari et al.* (2006)).

2.4.3 Current Field

Figure 2.13 presents monthly mean currents derived from geostrophic velocity computation, overlapped to density field. The most important structure emerging for all months, although with different intensity, is a clean separation of circulation systems between the area north and south of Ravenna. In general the circulation in the northernmost area is very variable throughout the year and reverses direction between summer and winter. In the southernmost area the current remains almost unchanged in direction and it generally flows southward.

The circulation north of Ravenna is characterized by a current field directed towards the open sea in November, December, January, February and April which closes up north of Ravenna with currents towards the coast. The two currents connect forming an anticyclonic eddy that we call the Porto Garibaldi anticyclonic eddy, which however is not well resolved by the mapping. This eddy produces a current directed to the shore which in part bifurcates, driving south all along the southern region sustained by a density gradient with lighter water close to the shore and denser water offshore.

Currents flowing towards the coast characterize the northernmost zone in March probably due to the minimum density value surrounding the Po delta. This pattern is more evident from May to October, when very low density values are present north of Reno River mouth. From June to September density is in general very low and exhibits a gradient parallel to the coastline. Currents flow towards the shore in most of the coastal area, with the exception of August, when the main current drives south meandering.

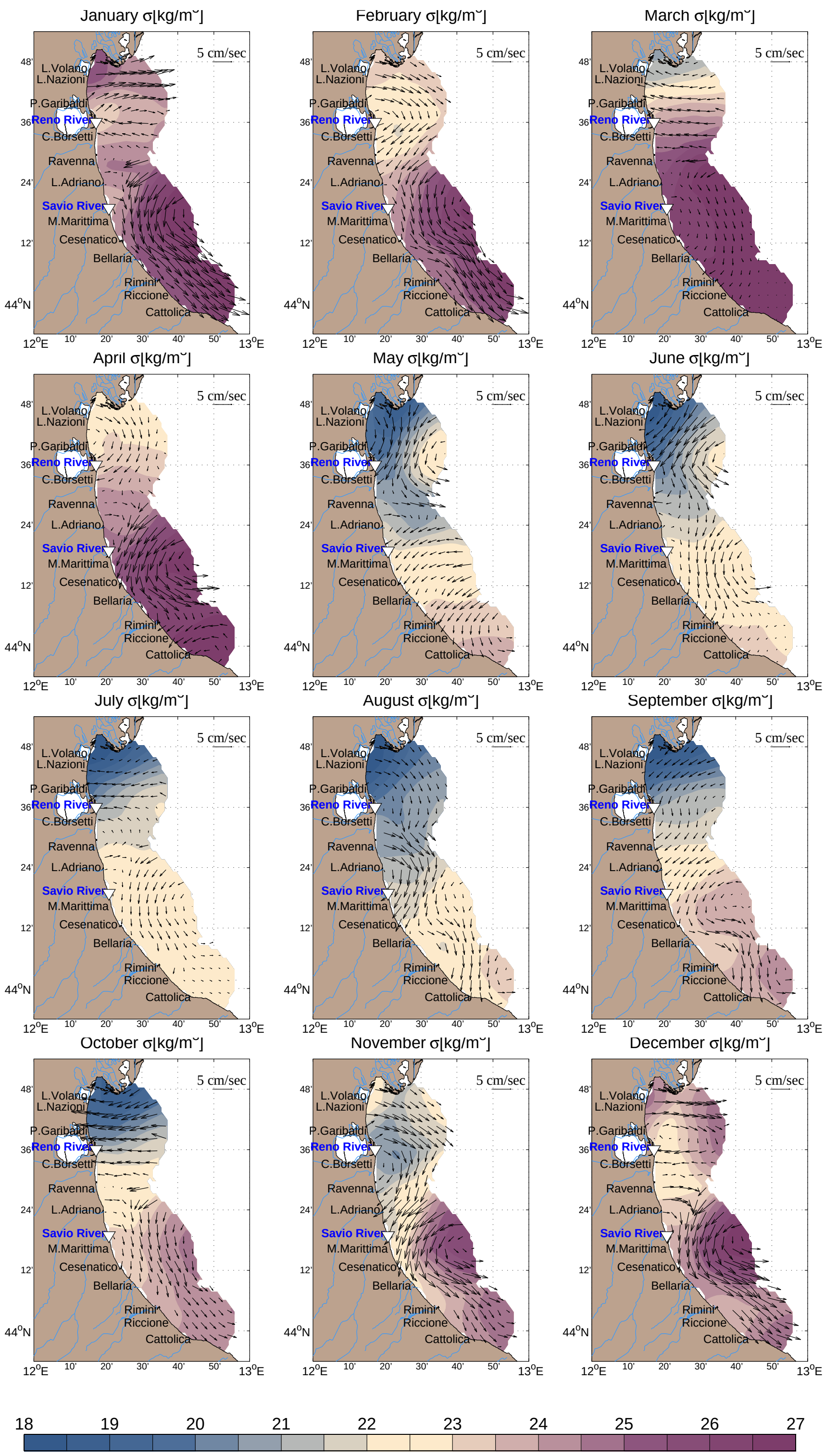

Figure 2.13: Climatological currents and the underlying density fields. (after *Montanari et al.* (2006))

2.5 Discussion

The Emilia Romagna coastal strip is a ROFI area and thus a buoyancy forced coastal system. However, as *Zavatarelli et al.* (2002) and *Zavatarelli and Pinardi* (2003) show, it is also influenced by winds which contribute during winter to form the WACC. On monthly basis, the Emilia Romagna coastal area appears fully stratified (see fig.2.5) implying a predominance, at this time scale, of a buoyancy-inertia balance as dynamical response to the density gradient, that allowed to derive baroclinic velocity field from temperature and salinity climatology.
Area average monthly temperature profiles capture the seasonal cycle modulated by surface heat flux and put on evidence unstable thermal winter conditions compensated in the density field by very low salinity values at the surface. Salinity profiles reveal a typical vertical gradient which lasts during the year with the first 10m layer highly influenced by freshwater input. Low salinity waters dominate the field north of Ravenna and the whole coastal strip up to the depth of 10 meters. Past this bathymetry waters of great salinity are present, which most probably come from the mixing of saltier Modified Levantine Intermediate Waters (MLIW), entering the Adriatic from the Mediterranean, with local waters.
Salinity stratification assists the onset of thermal stratification from May to September enhancing the offshore spreading of low salinity water above the thermocline. The onset of thermal stratification during spring and summer months inhibits vertical mixing process, already reduced by a concomitant weaker wind regime (fig.2.2a).
Figure 2.14 presents the subdivision Emilia Romagna coastal area into 3 zones and reproduces its surface climatological circulation scheme. The coastal strip is characterized by three areas:

- zone A north of Reno River outlet;
- zone B centered around Ravenna;
- zone C south of L. Adriano.

In general surface circulation of the Emilia Romagna coastal zone is characterized by an anti-cyclonic eddy (A1) in the zone A and by a southward current mainly aligned with the coast in the zone C. In zone B the circulation is weak or directed towards the coast particularly during the summer months.
Porto Garibaldi anti-cyclonic eddy (A1) is variable in time but particularly persistent in the summer months when it traps relatively fresh waters originating from the Po delta and presents a relative temperature maximum.

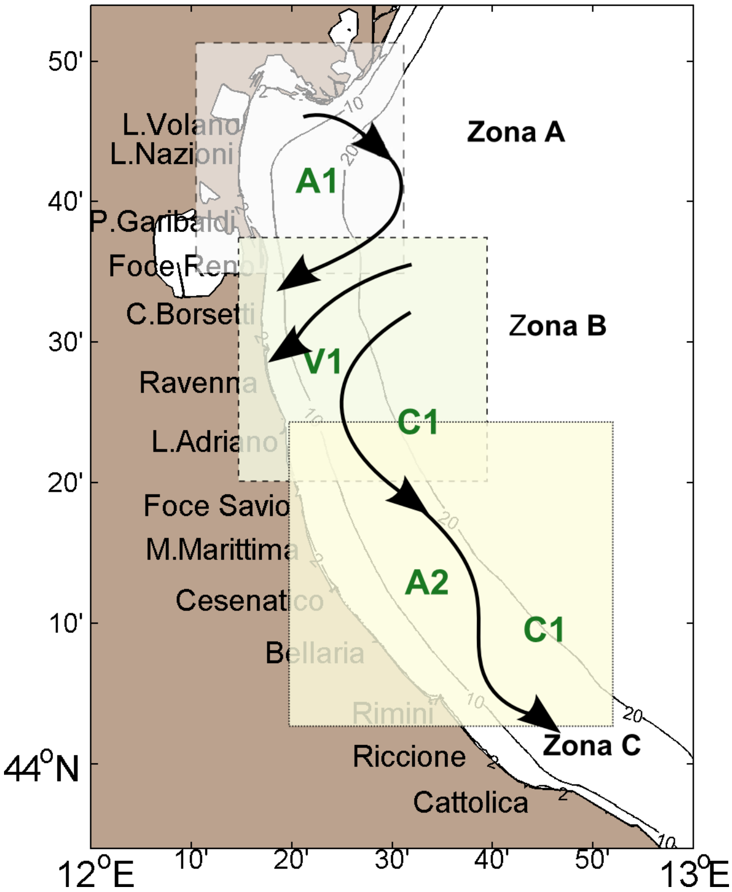

Figure 2.14: Schematic of the climatological coastal circulation (from *Montanari et al.* (2006)).

Both these conditions may favor eutrophication processes and consequent anoxic conditions. In April, May, August, November, and December the eddy is well developed and lies against the coast. The proximity of the eddy to the coast leaves evident only its eastern side attached to a meandering current heading south.

Zone C is characterized by a southward current which is a segment of the WACC persisting all year round, reaching its maximum intensity between November and January. This current segment is disconnected from the circulation north of Ravenna except in the months of February, June, September, November, when it seems to form a single meander positioned between the 10m and 20m bathymetric, which might prevent the coastal strip from exchanges with the open sea. WACC meandering gives origin to two cyclonic areas, the first off L.Adriano (C1), the second off Rimini (C2), and one anti-

cyclonic area centered between Cesenatico and Bellaria (A2). Wave length of the meander is approximately 40 km that is in good agreement with our estimation of correlation function and thus the de-correlation length scale set up for OA mapping technique. As the bathymetry does not present similar features it is supposed that the meander is due to the current instability.
There are months when the WACC is very weak (March, July), whilst the component perpendicular to coast is strong (May, July, August, September). This circulation is indicative of downwelling dynamics along the coast typical of Emilia Romagna's wind regime. Downwelling favorable north-easterly (Bora) wind induces in fact water accumulation phenomena towards the coast and successive movement of bottom water towards the open sea.
Downwelling phenomena may interest particularly zone B where currents heading towards the shoreline dominate. This region is a transitional area between the anti-cyclonic system prevalent to the north and and the intensified coastal current to the south. The hypothesis that emerges from the analysis of these distributions is that A1 eddy is able to create different hydrodynamic conditions depending from its proximity to the coast.
Emilia Romagna hydrodynamics on monthly climatological basis is in good accordance with climatological simulations of the Northern Adriatic circulation of *Zavatarelli and Pinardi* (2003) that pioneered a separated anti-cyclonic dynamics in zone A, a current heading towards the coast in zone B, which bifurcates driving south in zone C. Geostrophic currents confirms WACC intensification during winter and WACC weakening during summertime.
The subdivision of Emilia Romagna ROFI into three main zones can be explained as:

- zone A being the lee of Po River Delta directly influenced by the discharge plume;
- zone B being the re-attachment area of the discharge plume;
- zone C being the region where the plume adjust geostrophically to form the WACC.

On monthly basis Emilia Romagna coastal area may be considered a low mixing environment, since intense wind events (Bora and Scirocco) act on much smaller time scales, of the order of 1 to 5 days. In such environment the coastal current takes the form of a buoyant wedge that rests against the coast as shown in figure 2.15 from vertical sections of temperature and salinity climatologies along the transect off Cesenatico in January. During this month Bora wind is close to its maximum intensity bringing about

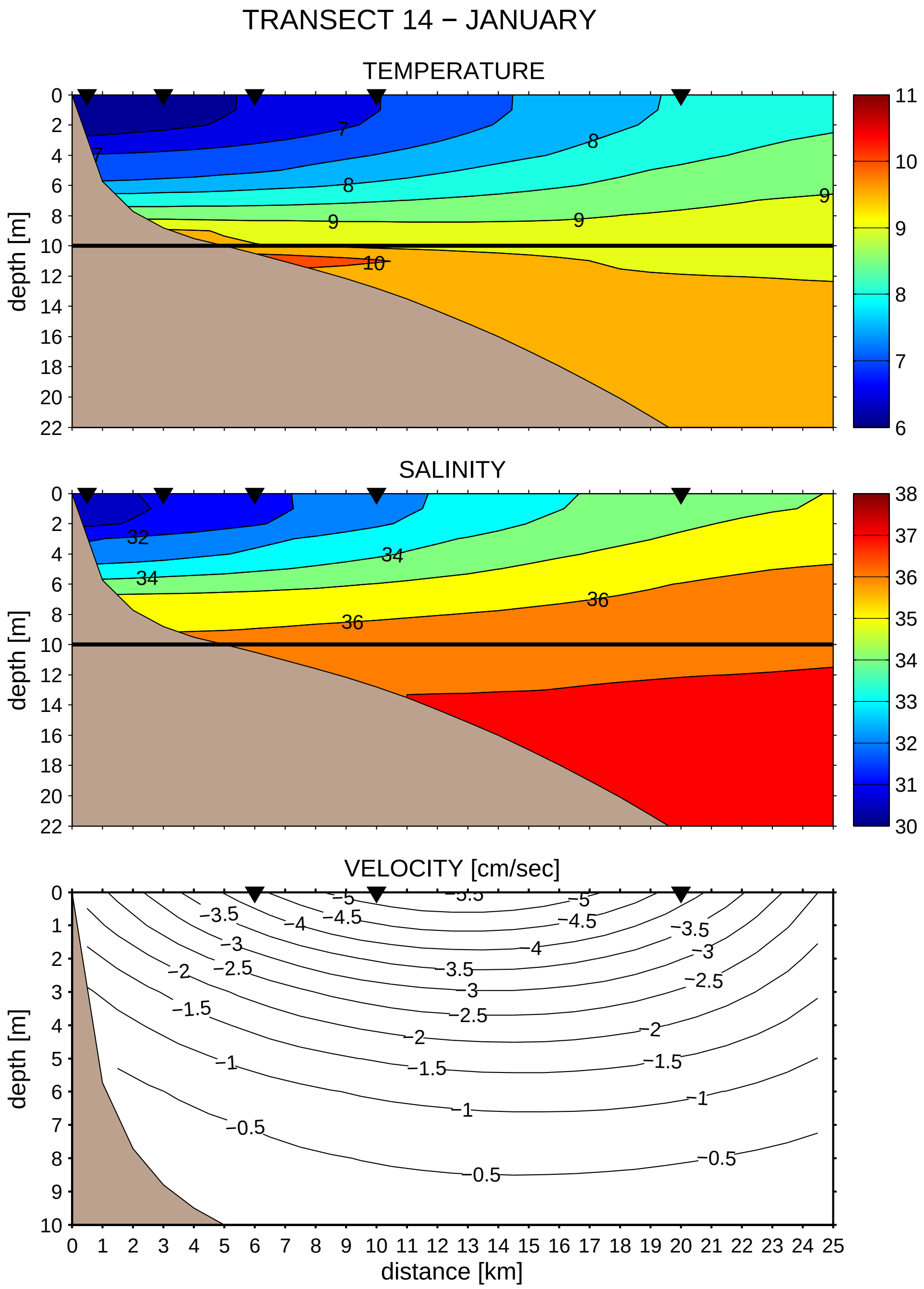

Figure 2.15: Vertical section of temperature (top), salinity (middle) and meridional component of geostrophic velocity along the transect off Cesenatico (bottom).

downwelling events that keep the current against the coast maintaining its alongshore integrity. Downwelling conditions are confirmed by both temperature and salinity isolines that clearly curve downward moving inshore. Meridional component of geostrophic velocity (fig.2.15, bottom panel) under these conditions attains in January its maximum speed.
Wedge type coastal current like WACC, during low vertical mixing conditions in summertime, are subject to baroclinic instability and consequent eddy production. Unstable WACC forms a meander which breaks generating cyclonic and anti-cyclonic pairs as we described in figure 2.14. Growing instabilities derive their energy from the available potential energy of the mean flow thus propagate downstream more slowly than the speed of the current itself.

2.6 Conclusions

Climatological data analysis from Emilia Romagna monitoring network allowed to estimate a monthly climatology of basic hydrodynamic parameters like temperature and salinity. Preliminary quality control procedure and basic statistical analysis depict the seasonal variability of the water column that indicate a persistent ambient stratification sustained mainly by the direct influence of the Po river waters. Under these circumstances we applied the geostrophic approximation to draw the climatological circulation which characterize the Emilia Romagna coastal area. The isolation of the lee area of Po River delta from the rest of Emilia Romagna coast is perhaps the most novel aspect of our analysis.

Chapter 3

Coastal Modeling in The Northern Adriatic Sea

3.1 Introduction

The objective of this study is the implementation of the Adratic shelf (ASHELF) high resolution numerical model, by using the Princeton Ocean Model (POM, *Blumberg and Mellor* (1987)), in the Northern Adriatic Sea, with a multi nesting approach that allows to bring outer and larger scale informations inside the model domain and gets a more realistic solution. Our intent is to establish a new tool to rapid assess the coastal ocean based on rapid initialization and short forecast. Rapid initialization procedure consists on downscaling interpolation technique of daily mean large scale fields onto the higher resolution grid.
ASHELF horizontal resolution is 800m which has never been adopted before in the Northern Adriatic sea. ASHELF is nested to the operational Adriatic Forecasting System (AFS, *Oddo et al.* (2005), *Guarnieri et al.* (2009)) which provides also the initial condition fields. AFS is nested within a basin scale operational model for the Mediterranean Sea, the Mediterranean Forecasting System (MFS, *Pinardi et al.* (2003), *Tonani et al.* (2008)).
ASHELF set up introduces a high resolution topography and new rivers data as first attempt to increase the realism of the numerical simulation. AFS and ASHELF models are forced by the same atmospheric data provided by European Centre for Medium-Range Weather Forecasts (ECMWF) operational products. Two short term experiments for different seasons will be presented to test ASHELF implementation and the applied nesting procedure. To this purpose we perform an extensive validation with remote and is situ observations for both AFS and ASHELF models, to determine the ability of ASHELF

to perform reliable short term simulation, and assess its performance versus AFS one, considered as the reference level.
Zavatarelli and Pinardi (2003) implemented for the first time a high resolution (1.5 km) model in the Northern Adriatic with a nesting approach but they focused on the study of the climatological circulation of the Adriatic and Northern Adriatic basins. Many other attempt were made in the framework of the MFSTEP, (Mediterranean Forecasting System: Towards Environmental Predictions) Project, to establish high resolution sub-basin prediction models nested within a basin scale prediction system (*Kourafalou and Tsiaras* (2007), *Natale et al.* (2006), *Gaberšek et al.* (2007), *Estournel et al.* (2009)) but none of these presented extensive model validation.
In *Section 2* is described in detail the ASHELF model implementation. *Section 3* presents the satellite and in situ data sets used for ASHELF and AFS model validation. *Section 4* introduces the validation analysis, while *Section 5* discusses the validation results. In *Section 5* we summarize our outcomes and make conclusions.

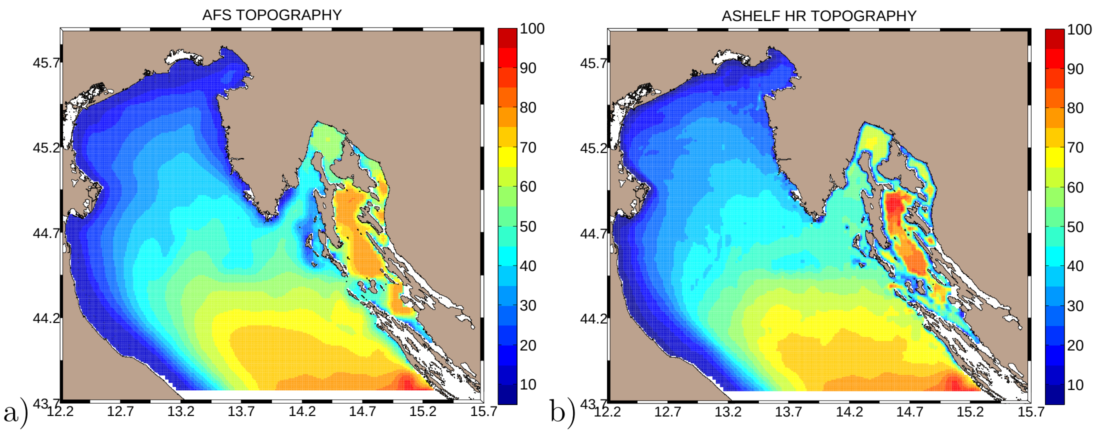

Figure 3.1: a) AFS topography interpolated on ASHELF grid; b) ASHELF high resolution topography

3.2 The Adriatic Shelf Model

ASHELF is a free surface, primitive equation model with hydrostatic and Boussinesq approximations, based on the Princeton Ocean Model (POM) code (*Blumberg and Mellor*, 1987). Horizontal eddy viscosity and diffusion vary in space and time. Eddy viscosity is provided by Smagorinsky parameterization (*Smagorinsky*, 1993) based on the local derivatives of the velocity field and the local grid size.Diffusivity is defined using the Prandtl number,

which is set equal to 0.1. The vertical mixing coefficients for momentum and tracers are calculated using the 2.5 Mellor and Yamada (*Mellor and Yamada*, 1982) turbulence closure scheme.
ASHELF is part of a nested modeling system, shown in figure 1.1, that comprehends the Mediterranean Forecasting System (MSF, *Pinardi et al.* (2003), *Tonani et al.* (2008)), at 6.5 km of horizontal resolution, and the Adriatic Forecasting System (AFS *Oddo et al.* (2006), *Guarnieri et al.* (2009)). AFS horizontal resolution is about 2.2 km and the vertical grid is made up of 31 double logarithmic σ layers. MFS is based on OPA code (*Estubier and M.Levy*, 2000) and it constitutes the modeling system in the outer domain, giving boundary conditions to AFS at its open boundary, located along the 39° parallel, in the Ionian Sea.
ASHELF domain covers the Northern Adriatic basin (fig. 3.1) with a horizontal resolution of 800 meters, which is the highest resolution ever applied in this domain, and a vertical discretization of 31 σ layers.
ASHELF and AFS use the same Monotonic Upstream centered Scheme for Conservation Laws (MUSCL) for tracers advection (*Estubier and M.Levy*, 2000) in order to give a more realistic representation of horizontal and vertical gradients. Up-stream advection scheme, as in *Oddo et al.* (2009), has been applied close to the lateral open boundary to increase diffusivity avoiding numerical instabilities.
ASHELF and AFS models characteristics are summarized in table 3.1 .

	ASHELF	AFS
Model	POM	POM
Horiz Resolution	0.8 km	2.2 km
Vert Resolution	31σ layers	31σ layers
Bathymetry	0.5 km res	DBDB1 1min res
Min depth	5m	10m
Po River	Daily Runoff and Temp.	Daily Runoff
Reno River	Daily Runoff	Monthly Runoff
Italian Rivers Runoff	*Raicich* (1994) Climatology	*Raicich* (1994) Climatology
Croatian Rivers Runoff	*Pasaric* (2004) Climatology	*Raicich* (1994) Climatology
Atmospheric Forcing	ECMWF (0.5°, 6 HR)	ECMWF (0.5°, 6 HR)
Lateral Open Boundary	from AFS	from MFS

Table 3.1: ASHELF and AFS sets up.

3.2.1 Topography

ASHELF uses a new high resolution topography (Richard Signell personal communication from ADRIA03 field experiment in the Northern-Central Adriatic, *Signell* (2003)) which has been blended with AFS topography at the lateral open boundary for about 30 km inside the domain (see fig.3.2). AFS minimum depth is set to 10m and the bottom has been flattened in shallower coastal areas, in order to preserve a realistic coastline. ASHELF minimum depth has been reduced to 5m to improve the realism of model results in near coastal areas. In figure 3.1 AFS topography interpolated on ASHELF grid (a) and ASHELF high resolution grid (b) are shown. The new high resolution topography is much more detailed and considerable different inside the Gulf of Trieste and between the Croatian Islands.
The lateral open boundary location, along the 43.7° parallel, was carefully chosen to minimize bathymetric discrepancies between the two models and to avoid big slopes that could create numerical instabilities in the boundary conditions. The coupling procedure between ASHELF and AFS took into account bathymetry blending in a layer 30km wide from the open boundary. AFS topography has been interpolated into the ASHELF grid and imposed on the first 14 longitudinal grid sections from the open boundary, while from the 15th to the 33rd section, a linear blending has been applied as function of the distance from the boundary.
Figure 3.2 shows the topography merging result that smoothed out small scale features from the high resolution topography to prevent spurious signals in model output. ASHELF land sea mask inside this boundary layer is maintained equal to AFS to avoid lateral extrapolation requirements during initialization and lateral nesting.

3.2.2 Nesting and Open Boundary Conditions

ASHELF is nested to AFS using the one-way off-line nesting approach. AFS provides to ASHELF daily mean fields of temperature, salinity, velocity and surface elevation that are linearly interpolated on the lateral open boundary. Interpolation in time assure a time evolving transfer of information. This nested approach has been first implemented by *Zavatarelli and Pinardi* (2003) to study the climatological circulation of the Adriatic and Northern Adriatic seas.
Open boundary condition for the normal component of the barotropic velocity uses the *Oddo and Pinardi* (2008) formulation of the Flather boundary

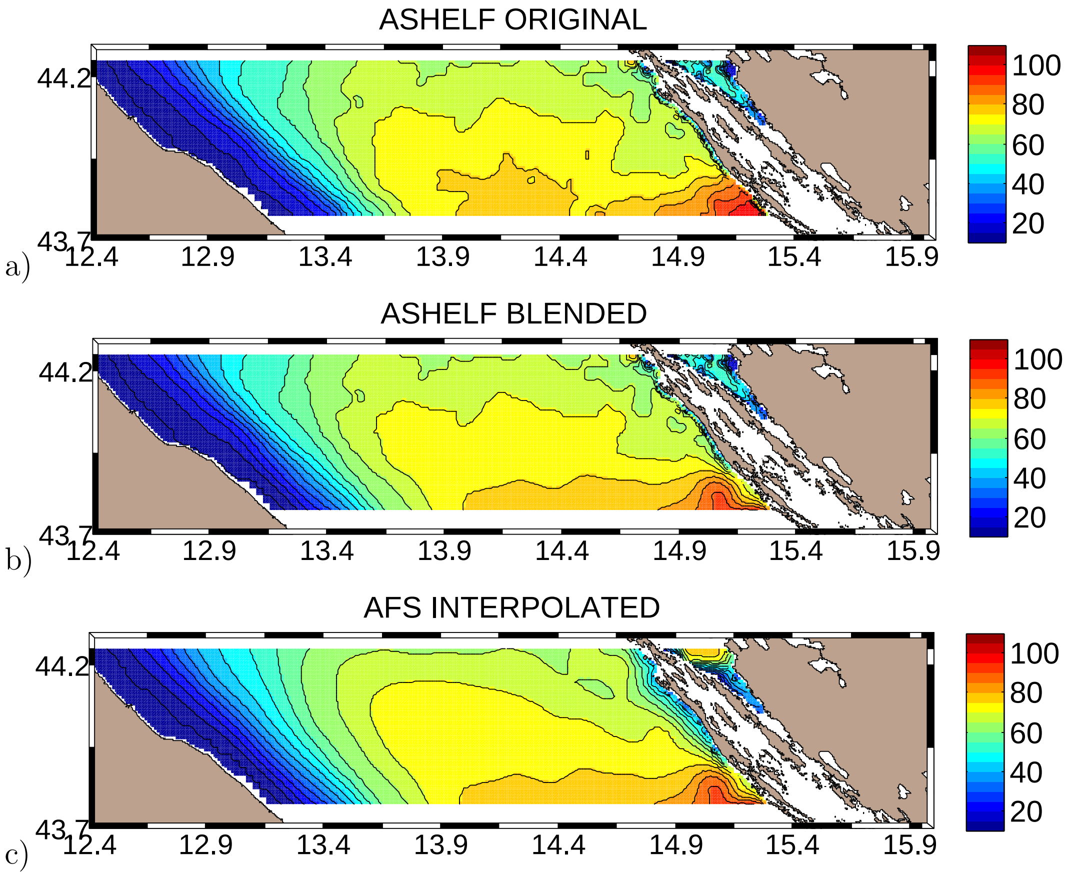

Figure 3.2: a) ASHELF original topography; b) blended ASHELF new topography; c) AFS topography interpolated on ASHELF grid.

condition (*Flather*, 1976):

$$V_{ASHELF} = V_{AFS} - \frac{\sqrt{gH}}{H}(\eta_{AFS} - \eta_{ASHELF}) \tag{3.1}$$

where V_{ASHELF} and V_{AFS} are respectively ASHELF and AFS meridional components of barotropic velocity, normal to the boundary, H is the bathymetry, which is identical for both models, g is the gravity, and $\eta_{ASHELF}, \eta_{AFS}$ are models surface elevation. The AFS velocity is imposed for the zonal component of the barotropic velocity tangential to the open boundary.
An advective condition is applied to active tracers (θ) temperature and salinity:

$$\frac{\partial\theta}{\partial t} + V_n\frac{\partial\theta}{\partial n} = 0 \tag{3.2}$$

R	Tolle	Pila	Maistra	Gnocca	Goro
1000	12.6	56.5	4.5	16.3	10.2
3000	15.7	54.9	3.9	18.6	11.3
4000	13.0	52.7	4.2	17.9	12.2
6000	12.5	52.9	5.0	17.9	12.0

Table 3.2: Po River runoff repartition percentages between its main delta arms as function of the total discharge in m^3/sec at Pontelagoscuro station.

If the velocity at the boundary is positive, tracers are advected out of the domain, otherwise the external data are advected inward at inflow boundary points.
A southern radiation boundary condition, according to Orlanski (*Orlanski*, 1976), is applied to the meridional component of total velocity, normal to the boundary:

$$\frac{\partial \phi}{\partial t} + C\frac{\partial \phi}{\partial y} = 0 \qquad , \qquad C = -\frac{\partial \phi}{\partial t}\Big(\frac{\partial \phi}{\partial y}\Big)^{-1} \tag{3.3}$$

where C is computed using an implicit numerical scheme:

$$C = \frac{\phi^{n-1}_{i,j-1} - \phi^{n+1}_{i,j-1}}{\phi^{n+1}_{i,j-1} + \phi^{n-1}_{i,j-1} - 2\phi^{n}_{i,j-2}} \tag{3.4}$$

The numerical stability requirements are that:

$$C = \begin{cases} 0 & C < 0 \\ C & 0 \leq C \leq \frac{\Delta y}{\Delta t} \\ \frac{\Delta y}{\Delta t} & C > \frac{\Delta y}{\Delta t} \end{cases}$$

The free surface elevation is not nested and a zero-gradient boundary condition is applied.

3.2.3 River Runoff

River discharge data considered in ASHELF has been extracted from different climatological data sets described in detail in appendix A. This is a major difference with AFS and it will be discussed in some detail. Mean daily outflow observed data have been included for Po and Reno Rivers.
The daily discharge has been divided between its main delta arms (Po di Tolle, Po di Pila, Po di Maistra, Po di Gnocca, Po di Goro) in different percentages, listed in table 3.2, that depend on the total runoff.

Figure 3.3a shows the daily Po River outflow for 2003 and the monthly climatology estimated for the time period 1995-2002 (the values have been inserted in table A.1). Maximum river discharge usually occurs in January, May and between October and November. The whole year 2003 is characterized by very low Po River runoff due to the extraordinary dryness and the high temperatures conditions recorded.
The Reno River daily outflow data were also available for 2003 during the periods of our simulations, and its time series is displayed in figure 3.3b, overlapped by the relative *Raicich* (1994) climatology which is used in AFS model. Reno daily runoff observations are in good accordance with *Raicich* (1994) climatology for 2003, especially during summertime.
ASHELF uses the complete fresh water flux parameterization, the vertical velocity w is written as

$$w|_{z=\eta} = E - P - \frac{R}{A} \tag{3.5}$$

where E is the evaporation rate in m/s, P is the precipitation rate in m/s and R is the river volume discharge in m^3/s, which is a non zero value only at the corresponding river mouth location on the model grid, divided by A, the area of the horizontal grid cell. This vertical velocity controls the salinity balance too. Salinity of precipitation and water vapor is assumed to be nil while it is set to S_{river} for rivers, parameterizing mixing and other processes (like resuspension) that are not explicitly resolved by our model implementation. There is no salt flux through the air-sea interface so the turbulent salt flux must exactly cancel out the advective salt flux:

$$\left(K_H \frac{\partial S}{\partial z}\right)\Bigg|_{z=\eta} = (E-P)S_{surf} - \left(\frac{R}{A}\right)(S_{surf} - S_{river}) \tag{3.6}$$

where K_H is the vertical turbulent diffusion coefficient and S_{surf} is the salinity at the sea surface and S_{river} is the river water salinity that has been set to $15psu$. The total salt is conserved and the local salinity change is due to freshwater dilution and concentration.
Po River Temperature data have been collected at Canavella station located just before the river delta. Figure 3.3 shows Po river temperature data versus surface temperature sampled at station 1002 of Emilia Romagna monitoring network, where it is evident the faster warming of Po river during spring time and its faster cooling during fall time. ASHELF model takes into account Po river temperature effects to the introduction of a new term into the heat flux boundary condition at the Po river delta outlets:

$$\rho_0 C_p \left(K_H \frac{\partial T}{\partial z} \right) \bigg|_{z=\eta} = Q + \frac{dQ}{dT} \bigg|_{T=T_{surf}} (T_{surf} - T_{river}) \tag{3.7}$$

The first term on the right-hand side of 3.7 represents the net heat flux at the sea surface and the second term the correction factor accounting for Po River temperature, where T_{surf} is the model surface temperature, T_{river} is Po river daily mean temperature and $dQ/dT = 47.3 \quad W/m^2C^\circ$ is the relaxation coefficient. This correction term is a non-zero value only at the Po river outlet grid points. The relaxation factor is:

$$\frac{dQ/dT}{\rho_0 C_p} = \frac{\Delta z}{\Delta \tau} \qquad\qquad \Delta\tau = \Delta z \frac{\rho_0 C_p}{dQ/dT} \tag{3.8}$$

and it corresponds to heat flux relaxation time $\Delta\tau$ of 1 day considering a surface layer thickness (Δz) of 1m.

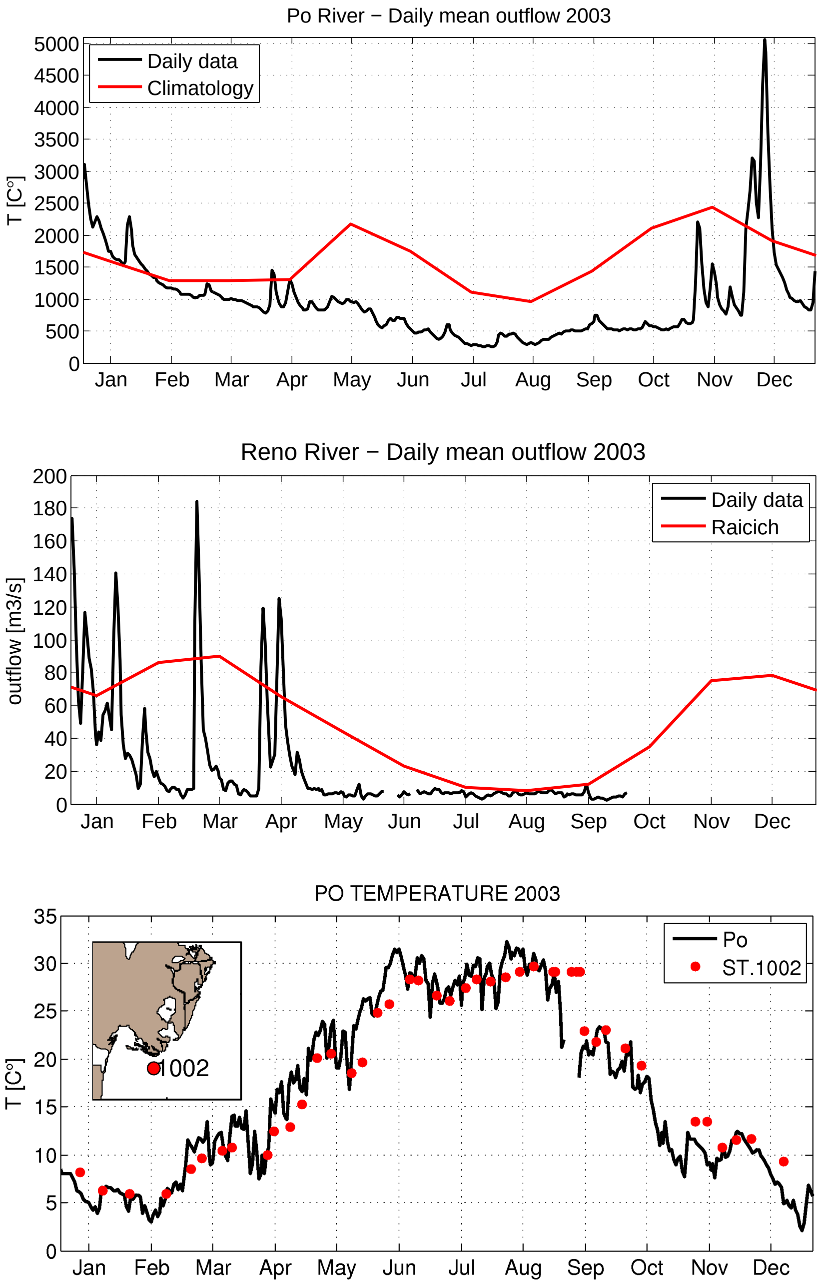

a)

b)

c)

Figure 3.3: a) Po River daily mean outflow for the year 2003 and monthly climatology calculated for the years 1995-2002. b) Reno River daily outflow for 2003 and Raicich monthly climatology. c) Po River daily temperature sampled at Canavella station and temperature sampled at station 1002 of Emilia Romagna coastal monitoring network, located just south the Po delta.

3.2.4 Simulation Experiments

Two model simulations of 70 days will be presented for spring and summer 2003. The first simulation starts on March 4th and the second starts on July 28th. These two periods have been chosen for the large number of measurements available allowing an extensively validation of ASHELF performances.

3.2.5 Atmospheric Forcing

ASHELF and AFS models are forced by the same atmospheric data obtained using bulk formulae and the ECMWF products, which provides data every 6 hours at a space resolution of 0.5°. Air temperature, dew point temperature, mean sea level pressure, cloud cover and wind speed are the variables considered. Precipitation data have been extracted from *Legates and Willmott* (1990) global monthly climatology having a 0.5° horizontal resolution.
In both models surface boundary conditions are computed through standard bulk formulae parameterization (*Castellari et al.*, 1998). Surface fluxes computation of heat-salt and momentum is carried out interactively every time step from atmospheric data and model predicted sea surface temperature (SST) (*Oddo et al.*, 2006).
Figure 3.4 shows the time series of air temperature and wind, averaged over ASHELF domain, during the simulation time periods. In March air temperature oscillates around $10C^{\circ}$ until the second week of April when it starts to raise reaching on average $20C^{\circ}$ in the first week of May. In March northeasterly Bora winds predominate while from April south-southeasterly wind altarnate to Bora events.
During summer simulation, air temperature keeps quite constant and it oscillates around $27 - 28C^{\circ}$. An abrupt cooling event occurs at the beginning of September when temperature drops and subsequently stabilizes around $20C^{\circ}$. Bora events predominate even during summertime when usually Scirocco wind does. One intense Scirocco episode took place at the end of August, preceding air temperature drop. Scirocco became more frequent from the second half of September.

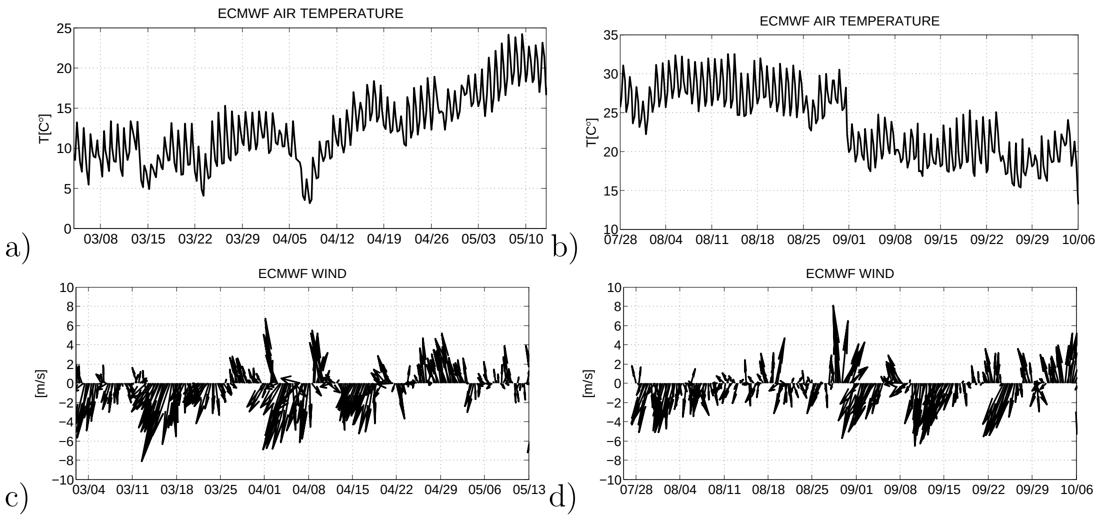

Figure 3.4: Air temperature time series from ECMWF analyses averaged on ASHELF domain: a) during the Spring Experiment; b) during the Summer Experiment. Wind time series from ECMWF analyses averaged on ASHELF domain: c) during the Spring experiment; d) during the Summer Experiment.

3.2.6 Initial Conditions

ASHELF has been rapidly initialized by a simple interpolation technique of AFS large scale fields. AFS daily mean fields of temperature, salinity and velocity have been first vertically interpolated from the AFS 31 vertical σ levels to 75 flat levels in order to preserve the vertical water column structure, since the implementation of a high resolution topography in ASHELF model created a displacement of the σ layers, even maintaining the same vertical discretization.
Constant vertical extrapolation is applied at the surface, where the first σ layer is brought at the surface.
Moreover the new topography made necessary to extrapolate values in those areas where the bottom depth is deeper than AFS grid. A threshold depth for extrapolation procedure equal to 20 meters has been defined under stratification conditions, so missing values shallower than 20 meters have been generated from AFS through a horizontal extrapolation technique that iteratively enlarges the field horizontally, averaging the available sea values while a constant vertical extrapolation has been applied for grid points deeper than 20 meters. This procedure assures to generate new bottom values preserving the vertical stratification. The successive step has been the horizontal bilinear interpolation on the finer resolution grid where the mismatch of models

coastlines, due to ASHELF better approximation of real coastline, required the same horizontal extrapolation procedure at the lateral boundaries.
Fields on the ASHELF horizontal grid and on the 75 flat levels have been backward interpolated on the ASHELF 31 σ levels.

3.3 Observations

ASHELF has been validated exploiting an extensive, in situ and remotely sensed, observational data set.

3.3.1 Satellite SST Observations

Satellite sea surface temperature (SST) data at high horizontal resolution have been employed. We exploited the AVHRR data set from NOAA 12, 13, 14, 15, 16 and 17 satellites, collected in the framework of DOLCEVITA Project (Dynamics of Localized Currents and Eddy Variability in the Adriatic, http://thayer.dartmouth.edu/adriatic/) and then elaborated by OGS (Istituto Nazionale di Oceanorafia e di Geofisica Sperimetale in Trieste, Italy). *Notarstefano et al.* (2006) computed SST field mapped on a 1.2 km horizontal resolution grid. The images from satellite nighttime passes are considered to avoid the diurnal warming effects. In particular we selected the closest available image to midnight which corresponds to the daily average centering time of both AFS and ASHELF model outputs. Data with cloud masking have been considered and only maps with more than the 50% of available points inside the model domain have been selected, to get more trustable skill scores. *Gaberšek et al.* (2007) conveys that RMSE calculation between model output and Satellite SST observations results in a much smaller variability if there is at least one third of the total number of pixel available.
SST data have been previously validated for the year 2003 with ADRICOSM in situ CTD observations in the Gulf of Trieste and the Emilia Romagna coastal area and annual average RMSE for 2003 in the Gulf of Trieste is equal to $0.6C^{\circ}$ and $0.8C^{\circ}$ in Emilia Romagna zone. The results of the validation are shown in appendix B.

3.3.2 ADRIA03 Observations

During ADRIA03 Field Trial (*Signell*, 2003) many CTD data were collected during springtime 2003 in the Northern and Central Adriatic Sea. ADRIA03 subsample within ASHELF model domain consists of 182 profiles collected between the 28th of April and the 4th of May. Data distribution map is shown in figure 3.5.

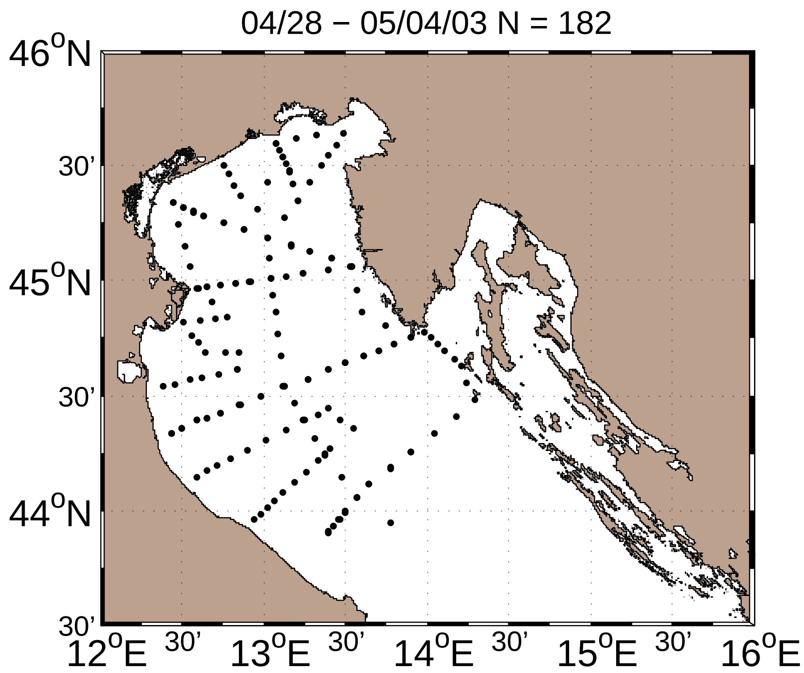

Figure 3.5: CTD data distribution map from ADRIA03 campaign conducted from April 28th to May 4th, 2003.

3.3.3 Coastal Observations

The three observational networks considered here are concentrated in the Emilia-Romagna, Gulf of Trieste and Rovinj coastal strips. CTD profiles of temperature and salinity were collected during the period of ADRICOSM Project. Their sampling array is displayed in figure 3.6, while the CTD collecting days during the two simulation time period are listed in table 3.3 for the spring experiment and in table 3.4 for the summer experiment.
Emilia-Romagna coastal monitoring network (fig.3.6a) is made up of 30 stations situated along many transects perpendicular to the coastline at distances of 500 m, 3, 6 or 10 km from the shoreline. Sampling activity occurs on weekly basis in two consecutive days. Emilia Romagna coastal area is sandy, shallow and gently sloping so the deepest stations reach 15 meters depth.

In the Gulf of Trieste bi-weekly (October 2002 - March 2003) and weekly (April - September 2003) cruises (*Celio et al.*, 2006) were performed over the sampling grid of 19 stations (fig.3.6b) providing an adequate spatial and temporal coverage of the area during one day cruise. The Gulf of Trieste is a semi-enclosed basin of about 30 km diameter with a complex topography. Its main NE-SW axis divides a deeper pool (maximum depths is 26m) in the southern-central part from a slope which characterizes the northern area influenced by the Isonzo River estuary.
The Rovinj coastal network is made up of 19 stations mainly arranged on three transects perpendicular to the coast (fig.3.6c). Here the sea bottom reaches few kilometers off the coast (44m).

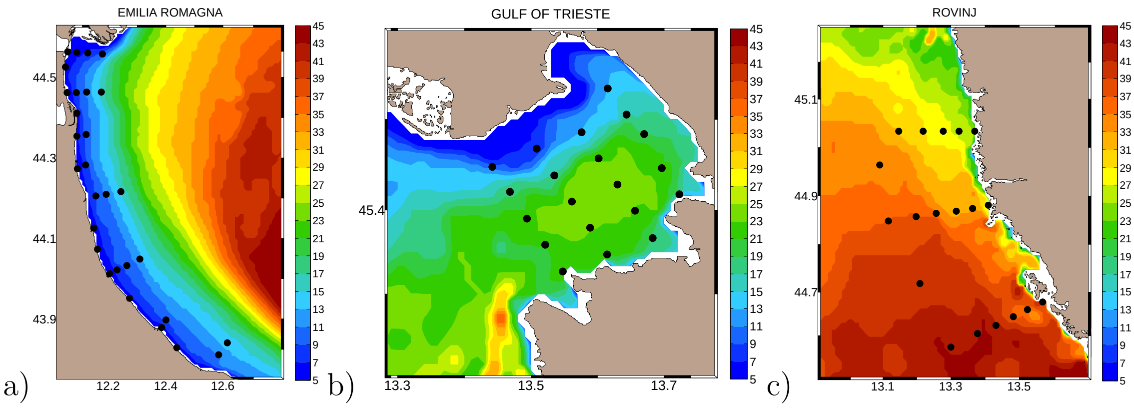

Figure 3.6: Coastal monitoring networks in the Northern Adriatic sea considered for ASHELF validation: a) Emilia Romagna; b) Gulf of Trieste; c) Rovinj.

3.4 Model Validation

Model simulations have been carried out to test if ASHELF model can perform reliable short term simulations when initialized from AFS daily mean field that also provides boundary conditions. We evaluate model performances through the quantitative comparison with satellite SST and in situ CTD data. Model validation is a necessary step to compare ASHELF and AFS model results, in order to ASHELF being able to reproduce AFS skills and adding small scale features allowed by the increased horizontal resolution of the grid.
Quantitative comparisons has been done using space and time mean esti-

Emilia Romagna	Gulf of Trieste	Rovinj Area
	Mar 04	
Mar 05-06		Mar 05
Mar 10-11		
Mar 18-20		Mar 18
Mar 24-25	Mar 24	Mar 24
		Mar 31
	Apr 05	
		Apr 08
Apr 09-11	Apr 11	
Apr 14-15		Apr 14
	Apr 17	
Apr 22-23		Apr 22
Apr 28		
	Apr 29	
May 05-06	May 05	May 05
May 12		
		May 13

Table 3.3: CTD data available from ADRICOSM observing system during the Spring Experiment time period.

Emilia Romagna	Gulf of Trieste	Rovinj Area
Jul 28-30	Jul 28	Jul 28
Aug 04-05		
Aug 11-12	Aug 11	Aug 11
Aug 18-19	Aug 18	Aug 19
Aug 26-27-28	Aug 26	Aug 26
		Sep 01
	Sep 04	
Sep 05		
Sep 09-11	Sep 09	Sep 09
		Sep 15
Sep 17-18	Sep 17	
Sep 22-23	Sep 22	Sep 22
		Sep 30
Oct 01-02		

Table 3.4: CTD data available from ADRICOSM observing system during the Summer Experiment time period.

mates of bias (BIAS), root-mean-square-error (RMSE) and pattern correlation coefficient (PCC):

$$BIAS = \sum_i \sum_j (\theta^M_{i,j} - \theta^O_{i,j}) \tag{3.9}$$

$$RMSE = \sqrt{\frac{\sum_i \sum_j (\theta^M_{i,j} - \theta^O_{i,j})^2}{n}} \tag{3.10}$$

$$PCC = \frac{\sum_i \sum_j (\theta^M_{i,j} - <\theta^M>)(\theta^O_{i,j} - <\theta^O>)}{\left[\sum_i \sum_j (\theta^M_{i,j} - <\theta^M>)^2 \sum_i \sum_j (\theta^O_{i,j} - <\theta^O>)^2\right]^{1/2}} \tag{3.11}$$

where $<>$ denote the average, θ^M represents model value and θ^O is the corresponding observed value. In the PCC calculation we considered the background mean estimate to be either the time series average for the period under consideration at each data point (i,j) or the spatial average per each sampling time.
Model behavior has been studied analyzing both time evolution of space mean skill scores or the space distribution of their time mean. In the first case the time evolution of model skill score allows to identify eventual trends in model behavior or some correlation of it with particular forcing events. In the second case the time averaged skill scores calculated for the simulation time period at each sampling location enable to pick out in which part of the domain the numerical model has major performance defects. In particular vertical skill scores profiles allow to evaluate if the model can well represent the water column dynamics (stratification or well mixed condition) and to identify whether some part of the water column is not well represented.

3.5 Results

3.5.1 Comparison with Satellite SST Observations

Model SST is the temperature at the first σ level whose depth differs if the models under investigation possess different topographies, like AFS and ASHELF. This must be taken into account in those areas of the domain where topographies substantially mismatch. AFS and ASHELF SST have been interpolated on the satellite observational grid and space averaged skill scores time series have been calculated considering daily mean fields, time centered at midnight.

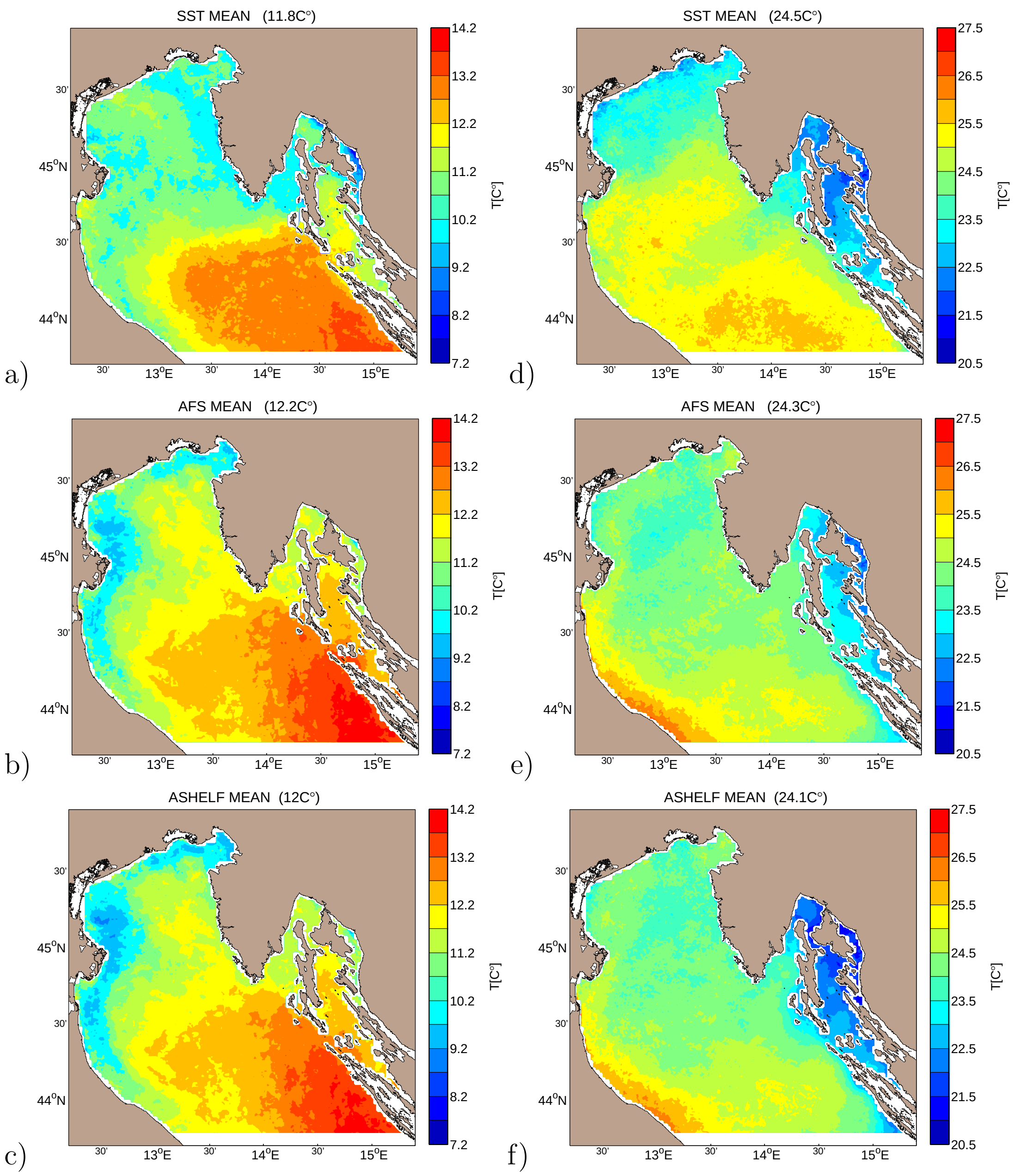

Figure 3.7: Time averaged SST maps for the simulated time periods. (Left) Spring Expriment results: a) Observed satellite SST; b) AFS SST; c) ASHELF SST. (Right) Summer Experiment results: d) Observed satellite SST; e) AFS SST; f) ASHELF SST.

In figure 3.7 we present mean maps of SST calculated for the two simulated time period from observations, AFS and ASHELF models. Spring observed SST map (fig.3.7a) presents a quite uniform cold temperature in the shallower north-western part of the domain, where temperature is on average below $12C^{\circ}$. Warm water remains confined in the south-eastern area where temperature reaches $14C^{\circ}$. AFS and ASHELF presents very similar patterns: a negative bias is detected around the Po river delta, inside the Gulf of Trieste and in the south-western area; a positive bias surrounds the Istrian peninsula, where the misfits are the highest.

Summer observed average SST (fig.3.7d) depicts cold areas along the northern coast and between the Croatian islands. The observed SST pattern places the coldest areas on the Bora wind main jets tracks, the Trieste jet which blows all along the northern coast towards Venice Lagoon and Senj jet blowing below the tip of Istria (*Dorman et al.*, 2007). In fact, northeasterly winds are frequent during summer 2003 as depicted in fig.3.4. AFS and ASHELF models give very similar results. They cannot reproduce the observed pattern since ECMWF atmospheric forcing does not fully capture the Bora wind spatial variability as stated by (*Signell et al.*, 2005).

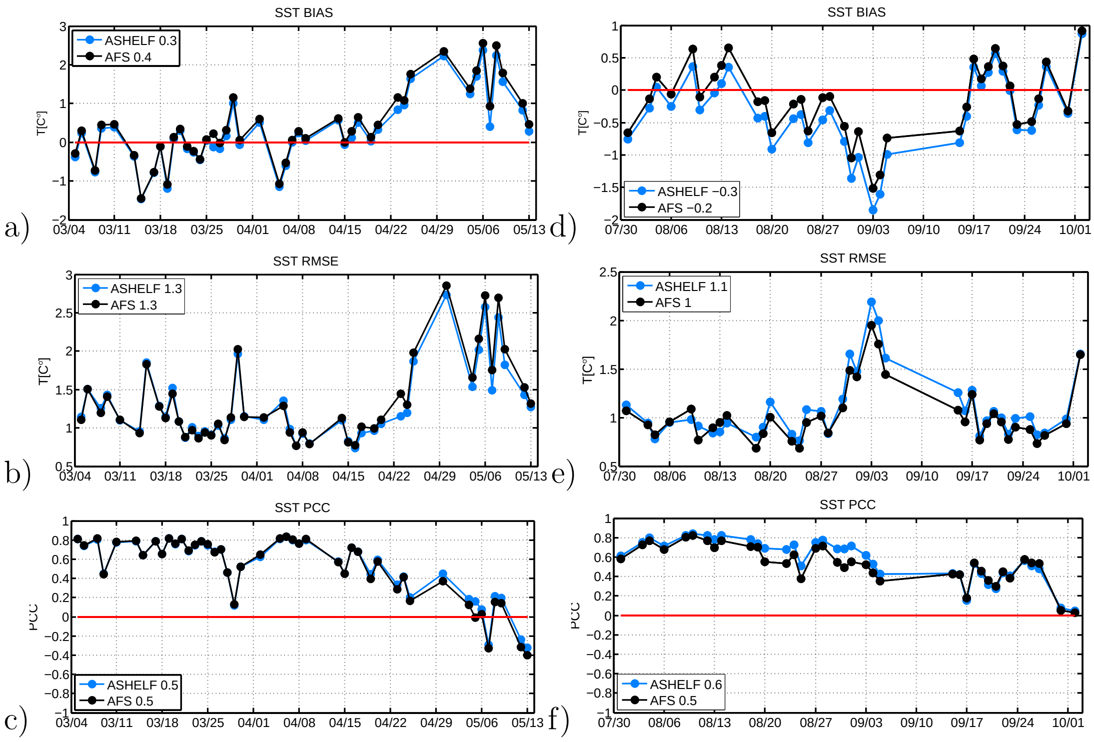

Figure 3.8: (Left) SST skill scores time series for the Spring Experiment: a) BIAS; b) RMSE; c) PCC. (Right) SST skill scores time series for the Summer Experiment: d) BIAS; e) RMSE; f) PCC

Skill scores time series for the spring experiment (fig.3.8a-b-c) show same AFS and ASHELF results with a little bias and rmse reduction and pcc enhancement in ASHELF starting from middle April, when air temperature start to increase. We might ascribe this small positive signal to Po river temperature implementation within ASHELF. River temperature (see fig.3.3c) in spring warms up faster than seawater and its signature is quite evident from SST maps, like in figure 4.10a of the next chapter.
ASHELF mean bias is $0.3C^\circ$ while mean rmse is about $1.3C^\circ$. Pattern correlation falls abruptly to negative values at the beginning of May when, due to the surface warming, the water column starts to stratify.
During summer simulation both models present a small negative bias that peaks during the first days of September in concomitance with the air temperature drop. RMSE usually oscillates around $1C^\circ$ but it peaks too during the first week of September overpassing $2C^\circ$. ASHELF results in general slightly colder than AFS but its PCC is on average higher than AFS one, indicating a better dynamics representation.

3.5.2 Comparison with ADRIA03

Observed mean temperature profile (fig.3.9) shows a surface maximum value of $15C^\circ$ and a subsurface minimum at 30m depth. Observed mean salinity profile displays a surface minimum of 36.5psu, a marked halocline at 10m depth and a maximum salinity of 38.5psu on the bottom.
ASHELF gives on average same results than AFS. Models temperature have a mean negative bias of $1C^\circ$ with minimum values at the surface and at 30m. Maximum temperature discrepancy is on the deepest part of the domain, below 40m of depth. Temperature RMSE is maximum at 10m depth and on the bottom where it reaches $1.5C^\circ$.
Salinity mean bias profile indicates a slight models overestimation of surface value and a quite constant negative bias below 10m depth. Salinity mean RMSE is maximum at the surface (1psu), it keeps constant between 15 and 40m and it rather increases at the bottom, below 40m of depth.

3.5.3 Comparison with Coastal CTDs

Second models CTD validation considers the three coastal and shallow areas, being a strict verification of model performances. Synthetic profiles have been extracted interpolating the model on each CTD space/time location.
Hovmoller plots in figure 3.10 show the evolution in time of temperature and salinity in the Emilia Romagna coastal area during spring experiment where,

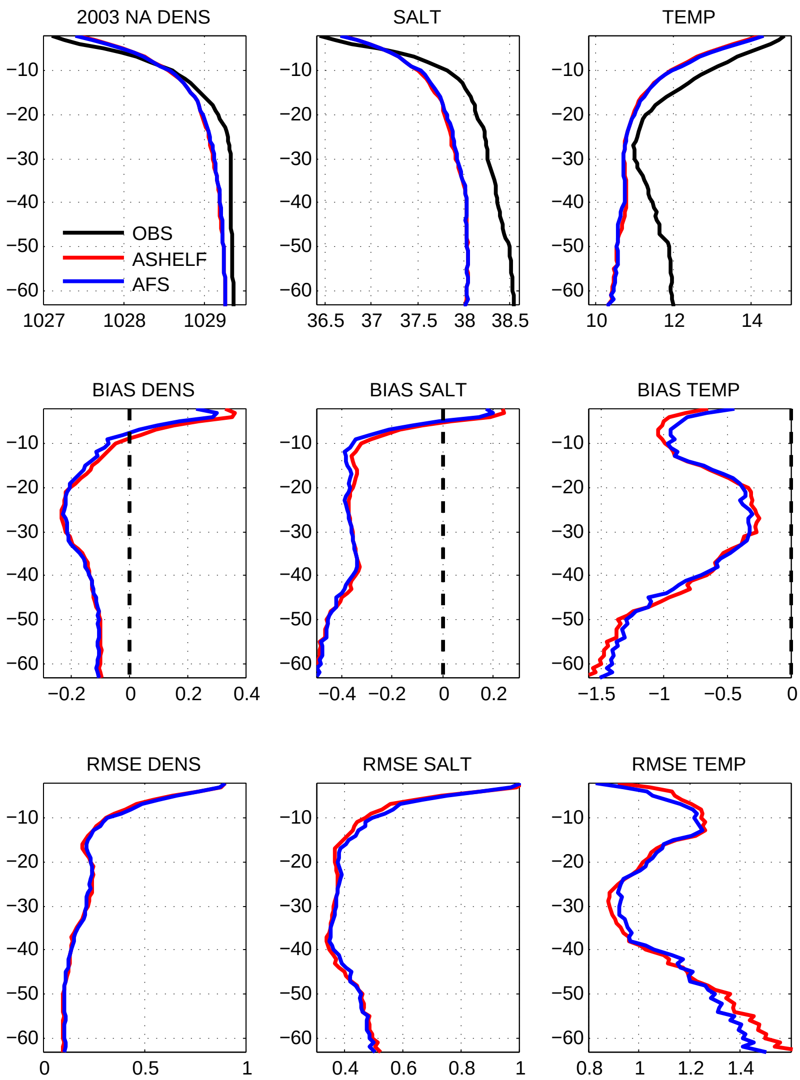

Figure 3.9: (Top) Area averaged density, salinity and temperature profiles from CTD observations, ASHELF and AFS models. (Middle) AFS and ASHELF bias profiles of density, salinity and temperature. (Bottom) AFS and ASHELF RMSE profiles of density, salinity and temperature .

for each sampling day, the areal mean profile has been computed. Oscillations on the profile depth are due to the sampling array, that in this area covers the entire network into two consequent days without a defined scheme but depending on the weather conditions. Also the number of sampled stations varies. This does not happens for the other two monitoring networks where the same stations are all sampled in one day.

Observed temperature (fig.3.10A) looks quite homogeneous till middle April when it starts to warm up at the surface and a well developed thermocline establishes in May. Observed salinity (fig.3.10E) conversely presents a permanent vertical gradient due to the direct influence of Po river freshwater discharge.
AFS temperature (fig.3.10B) follows the observed temperature behavior, but its value is lower than the observed one in early March, thus determining an initial ASHELF temperature bias (fig.3.10C). Both models heat up at the surface in May but not as much as observed. Models temperature RMSE time series (fig.3.10D), whose mean value settle at $1.4C^{\circ}$, confirm that maximum temperature error occur on early March and May with values over $2C^{\circ}$. AFS salinity vertical gradient (fig.3.10F) is much weaker than observed with saltier water at the surface (positive bias) and fresher on the bottom (negative bias) respect to observed salinity field. This determines on average a small bias value (0.5psu) but a large RMSE that for AFS is equal to $2.2psu$ and for ASHELF slightly reduces to $2psu$ (fig.3.10H). In general, ASHELF tendency follows AFS one but it exhibits an increased realism due to both the introduction of a high resolution bathymetry and the reduction of model's minimum depth from 10 to 5m.

Figure 3.11 shows mean RMSE temperature and salinity profiles for the spring experiment. Emilia Romagna RMSE profiles (fig.3.11a) indicate for both temperature and salinity maximum misfits within the first 5 meters of the water column which is highly influenced by river freshwater. In the Gulf of Trieste (fig.3.11b) the RMSE profiles reveals a slight worsening of temperature and conversely an improvement of surface salinity owing to the introduction of a new Isonzo river climatology form *Malačič and Petelin* (2009) with respect to AFS. In Rovinj coastal area (fig.3.11c) AFS and ASHELF produce the same temperature and salinity RMSE profiles.

Hovmoller plots in figure 3.12 relative to the summer experiment depict a warm temperature during August with a weak vertical gradient in the central part of the month. An abrupt cooling event occurs during the first days of September that lowers the area mean temperature of approximately $3C^{\circ}$ in the overall water column. AFS and ASHELF follow temperature evolution with an increased realism of ASHELF solution. Observed salinity (fig.3.12E) keeps fresher values at the surface for the most part of the simulation time period, with minimum values at the surface of $33psu$ in September. During the first days of September when temperature drops, salinity is homogeneous within the water column. This indicate that the intense Scirocco event followed by Bora wind between August and September (see fig.3.4d) fully mixed and cooled down the Emilia Romagna coastal area.
ASHELF (fig.3.12G) better reproduces salinity evolution increasing the bot-

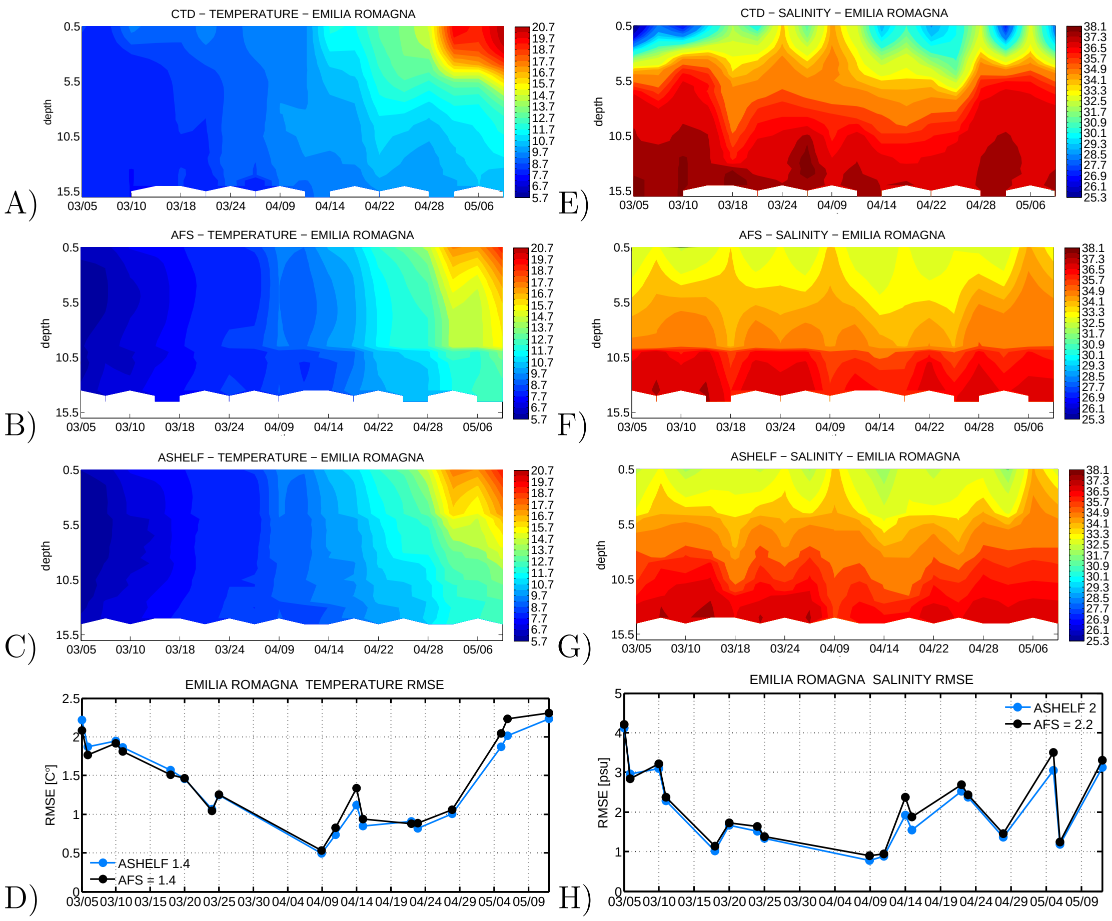

Figure 3.10: Temperature hovmoller plots in Emilia Romagna Coastal area during Spring experiment. A) Observations; B) AFS; C) ASHELF. D) Temperature RMSE time series. Salinity hovmoller plots in Emilia Romagna Coastal area during spring experiment. E) Observations; F) AFS; G) ASHELF. H) Salinity RMSE time series.

tom salinity value, but like AFS (fig.3.12F) fails in reproducing the minimum salinity values at the surface. Temperature PCC (fig.3.12D) oscillates around zero between the end of August and the beginning of September, when vertical mixing occurs, probably owing to the coarse ECMWF atmospheric forcing which does not fully resolve the space variability of wind, underestimates its intensity or misses the exact timing of the events. ASHELF reproduces better than AFS the water column dynamics in September, doubling the AFS overall PCC value. Salinity PCC (fig.3.12H) exhibit negative values between August and September, strengthening the previous outcome on ECMWF atmospheric forcing. ASHELF value is higher than AFS one on the majority

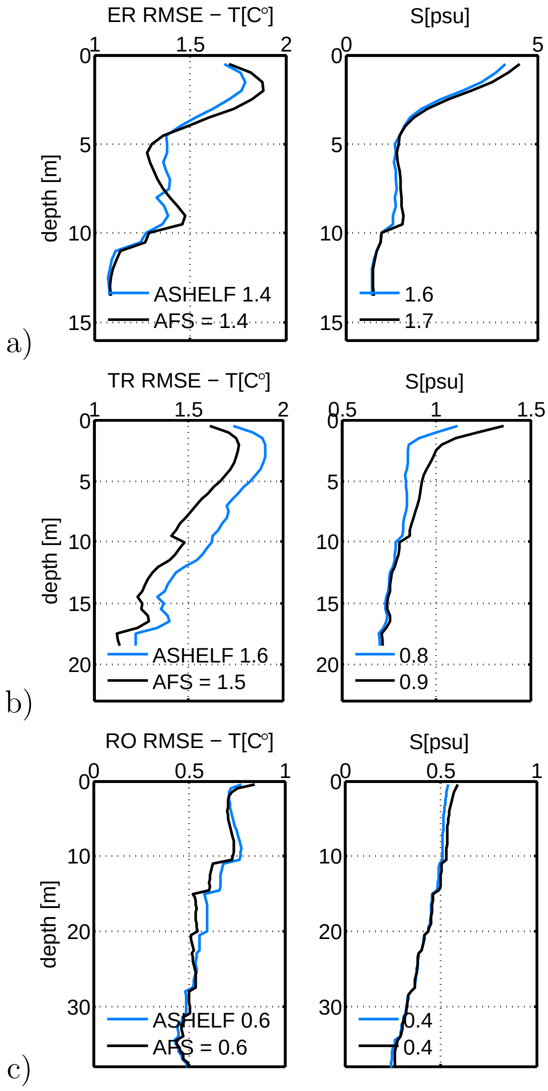

Figure 3.11: RMSE temperature and salinity profiles calculated fROM the Spring Experiment: a) Emilia Romagna; b) Gulf of Trieste; c) Rovinj.

of the sampling days, especially in September.
Vertical RMSE profiles for summer experiment (fig.3.15a) show in the Emilia Romagna area an ASHELF temperature RMSE increase below 10m depth but an overall salinity RMSE reduction of 0.3psu.

Observed temperature in the Gulf of Trieste (fig.3.13A) reveals a strong vertical gradient and a strong thermocline oscillating between 10 and 15 meters with cold water on the bottom which totally misses in models simulations. Summer thermocline starts to break down in September when the

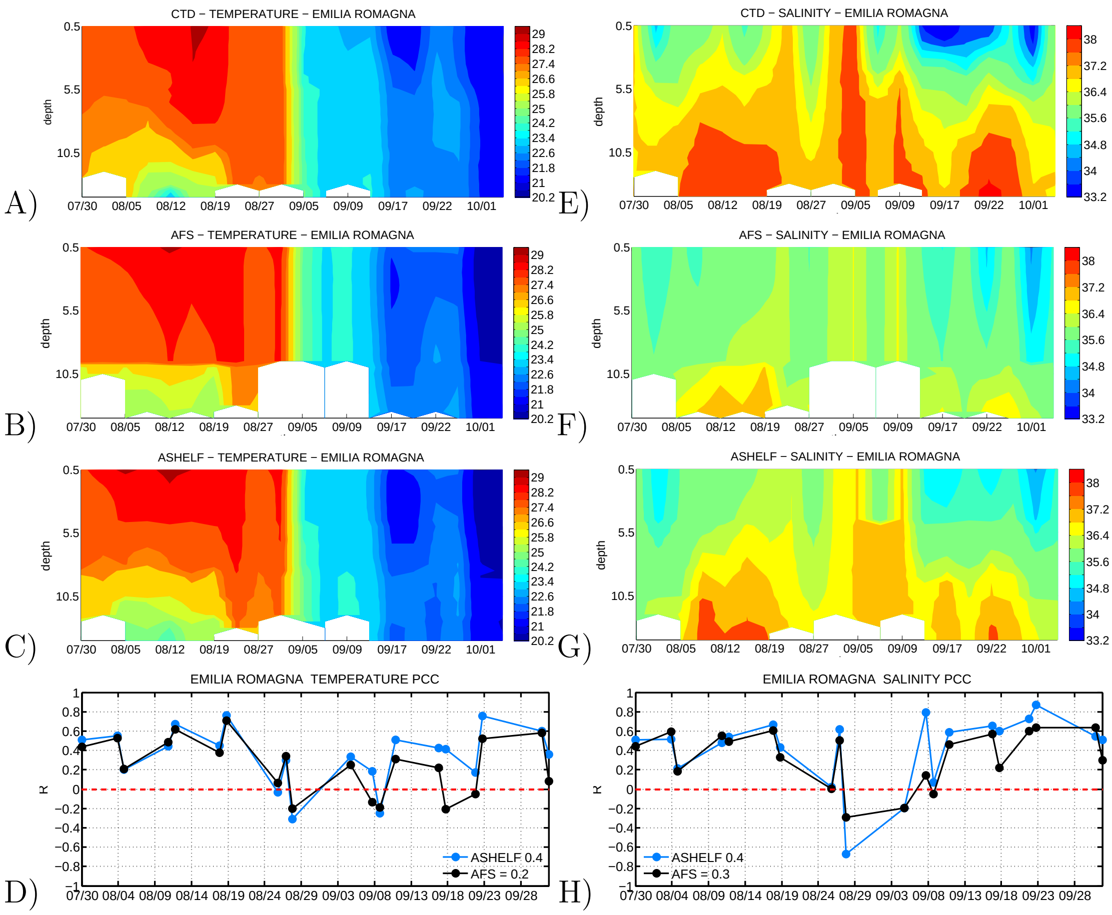

Figure 3.12: Temperature hovmoller plots in Emilia Romagna Coastal area during Summer experiment. A) Observations; B) AFS; C) ASHELF. D) Temperature PCC time series. Salinity hovmoller plots in Emilia Romagna Coastal area during Summer experiment. E) Observations; F) AFS; FG) ASHELF. H) Salinity PCC time series.

water column mixes up to 15m depth still maintaining a cold bottom layer. In AFS (fig.3.13B) totally misses the cold bottom layer thus determining a wrong ASHELF initial condition. ASHELF (fig.3.13C) temperature presents a shallower thermocline than AFS one, but it deepens unrealistically on August 26th.
Observed salinity (fig.3.13D) exhibits very high values during all the simulated time period. Summer 2003 has been anomalous due to the high temperature recorded and the consequent dryness, as it is clearly noticeable from Po river daily mean outflow time series (fig.3.3a) if compared with its relative climatology. Models are much fresher than observations due to the

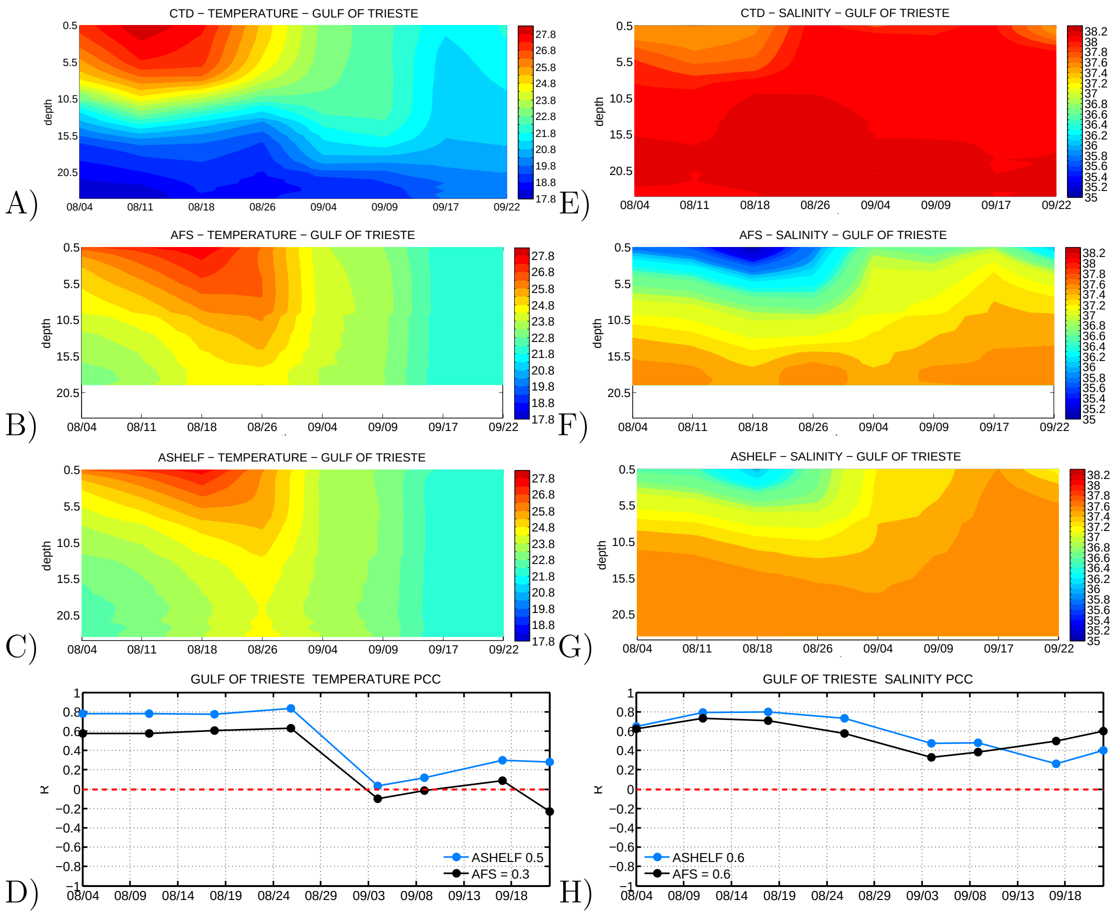

Figure 3.13: Temperature hovmoller plots in Gulf of Trieste during Summer experiment. A) Observations; B) AFS; C) ASHELF. D) Temperature PCC time series. Salinity hovmoller plots in Gulf of Trieste during Summer experiment. E) Observations; F) AFS; G) ASHELF. H) Salinity PCC time series.

monthly climatological rivers forcing applied (except for Po and Reno rivers) that overestimates the real discharge. Both temperature and salinity PCC time series confirm the goodness of the adopted initialization technique in recreating missing values on the bottom, without compromising ASHELF dynamics, that ameliorates with respect to AFS. Temperature RMSE profile (fig.3.15b) depicts an error reduction below 10m depth. ASHELF salinity RMSE profile proves a general improvement within the water column with a total lowering of $0.3psu$ with respect to AFS.

Temperature in Rovinj coastal area brings about similar results to Trieste ones. Observations depict strong stratification persisting till middle Septem-

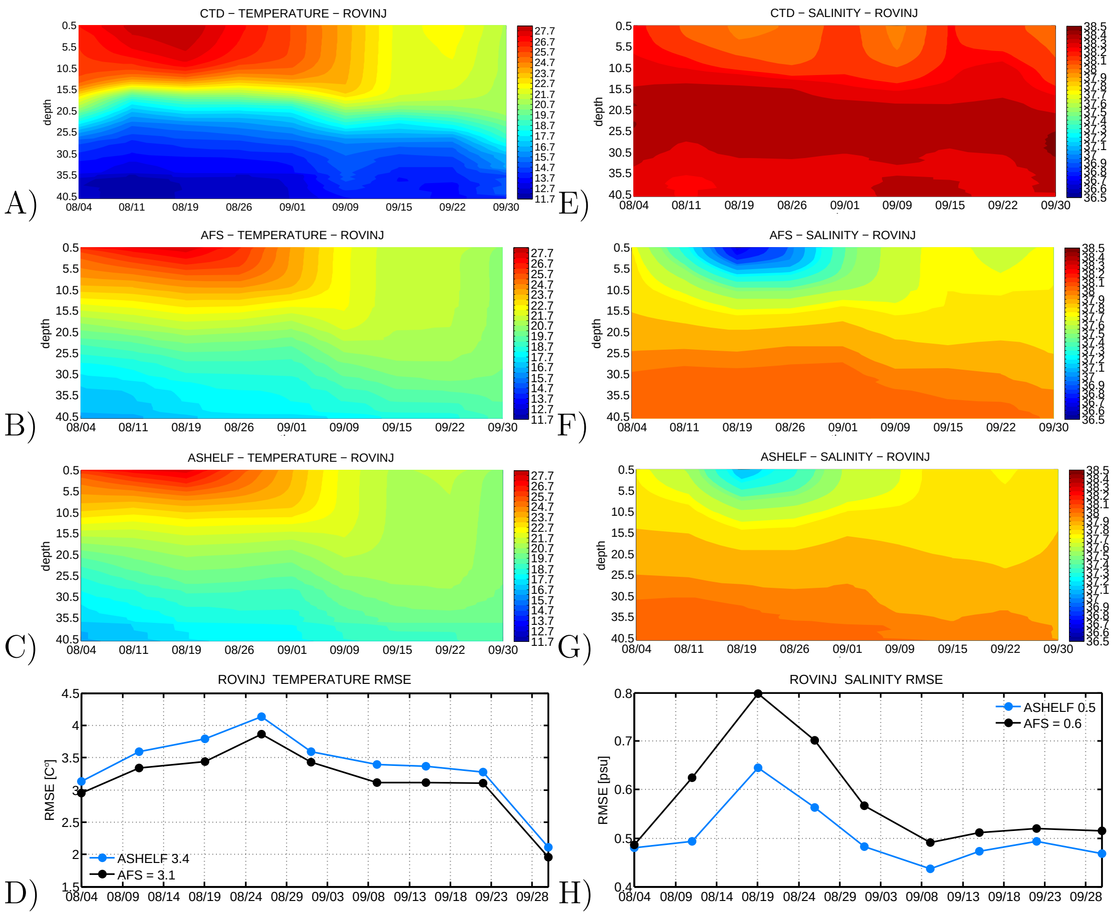

Figure 3.14: Temperature hovmoller plots in Rovinj coastal area during Summer experiment. A) Observations; B) AFS; C) ASHELF. D) Temperature RMSE time series. Salinity hovmoller plots in Rovinj coastal area during Summer experiment. E) Observations; F) AFS; FG) ASHELF. H) Salinity RMSE time series.

ber which both models cannot reproduce. The lack of the cold bottom layer in AFS temperature field negatively affects ASHELF initial condition, determining a very high RMSE value (fig.3.15c) for both models overpassing $3C^{\circ}$. ASHELF RMSE is higher than AFS one within the first 10m depth. Salinity is again slightly biased (0.5psu) and ASHELF RMSE rather diminishes above 20m of depth.

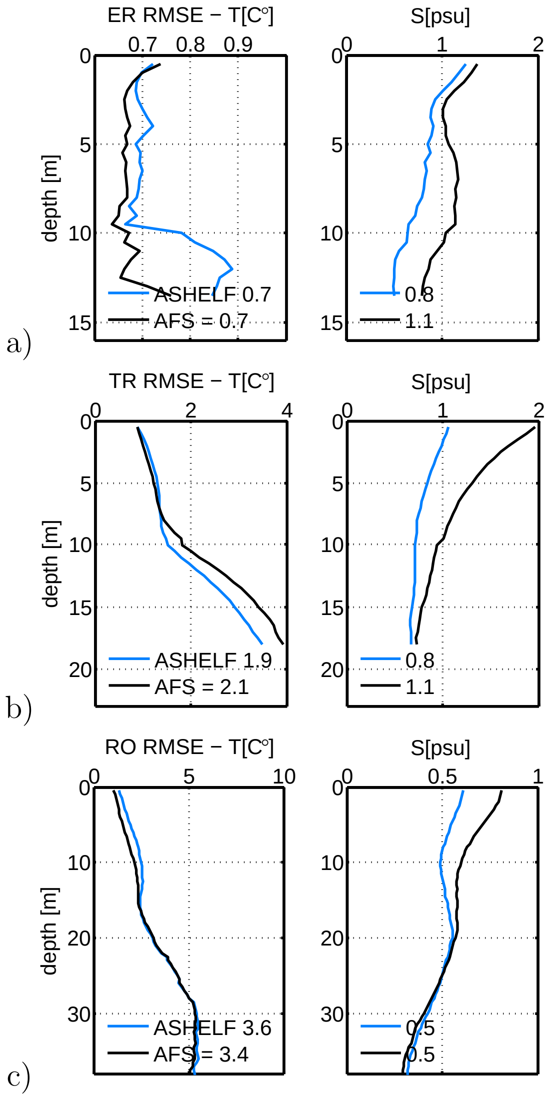

Figure 3.15: RMSE temperature and salinity profiles calculated from the Summer Experiment: a) Emilia Romagna; b) Gulf of Treste; c) Rovinj.

3.6 Summary and Conclusions

SST validation presents same results for AFS and ASHELF models. AFS and ASHELF biases oscillates on average within the $\pm 1C^{\circ}$ interval except during the period of thermocline formation on May, when models are warmer than observations, and during the sudden cooling event in early September, when models are colder than observed. RMSE during these periods expresses maximum values over $2C^{\circ}$. When these transition events occur and the wa-

ter column passes from homogeneous to stratified ambient conditions, and vice versa, model performances reduce abruptly, probably because the atmospheric forcing does not fully represent the real spatial pattern or its exact timing.
ADRIA03 campaign allowed an extensive model validation for spring experiment between April and May, when surface warming brings about the establishment of the seasonal thermocline. Observed temperature is in fact warmer at the surface. Again AFS and ASHELF reproduce the same temperature, salinity and density pattern.
AFS and ASHELF validation with coastal CTD showed an increased realism of ASHELF model suggested by a slight increase of PCC, that we may ascribe to the introduction of the high resolution topography and a shallower minimum depth. ASHELF rapid initialization through interpolation/extrapolation of AFS large scale fields was successful in recreating new data on the bottom and at the lateral boundary without generating model disturbances, as we have seen in the Gulf of Trieste, where topography mismatch is maximum.
In general we detected a small improvement of ASHELF salinity which confirms the goodness of the new rivers data set used in ASHELF. ASHELF temperature instead does not improve AFS result. This outcome may indicate that phase errors of higher resolution ASHELF are more frequent than coarser AFS ones in coastal areas, reducing the overall skill of the simulation and masking the positive effect of increasing the resolution and introducing a more realistic topography.
This work regarded the implementation of ASHELF model in the Northern Adriatic embedded into an operational modeling system consisting of the MFS in the outer domain and the AFS in the intermediate domain. The main goal was the validation of ASHELF performances in the near coastal area as preliminary step towards the application of a Rapid Environmental Assessment strategy which employs coastal observations to correct AFS large scale initial conditions.
Two simulations have been performed during spring and summer 2003 to test ASHELF set up, the nesting procedure and the rapid initialization technique which interpolate/extrapolates AFS large scale daily fields into ASHELF grid. ASHELF and AFS models were forced by the same atmospheric data from ECMWF.
AFS and ASHELF have been validated by an extensive pool of remote and in situ observations with the final result of a successful implementation of ASHELF model and the nesting technique. ASHELF increased resolution was not sufficient to improve model results versus AFS, that represents our reference level. AFS initial conditions and boundary conditions together with

ECMWF forcing drive and keep ASHELF solution close to AFS one.
ASHELF and AFS present on average same temperature predictive skills and we may ascribe it to the occurrence of phase type errors that are more probable when new high resolution circulation features are introduced by the enhanced resolution. ASHELF shows respect to AFS a small refinement in salinity representation and a major realism in the near coastal area thanks to the introduction of new river data and a high resolution topography.
Future developments will regard the introduction of higher resolution atmospheric forcing and the implementation of a data assimilation technique which will correct AFS fields with opportunity coastal observations to generate the best initial conditions and ameliorate ASHELF predictive capabilities in the near coastal area.

Chapter 4

Rapid Environmental Assessment in The Northern Adriatic

4.1 Introduction

The concept of Rapid Environmental Assessment (REA) originates with the applications that need to predict changes in the ocean within a short time besides a description of the present status. The nowcasts and forecasts must be accurate and efficient because they have to support operational and management activities effectively. A modelling and observational system that meets these requirements is called REA (*Robinson*, 2002).
In the past fifteen years many REA study cases were carried out in the open ocean and in coastal environments,(*Robinson* (1999), *Robinson* (2002), *Ferreira-Coelho and Rixen* (2008)).
REA requires an Ocean Observing and Prediction System (OOPS) made of an observational network, a numerical dynamical modeling system and data assimilation scheme. The general goal is to assimilate data of the observational network into the prediction model to generate the best field estimates, this reducing the forecast uncertainty. In the past efforts the observations were collected ad hoc since only climatology was available in the area of interest. However with the advent of operational oceanography, accurate initial conditions could be created using operational analyses, thus it is possible to apply REA in the coastal domain (CREA) using first guess fields from large scale models adding coastal observations.
We present a CREA strategy that is based on a regional forecasting system and coastal observational networks to initialize a high resolution coastal

model and produce short range predictions. The general objective is to develop a methodology to reduce forecast uncertainty in the coastal area using opportunity observations. In this case the observational network has been designed for other purposes and we try to make use of it within a REA strategy.
CREA will be applied to the Northern Adriatic Sea (see fig.4.1a), where a high resolution, O(800m) Adriatic SHELF model (ASHELF) will be implemented and nested within the Adriatic Forecasting System (AFS) (*Oddo et al.*, 2006). The methodology wishes to blend the large scale AFS fields with coastal observations to produce the best initial condition for ASHELF. The blending of the two data sets has been carried out with a multi-scale optimal interpolation technique developed by *Mariano and Brown* (1992). This assimilation technique consists of a correction of the initial field provided by AFS on the basis of the available opportunity observations.
CREA utilizes the observational system established in the framework of ADRICOSM Pilot Project (*Castellari et al.*, 2006). The Project set-up a coordinated network of observations in three coastal areas of the Northern Adriatic basin: Emilia-Romagna, Gulf of Trieste and Rovinj (fig.4.1b-c-d). They performed weekly coastal monitoring campaigns on coincident sampling days, when weather conditions were favorable.

Two weekly CREA experiment will be discussed for spring and summer 2003, when the three coastal zones were synchronously monitored. Our objective is to demonstrate the feasibility and the efficacy of a CREA system which uses monitoring coastal network of opportunity and an existing low resolution operational model to forecast for a week the near coastal areas of the Northern Adriatic.
The Northern Adriatic is a landlocked basin located at a midlatitude in the northernmost part of the Adriatic Sea, confined north by the Alps and laterally between the Apennine and the Balkan peninsulas. It constitutes the shelf of the Adriatic basin that gently slopes towards the shelf break identified by the 120m bathymetric. Its mean depth is 35 m with sandy and smooth coastal areas on its western side and an irregular eastern rocky shore, characterized by numerous channels and islands.
The Northern Adriatic presents three main ambient stratification regimes, widely described in *Artegiani et al.* (1997a) and *Jeffries and Lee* (2007), with strong stratification from June through September and a weak stratification from December through March. A transitional stratification regime characterizes April, May, October and November. Fresh water input is a major forcing owing to the presence of many rivers but mainly to the Po River which accounts for almost 80% of the total fresh water contribution of the Adriatic Basin. Wind is also a major forcing characterized by northeasterly

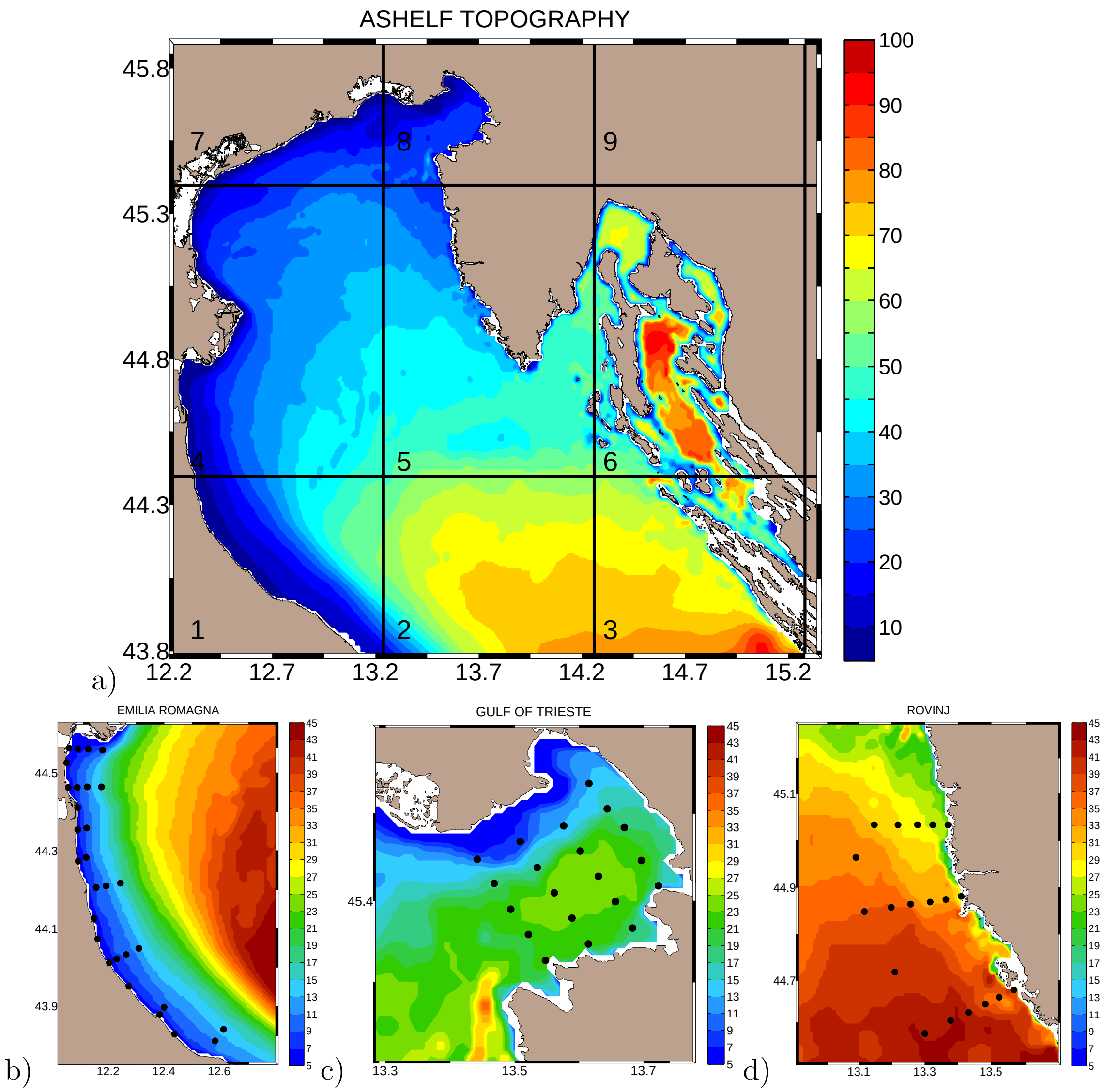

Figure 4.1: a) ASHELF model domain and topography. ASHELF domain has been divided in squared bins to define an heterogeneous Parameter Matrix for the OA technique; b) Emilia Romagna; c) Gulf of Trieste; d) Rovinj coastal areas and monitoring networks.

Bora winds and sporadic southeasterly Scirocco winds.
In this paper we concentrate the attention on the three coastal areas of the Northern Adriatic Sea and we apply the new CREA methodology for the year 2003. The model employed (ASHELF) is the highest resolution model used in this area and it is nested in AFS.

The paper is organized as follows. A description of the modeling system and the ASHELF model is given in *Section 2*. *Section 3* presents the coastal observational networks and data. In *Section 4* we explain the applied initialization procedure, first the interpolation/extrapolation method and then the multi-scale optimal interpolation technique. *Section 5* explains the CREA experimental design. In *Section 6* we discuss CREA results, while in *Section 7* we summarize our conclusions.

4.2 The Adriatic Shelf Model

ASHELF is embedded in a modeling system which consists of a hierarchy of three numerical models (Mediterranean Sea, Adriatic Sea, Northern Adriatic basin) nested within each other to downscale the larger scale flow field and resolve the coastal scale fields. This nested approach has been first implemented by *Zavatarelli and Pinardi* (2003) to study the climatological circulation of the Adriatic and Northern Adriatic seas.
The Mediterranean ocean Forecasting System (MFS) (*Pinardi et al.*, 2003) constitutes the modeling system in the outer domain, giving boundary conditions to the Adriatic Forecasting System (*Oddo et al.*, 2006).
AFS produces once a week, with a daily system, 9 days forecast (*Guarnieri et al.*, 2009) of the main hydrodynamics state variables (currents, temperature, salinity, sea level and air-sea fluxes). AFS horizontal resolution is about 2.2 km and the vertical grid is made up of 31 double logarithmic σ layers. Model bathymetry has been modified to have a minimum depth of 10m and flattening the coastal area between the coastlines and the 10m bathymetry.
ASHELF domain covers the Northern Adriatic basin (fig. 4.1) with a horizontal resolution of 800 meters and a vertical discretization of 31 σ layers. ASHELF uses a new high resolution topography (Richard Signell personal communication from ADRIA03 field experiment in the Northern-Central Adriatic) which has been blended with AFS at the open boundary of ASHELF for about 30 km inside the domain.
ASHELF and AFS use the same Monotonic Upstream centered Scheme for Conservation Laws (MUSCL) for tracers advection (*Estubier and M.Levy*, 2000) in order to give a more realistic representation of horizontal and vertical gradients. Up-stream scheme, as in *Oddo et al.* (2009), has been applied close to the lateral open boundary to increase diffusivity avoiding numerical instabilities.
AFS provides daily mean fields of temperature, salinity, velocity and surface elevation that are linearly interpolated on the lateral open boundary. Interpolation in time assure a time evolving transfer of information from one

model to the other. Open boundary condition for the normal component of the barotropic velocity uses the *Oddo and Pinardi* (2008) formulation of the Flather boundary condition (*Flather*, 1976):

$$V_{ASHELF} = V_{AFS} - \frac{\sqrt{gH}}{H}(\eta_{AFS} - \eta_{ASHELF}) \tag{4.1}$$

where V_{ASHELF} and V_{AFS} are respectively ASHELF and AFS meridional components of barotropic velocity, normal to the lateral open boundary, H is the bathymetry, which is identical for both models, g is the gravity, $\eta_{ASHELF} and \eta_{AFS}$ are models surface elevation. The AFS velocity is imposed for the zonal component of the barotropic velocity tangential to the open boundary.
An advective condition is applied to tracers (θ) temperature and salinity:

$$\frac{\partial \theta}{\partial t} + V_n \frac{\partial \theta}{\partial n} = 0 \tag{4.2}$$

If the velocity normal to the boundary is positive (outflow), tracers are advected out of the domain, otherwise the external data are advected inward at inflow boundary points.
A southern radiation boundary condition, according to Orlanski's scheme (*Orlanski*, 1976), is applied to the meridional component of the total velocity (ϕ), normal to the lateral open boundary:

$$\frac{\partial \phi}{\partial t} + C\frac{\partial \phi}{\partial y} = 0 \qquad , \qquad C = -\frac{\partial \phi}{\partial t}\Big(\frac{\partial \phi}{\partial y}\Big)^{-1} \tag{4.3}$$

The free surface elevation is not nested and a zero-gradient boundary condition is applied.

4.2.1 River Runoff

River runoff and river parameterization have been described in details in section 3.2.3 on page 48.

4.2.2 Atmospheric Forcing

Surface boundary conditions are computed through standard bulk formulae parameterization (*Castellari et al.*, 1998). Surface fluxes computation of heat and momentum is carried out interactively every time step from atmospheric data and model predicted sea surface temperature (SST) (*Oddo et al.*, 2006). Two different atmospheric data sets were used to calculate heat and momentum fluxes: a coarse resolution data set from European Centre

for Medium-Range Weather Forecasts (ECMWF) and a high resolution data set from Limited Area Model Italy (LAMI).
ECMWF provides data every 6 hours at a space resolution of 0.5°. Air temperature, dew point temperature, mean sea level pressure, cloud cover and wind speed are the variables considered. Precipitation data have been extracted from *Legates and Willmott* (1990) global monthly climatology having a 0.5° horizontal resolution.
LAMI is the Italian operational implementation of the Lokal-Modell (LM), (www.cosmo-model.org). LAMI supplies data every 3 hours and produces a 72 hours forecast once per each day on a 7 km grid. LAMI variables considered for surface fluxes computations are: air temperature, cloud fraction, relative humidity, rain and wind speed.
Figure 4.2 shows the time series of air temperature and wind speed space averaged over ASHELF domain for the two time periods in spring and summer 2003 considered in our simulations. LAMI and ECMWF air temperature general trend overlap quite well exhibiting, a warming trend that starts on the second week of April during spring time, and stable warm conditions during all August with an abrupt cooling event at the beginning of September. Diurnal cycles are instead very different, as it can be seen in the small square plot depicting the mean cycles estimated for the period under consideration, since ECMWF presents a wider diurnal cycle with maximum temperature at noon while LAMI maximum temperature occurs between 15 and 18PM, which is more realistic over the ocean.
LAMI and ECMWF wind speed are in overall good agreement on ASHELF domain (fig.4.2) since mean direction and timing are very similar, alternating intense Bora (northeasterly wind) and Scirocco (southeasterly wind) events with periods of wind stagnation. LAMI winds magnitude is on average larger than ECMWF one, consistently with prior studies like *Signell et al.* (2005).

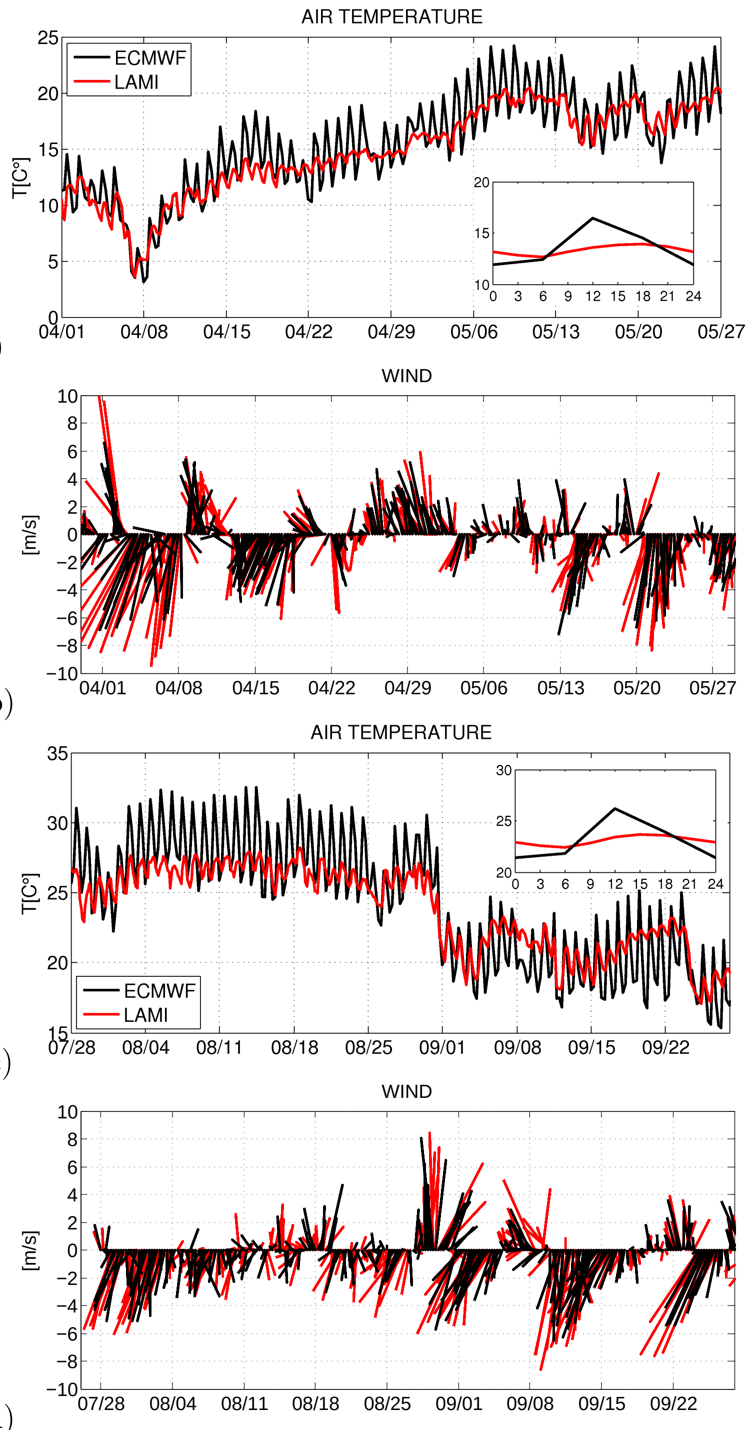

a)

b)

c)

d)

Figure 4.2: Area average air temperature time series from ECMWF (black) and from LAMI (red) calculated on ASHELF domain for 2 periods: a) Apr-May 2003; c) Aug-Sept 2003. Small subplot displays the mean air temperature diurnal cycle. Area average wind velocity time series over ASHELF domain: b) Apr-May 2003; d) Aug-Sept 2003.

Emilia Romagna	Gulf of Trieste	Rovinj Area
May 05-06	May 05	May 05
May 12		May 13
Aug 11-12	Aug 11	Aug 11
Aug 18-19	Aug 18	Aug 19

Table 4.1: CTD data collection periods.

4.3 Coastal Observations

The three opportunity observational networks considered here are concentrated in the Emilia-Romagna, Gulf of Trieste, Rovinj coastal strips. The sampling arrays are displayed in figure 4.1b-c-d.
Emilia-Romagna coastal monitoring network (fig. 4.1b) is unique in the overall Mediterranean Sea since it has been the first one established in the late seventies to face the environmental emergency related to eutrophication processes and then maintained from the regional environmental protection agency (ARPA) to control water quality and study the marine ecosystem and coastal hydrodynamics. The monitoring array is made up of 30 stations situated along transects perpendicular to the coastline at distances of 500 m, 3, 6 or 10 km from the coastline sampled on a weekly basis on two consecutive days. Emilia Romagna coastal area is sandy, shallow and gently sloping so the deepest stations reach 15 meters depth.
In the Gulf of Trieste bi-weekly (October 2002-March2003) and weekly (April-September 2003) cruises (*Celio et al.*, 2006) were performed over the sampling grid of 19 stations (fig. 4.1c) providing an adequate spatial and temporal coverage of the area during one day cruise. The Gulf of Trieste is a semi-enclosed basin of about 30 km diameter with a complex topography. Its main NE-SW axis divides a deeper pool (maximum depths is 26m) in the southern-central part from a narrow slope which characterizes the northern area, influenced by the Isonzo River estuary.
The third coastal network is made up of 19 stations mainly arranged on three transects perpendicular to the coast (fig.4.1d). Here the sea bottom reaches the maximum depth (44m) few kilometers off the coast . *Lyons et al.* (2007) present a detailed analysis of all the CTD data collected in this area.
The CTD data used in our CREA exercises are listed in table 4.1. They belong to two different weeks, the first goes from May 5th to May 13th, the second goes from August 11th to August 19th.

4.4 Initialization Methods

4.4.1 Interpolation-Extrapolation Procedure

ASHELF has been initialized by a simple interpolation technique of AFS large scale fields to first assess model performances without exploiting any information from coastal observations. AFS daily mean fields of temperature, salinity and velocity have been first vertically interpolated from the AFS 31 vertical σ levels to 75 flat levels in order to preserve the vertical water column structure, since the implementation of a high resolution topography in ASHELF model created a displacement of the σ layers, even maintaining the same vertical discretization.
Constant vertical extrapolation is applied at the surface, where the first σ layer value is brought at the surface. Moreover the new topography made necessary to extrapolate values in those points where the bottom value is deeper than AFS one.
Our approach takes into account the mean vertical water column structure in the Northern Adriatic Sea which exhibits an evident seasonal thermal cycle with a well-developed thermocline in spring and summer down to 30m depth (*Artegiani et al.*, 1997a) in the open waters and shallower in the near coastal zone. A threshold depth for extrapolation procedure equal to 20 meters has been defined under stratification conditions. Missing values shallower than 20 meters have been generated from AFS through a horizontal extrapolation technique that iteratively enlarges the field horizontally, averaging the available sea values. A constant vertical extrapolation has been applied for grid points deeper than 20 meters. This procedure assures to generate new bottom values preserving the vertical stratification.
The successive step has been the horizontal bilinear interpolation on the higher resolution grid where the mismatch of models coastlines, due to ASHELF better approximation of real coastline, required the same horizontal extrapolation procedure at the lateral boundaries. Lastly, fields on the ASHELF horizontal grid and on the 75 flat levels have been backward interpolated on the new ASHELF 31 σ levels.
Figures 4.3 and 4.4 display the result of the interpolation-extrapolation procedure of AFS fields (IAFS hereafter) compared to observations. Synthetic profiles have been extracted from IAFS fields on CTD space/time locations and then area averaged like observations.
The IAFS fields in Emilia Romagna area on May 5th (fig.4.3a) reveals unrealistic smoothen temperature and salinity profiles with a surface temperature bias on the order of $2C^{\circ}$ and a surface salinity bias of about $6psu$. Inside the Gulf of Trieste (fig.4.3b) and off Rovinj (fig.4.3), IAFS is still too mixed and

generally fresher. Rovinj salinity field shows on average a small misfit, less than $0.5psu$.
In summer case (fig.4.4a) vertical stratification is again less pronounced. IAFS temperature matches on average the observed value in Emilia Romagna, while it is fresher above the thermocline located between 10 and 15 meters in Trieste and Rovinj regions where it shows also a large positive bias on the bottom layer. IAFS salinity profiles present in all three areas a almost constant negative bias of about $1psu$.

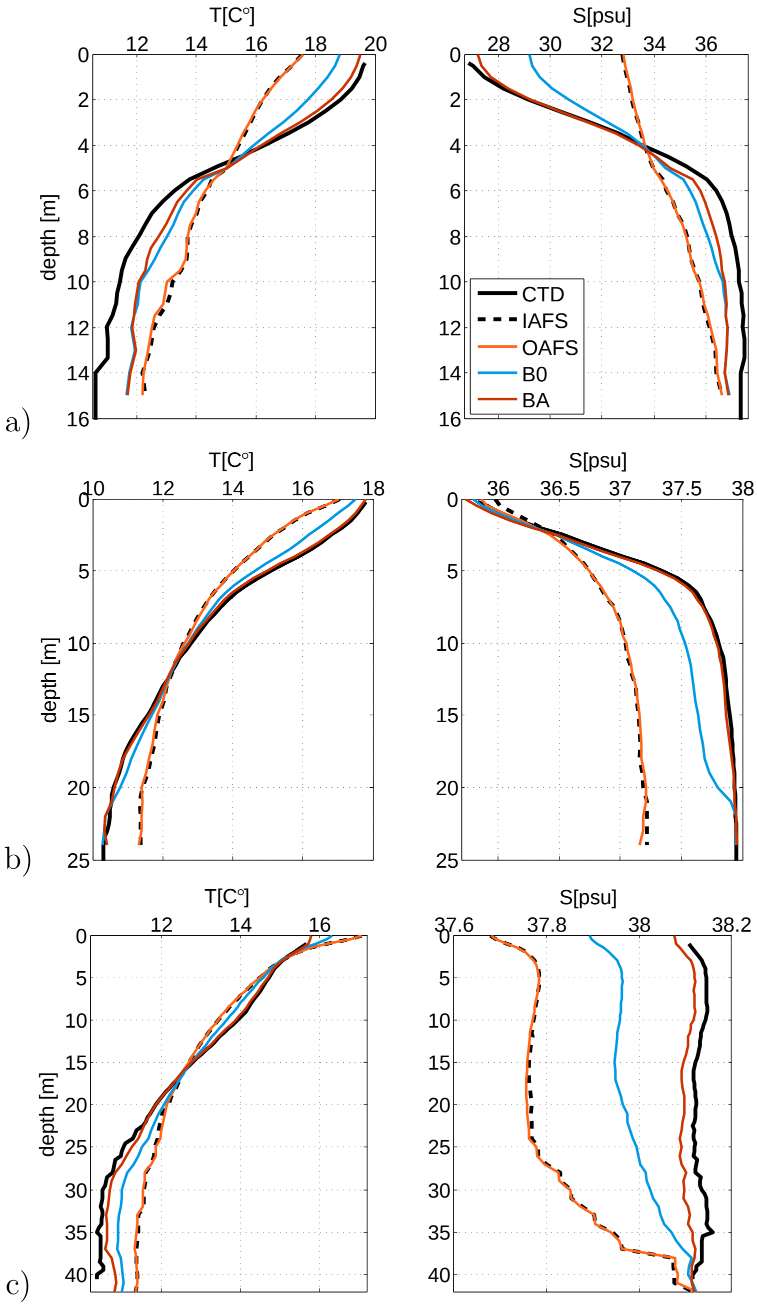

Figure 4.3: Initial condition area averaged profiles on May 5th: a) Emilia Romagna; b) Gulf of Trieste; c) Rovinj. Black solid line represents observations. Dashed black line stands for the synthetic profile from interpolated AFS (IAFS). OAFS is the OA result of AFS field mapped using B0 correlation length scales (see tab.4.2). B0 is OA result from blending AFS with observation using B0 correlation length scales. BA is OA result from blending AFS with coastal CTD using BA correlation length scales (see tab.4.3).

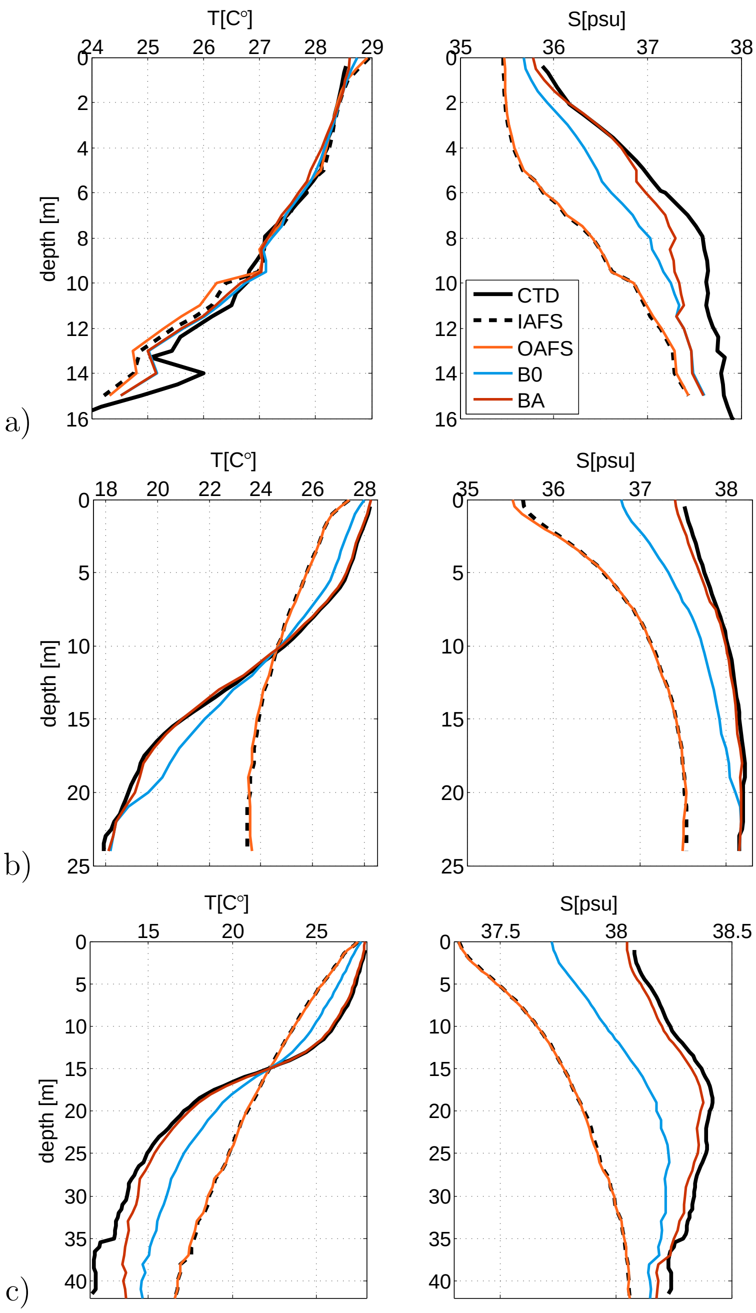

Figure 4.4: Initial condition area averaged profiles on August 11th. Details in fig.4.3.

4.4.2 Blending Large Scale Fields and Coastal Observations

IAFS initial has been corrected taking into account coastal temperature and salinity observations and blending them with AFS large scale field through the multi-scale optimal interpolation technique developed from *Mariano and Brown* (1992) who established a generalized approach for the objective analysis (OA) of non-stationary and dynamically heterogeneous fields via the "parameter matrix algorithm" (PM). This powerful algorithm allows to define different correlation lengths scales in different areas of the analysis domain and to subtract from observations a large scale trend, which are both fundamental issues in coastal areas where statistics and dynamics are far from being homogeneous and stationary.
Principal assumption in optimal estimation is that the statistics of the subject data field does not vary in the time interval and spatial domain considered and a practical approach to ensure it, is to decompose the data field (T_o) into three components:

$$T_o(x, y, t) = T_m(x, y, t) + T_e(x, y, t) + e_s(x, y, t) \tag{4.4}$$

where T_m is the contribution of the large scale or trend field (subscripted m for mean), T_e is the natural field variability, important on the mesoscale or synoptic time scale (subscripted e for eddy), and e_s is the combined effect of sub-grid scale noise and measurement error. The choice of the trend field T_m should make the mean value of T_e as small as possible and the field more homogeneous and isotropic. This method objectively interpolates just the deviations from the mean and the final field estimate is the sum of the large scale trend and the OA of the small scale deviation field. Moreover for each interpolation location only few influential de-trended data points are considered and their weighted average is also subtracted to remove local biases.
Another advantage of this technique comes from the possibility to assign different noise levels at different data sets if, for example, they were sampled from different instruments, or like in our case, if data are from observations on one side and from a numerical model on the other. Random errors e_s have zero mean and it is assumed that they are not correlated with one another and with the observed variable but have known variance. The numerical value of the error is given as a fraction of total field variance.
The PM algorithm uses a nine parameter, anisotropic, time dependent correlation model with correlation parameters that can vary in space and time. We used a simplified version of it which does not take into consideration

phase speeds.

$$C(dx, dy, dt) = \\ = C(1)\left[1 - \left(\frac{dx}{C(2)}\right)^2 - \left(\frac{dy}{C(3)}\right)^2\right] e^{\left[1-\left(\frac{dx}{C(4)}\right)^2+\left(\frac{dy}{C(5)}\right)^2+\left(\frac{dt}{C(6)}\right)^2\right]} \tag{4.5}$$

where:

- C(1) is the correlation at zero lag and equals one minus the normalized (by the field variance) measurement variance (which includes a subgrid scale component);
- C(2) and C(3) are the zero crossing scales in the east-west and north-south direction;
- C(4) and C(5) are the spatial decay (e-folding) scales in the east-west and north-south direction;
- C(6) is the temporal decay scale.

This correlation function can be rotated in space by an arbitrary angle C(7). PM algorithm consists on dividing the interpolation grid and data domain in even space-time bins, whose size depends on the correlation scales and how the correlation parameters change in space and time. Each bin contains one set of correlation parameters. We defined a parameter matrix, displayed in figure 4.1a, made by 3*3 space bins with a bin size of one degree.Data preparation (Pre-OA) was required before OA data injection because of the mismatch of model topographies. AFS data have been vertically interpolated on the pre-defined 75 standard z levels applying the previous interpolation-extrapolation approach for data deeper than 20 meters. In this case bottom missing values, shallower than 20m, would be generated from OA.
Observed CTD data have been checked at the bottom too. The deepest observed values were never at constant depths owing to sampling conditions, though we decided to assign the last temperature and salinity values to the nearest and deeper standard z level to prevent discontinuities in the bottom layer. Coastal observations sampled on initialization day have been considered as synoptic ad their sampling time have been set at noon, while AFS daily mean fields are centered at midnight. Estimation time is noon.
T_m has been estimated by least-square fitting of a two dimensional bi-cubic spline surface to the data and subtracted before OA since the area considered is dynamically complicated and AFS data, already gridded, ensure a good spatial coverage avoiding spurious oscillation (over-shooting). These least square finite element splines have adjustable smoothness (ρ) and tension (τ)

EXP	C(2)	C(4)
B0	0.4	0.25
B1	0.6	0.375
B2	0.8	0.5
B3	1.0	0.625

Table 4.2: List of blending experiments with homogeneous parameter matrix and isotropic correlation length scales expressed in degrees. C(2) is the zero crossing scale and C(4) is the e-folding scale.

parameter and allow variable data errors. The smoothness parameter, ρ controls the tradeoff between the fitness to the data and total smoothness. We chose a small $\rho(10^{-2})$ to have a smooth fit to the data which mimics a low pass filter, and a $\tau(0.99)$ close to 1 to avoid unrealistic values at the boundaries.
We associated a noise level of 0.16 to AFS field and of 0.03 to coastal observations that multiplied by the standard deviation of the considered field variability means an error level that ranges for AFS temperature between $0.05 - 0.25C^{\circ}$ and salinity between $0.18 - 0.25psu$. The noise level assigned to coastal observation stands for a measurement error ranging from $0.003 - 0.6$ for both temperature and salinity that matches quite well sensors specifications, verified during ADRICOSM inter-calibration campaign (*Celio et al.*, 2006).
We chose six influential data for each OA estimation point to limit the computational time. Since AFS data are already on a regular grid and highly resolved respect to CTD observations, OA technique would consider the nearest AFS points plus the nearest CTD observation, where available.
Correlation function parameters have been tuned to create the best data melding without smoothing out AFS field variability or high resolution coastal informations. We started defining a homogeneous parameter matrix and an isotropic correlation function where $C(2) = C(3)$ and $C(4) = C(5)$. C(1) is set to 0.98, the temporal decay scale is 2 days. The first experiment uses B0 correlation length scales listed in tab.4.2 that are in agreement with the ones estimated by *Jeffries and Lee* (2007) in the Northern Adriatic sea from a large historical data set. They computed covariance functions for weak and strong ambient stratification and found a zero crossing scale from 40 to 50 kilometers with shorter correlation scales during strong stratification.

The first step has been the OA of AFS data only (OAFS) using B0 length scales, to test our pre-OA and OA procedure versus the previous interpolation-extrapolation one (IAFS). The result correspond perfectly as

AREA	BIN	C(2)	C(3)	C(4)	C(5)	C(7)
ER	1	0.8	1.0	0.5	0.625	315
ER	4	0.8	0.8	0.5	0.5	0
RO	5	1.2	1.4	0.75	0.825	330
TR	8	0.6	0.6	0.375	0.375	0
others		0.4	0.4	0.25	0.25	0

Table 4.3: Heterogeneous Parameter Matrix (PM) defined for BA initial condition estimation. Each area, displayed in figure 4.1a and sorted by bin number, has its own set of correlation parameters. The other bins uses B0 correlation parameters as in table 4.2.

proven by IAFS and OAFS profiles that overlap in figures 4.3 and 4.4 in all three coastal areas, with the only one exception for the Gulf of Trieste (fig.4.3b and 4.4b), where OAFS surface salinity is fresher than IAFS because of the strong gradient generated from the Isonzo River plume that OA tend to slightly spread out having a wider influential range respect to IAFS procedure.
The second step has been the blending of AFS fields with coastal data using B0 length scales. The result brings B0 profiles closer to the observations, as can be seen in figures 4.3 and 4.4. We progressively enlarged the correlation scales in B1, B2 and B3 experimets, whose correlation lengths are listed in tab.4.2, assuming that the closer the blended field went to observations and more successful were our initial condition. This tuning process highlighted the necessity to define different correlation scales in the three areas to correct AFS, owing to the different sampling schemes which strongly influences the final solution, nonetheless the different topographies and local dynamics. The outcome of tuning process is BA initial condition field estimated using an heterogeneous PM, whose parameters, that vary from bin to bin, are listed in tab.4.3. BA temperature and salinity profiles are in all three regions very close to the observed ones. In Emilia Romagna the correction is not fully efficient on the bottom layer due to the sampling scheme which does not provide at those depths enough data to correct AFS fields.

The validation of the blending technique has been carried out by visual inspection using high resolution satellite sea surface temperature (SST) data collected within the framework of DOLCEVITA Project (Dynamics of Localized Currents and Eddy Variability in the Adriatic) and then elaborated by OGS (Istituto Nazionale di Oceanorafia e Geofisica Sperimetale, Trieste) (*Notarstefano et al.*, 2006). An example is shown in figure 4.5 for the Rovinj coastal area. Figure 4.5a is the satellite image for May 5th at 6.52AM, where

an upwelling front is evident along the Istrian coastal area which is totally absent in the IAFS corresponding SST field (fig.4.5b). CTD data have been mapped using B0 (fig.4.5c) and BA (fig.4.5e) implementations together with their corresponding blended fields, plotted in figure 4.5d-f. CTD data confirm the presence of a cold front close to coast.
B0 mapping corrects AFS SST field in a small area surrounding each observation which influences only the adjacent observations on the same transect. The resulting field is patchy and shows up the transect geometry. BA mapping uses a rotated correlation function to define a longer correlation scale parallel to the coastline and to enable observations on a transect to feel the effect of observations on the adjacent ones. The resulting BA initial condition (fig. 4.5f) is in good agreement with the satellite image and does not look patchy anymore.
Figure 4.6 shows BA initial condition for the Emilia Romagna region and the Gulf of Trieste together with the corresponding IAFS fields and observed maps. IAFS SST is colder than observations in both areas, but BA initial condition corrects it and brings it good agreement with satellite images (not shown).
Emilia Romagna observed map (fig.4.6) confirms the strong Po River fresh water influence detected from the mean salinity profile in fig. 4.3b. Po River fresh water heated up faster than sea water warming up all the coastal surface layer. BA generates a strong temperature gradient parallel to the shoreline. Inside the Gulf of Trieste IAFS has a cold plume in front the Isonzo River mouth that totally lacks in observations while warmer water characterizes the southern-central area. The observed temperature is even higher in the lower zone. BA smoothed the cold plume and creates a warm water pool in the deepest part of the basin.

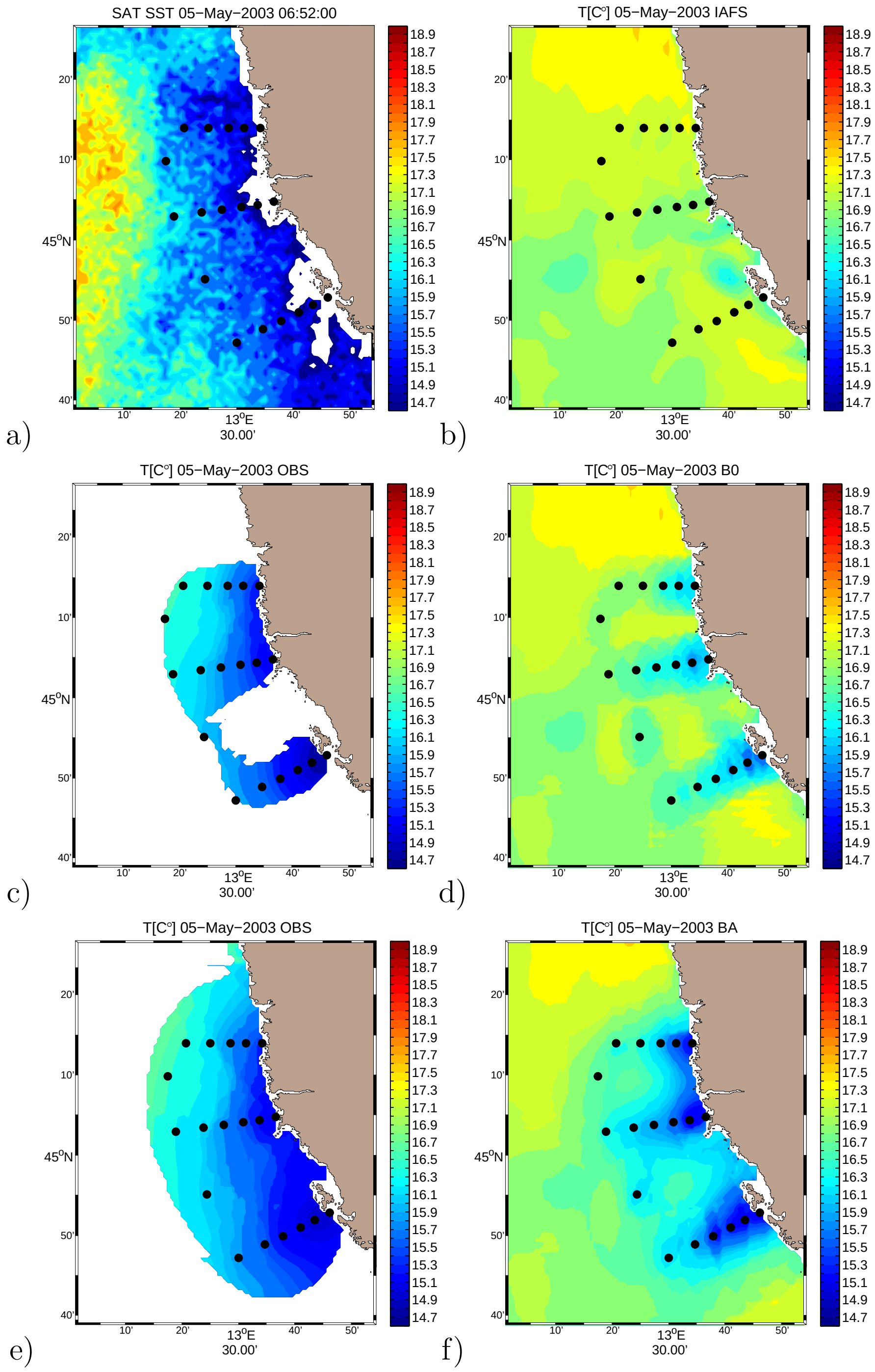

Figure 4.5: SST fields on May 5th for the Rovinj coastal area: a) satellite high resolution SST image; b) IAFS SST field; c) B0 observed SST; d) B0 blended SST; e) BA observed SST; f) BA blended SST. (SST fields have been masked for mapping error greater than 30%)

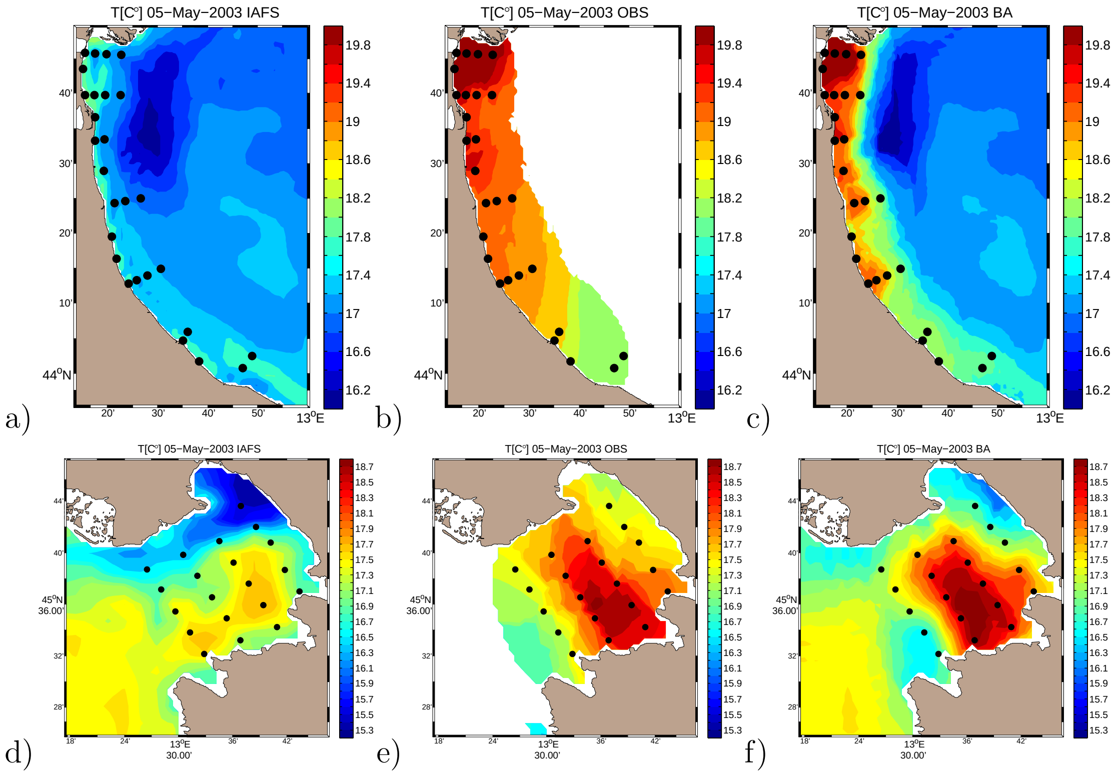

Figure 4.6: SST fields on May 5th for the Emilia Romagna coastal area and the Gulf of Trieste. a) Emilia Romagna IAFS SST field; b) BA observed SST; c) BA blended initial condition SST; d) Gulf of Trieste IAFS SST; e) BA observed SST; f) BA blended SST. (SST fields have been masked for mapping error greater than 30%)

4.5 Coastal REA Experimental Design

The CREA experimental design originates from the fundamental hypothesis that exploiting coastal observations to correct large scale IC of a high resolution numerical model would highly improve our short range predictive capabilities in the coastal environment. We chose two different periods to test this hypothesis, the first at the beginning of May (spring experiment) and the second in middle August (summer experiment), looking at the availability of all coastal observation in the initialization day (IC Day) and one week later (REA Day) to validate model results and verify our predictive skills after one week of simulation. This two test cases would strengthen our outcome since IAFS IC fields have different initial skills and simultaneously

ASHELF must face different ambient conditions and dynamics.
The first case named D (from downscaling), as depicted in fig.4.7 starts from IAFS and it is carried out first applying ECMWF atmospheric forcing (DE) and then LAMI higher resolution forcing. The second case, named B (from blending) starts from BA IC. The third case, named SU (from spin up), would start a certain time in advance from IAFS to spin up the smaller scales of the circulation allowed by the increased resolution and run till IC day when ASHELF is re-initalized blending its temperature and salinity fields with observations using the same BA mapping approach. We defined the required spin up time through a dedicated experiment presented in the next section.

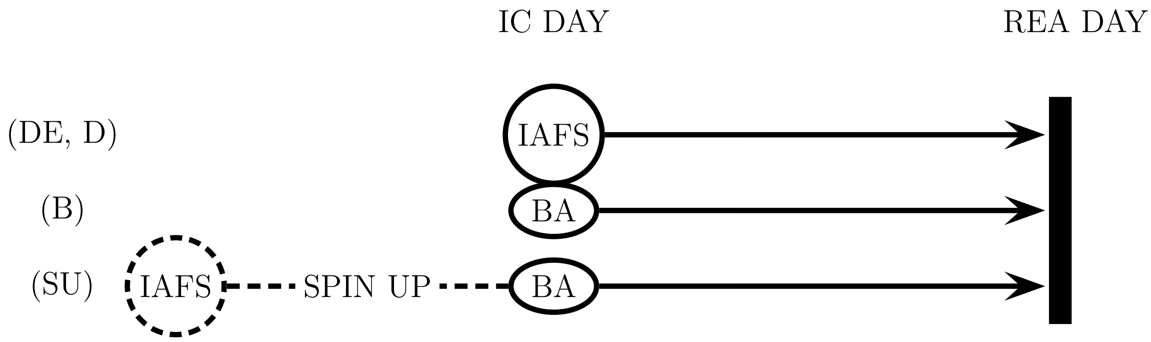

Figure 4.7: CREA initialization and forecast procedure.

4.5.1 Spin Up

The spin up time is the time needed by an ocean model to reach a dynamical balance with its forcings. Spin up evaluation is a critical issue in short range prediction and rapid assessment of coastal environment where nested modeling systems allow to reach very high resolution through a successive downscaling process of boundary conditions. Initial and lateral boundary conditions provided from parent models are in dynamical balance with the applied forcings but the child model would need a certain time to generate new circulation features enabled by the increased resolution. *Gaberšek et al.* (2007), reviewing different spin-up strategies, defined this approach a kind of "cold start".
The objective is to understand how log ASHELF takes to reach this new

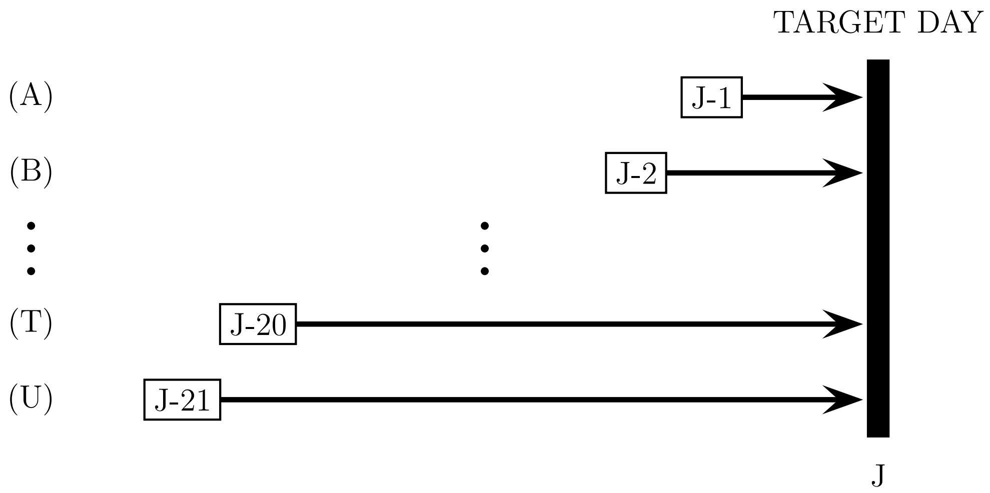

Figure 4.8: Spin Up experiment diagram.

dynamical equilibrium and settle at a higher energetic level with a different method from previous studies. A dedicated experiment has been performed fixing a target day (J). We run ASHELF 21 times up to J, starting at sequential days, from day J-1 (A) till day J-21 (U) as described from diagram in figure 4.8. ICs are from IAFS. This experimental design permits to analyze 21 ASHELF realizations of the same day. We calculated ASHELF Total Kinetic Energy (TKE):

$$TKE = \frac{1}{VOL}\int_V \frac{(u^2+v^2)}{2}dxdydz \tag{4.6}$$

at the target day for the 21 realizations and the corresponding AFS TKE on ASHELF domain to study the ratio between the two.

We repeated the experiment 2 times considering as target days our initialization days, May 5th and August 11th, to evaluate different ambient conditions and obtain more general results.

Figure 4.9a illustrates the ratio between ASHELF and AFS TKE level as function of time of integration for the two target days. Both cases exhibit a similar behavior. Initializing ASHELF at J-1 (A) results in a TKE ratio value smaller than one, indicating that our initialization procedure induces a sort of inertia, probably due to the use of AFS daily mean fields instead of snapshots. ASHELF rises to AFS TKE value after two days of integration (B) and then increases until it reaches a plateaux when intergration time overtakes 7 days (G). The two curves adjust to different energetic levels owing to the external forcing regime on the corresponding target day, with highest value over 1.5 on the 11th of August.

We further investigated model behavior related to the time of integration comparing model temperature and salinity to observed CTD profiles in the three coastal areas. Temperature and salinity RMSE have been estimated between each model realization and observed data with the aim to understand if model results improve as function of spin up time. Area averaged RMSE have been calculated extracting ASHELF synthetic profiles on space/time CTD locations through equation 4.7:

$$RMSE = \sqrt{\frac{\sum_{ij}(\theta^{m}_{i,j} - \theta^{o}_{i,j})^2}{N}} \tag{4.7}$$

and the results for Emilia Romagna coastal area on target day, May 5th, are plotted in fig.4.9b-c. An exponential reduction of RMSE for both ASHELF temperature (b) and salinity (c) occurs if ASHELF is initialized from one (A) up to seven (G) days in advace, while results keeps constant for longer integration times. Temperature improvement after a week of spin up is on the order of $0.3C^{\circ}$ while salinity improvement is about $0.7psu$, suggesting that one week of model spin up might highly improve our simulation in Emilia Romagna coastal area on the target day.
Salinity response in the other coastal areas and on the summer target day (not shown) is similar with a progressive reduction of RMSE as function of model spin up time of about 11% after 7 days and 15% after 14 days.
Temperature RMSE on May 5th in Rovinj and Trieste does not follow the same trend but it oscillates around the same value for a spin up time less than 14 days and it grows for longer integration times. In the summer case Rovinj area temperature RMSE is not sensitive to spin up time while Emilia Romagna and Trieste do not reveal any tendency.
ASHELF salinity reaction can be addressed to a more precise river outlets positioning and the introduction of new river discharge data respect to AFS, which determines the initial error level. Temperature behavior instead cannot be generalized since any new model parameterization has been introduced and the atmospheric forcing applied is the same. The Emilia Romagna exception (fig.4.9b) can be addressed to the Po River temperature signal introduced into the surface heat flux that highly ameliorate the model results in one week of spin up with the effect of warming up the surface layer strongly influenced by fresh water input.
Evaluation of the model energetics demonstrate that for the Northern Adriatic Sea and for the forcing considered, a spin-up period of one week allows the total kinetic energy to reach equilibrium with the higher resolution nested model simulation results. Moreover the comparison with observations indicates that temperature and salinity results might improve after 1 week of spin up owing to a better representation of river runoff or the introduction of Po river temperature, more than the addition of small scale features which,

on contrary might magnify phase errors due to feature displacement. Salinity common trend demonstrate its more conservative behavior regard to temperature, whose forcing act on much smaller temporal scales.

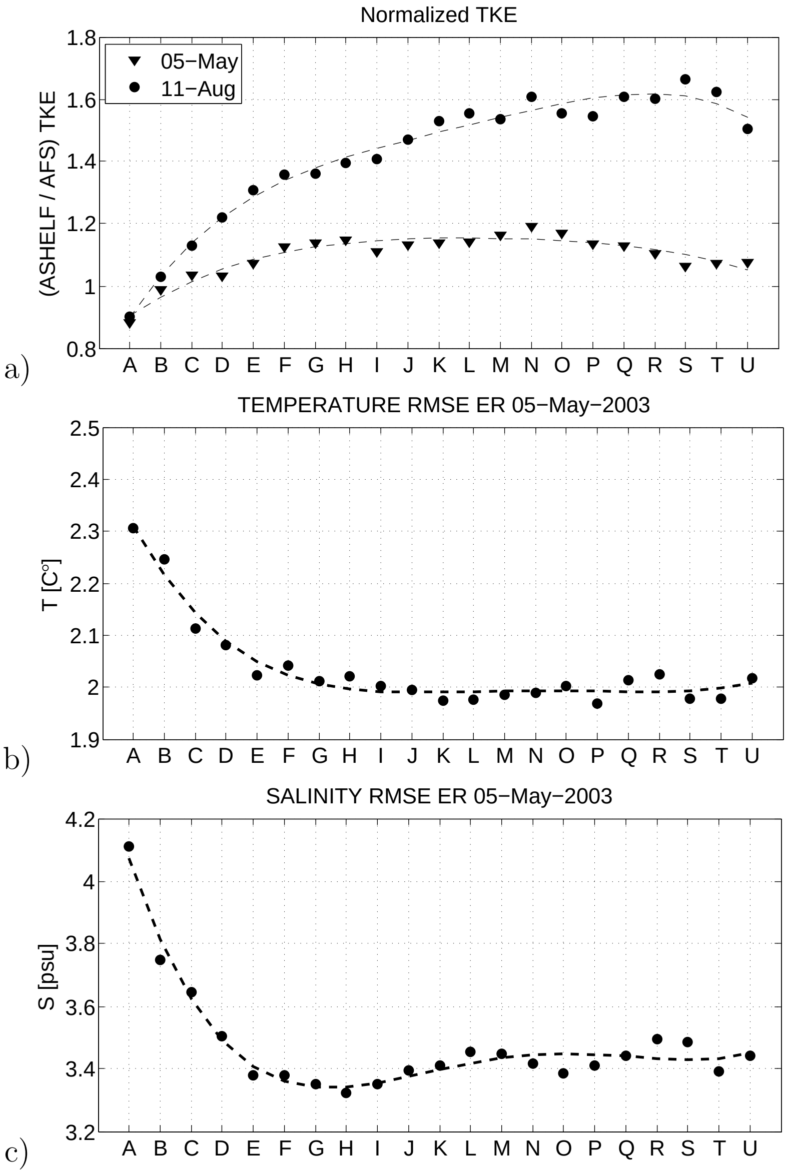

Figure 4.9: (a) Total Kinetic Energy ratio between ASHELF and AFS calculated on target days, May 5th and August 11th. (b) Temperature RMSE (c) salinity RMSE calculated on day May 5th for the Emilia Romagna area.

EXPERIMENT	RMSE	AFS	DE	D	B	SU
Emilia Romagna						
Spring	T	2.3	2.2	2.1	2.0	2.0
	S	3.4	3.2	3.2	3.0	3.0
Summer	T	0.9	0.8	0.7	0.8	0.7
	S	1.1	1.0	1.1	0.9	0.9
Gulf of Trieste						
Summer	T	2.4	2.1	2.0	1.5	1.5
	S	1.7	1.3	1.0	0.6	0.5
Rovinj						
Spring	T	1.0	1.0	1.0	0.8	0.8
	S	0.5	0.5	0.4	0.3	0.3
Summer	T	3.4	3.5	3.6	2.6	2.6
	S	0.8	0.8	0.6	0.4	0.3

Table 4.4: RMSE calculated from AFS and CREA Summer and Spring experiments. AFS and DE have been forced by ECMWF atmospheric data, while the others consider LAMI high resolution forcing.

4.6 Results

CREA results have been evaluated extracting synthetic profiles from ASHELF on CTD space/time location and computing the area average profiles for temperature and salinity in the three coastal zones. Only most significant cases were plotted in figures 4.12 and 4.13 while tab.4.4 lists all the RMSE.
DE in general reproduces AFS result and enhances it in the Gulf of Trieste in terms of RMSE. In Emilia Romagna the synthetic profile (not shown) presents a more realistic shape owing to ASHELF better representation of topography respect to AFS. It reduces AFS negative temperature bias and salinity positive bias at the surface, but without a consistent RMSE reduction. Inside the Gulf of Trieste *DE* is colder at the surface but is doing much better below the thermocline reducing AFS positive bias of $1C^{\circ}$. Salinity bias extremely decreases too in particular at the surface. In the Rovinj coastal area *DE* tends to be colder at the surface (upper 15 meters) and warmer at depth but, on average, both models produce the same RMSE.
Introducing LAMI atmospheric forcing (D) ameliorates temperature in Emilia Romagna, salinity in the Rovinj coastal area and inside the Gulf of Trieste. In Emilia Romagna, D establishes a warming of the overall water column of approximately $0.5C^{\circ}$ thus getting better at the surface but not on the bottom layer. In the Gulf of Trieste the salinity bias further reduces of a 50%. D

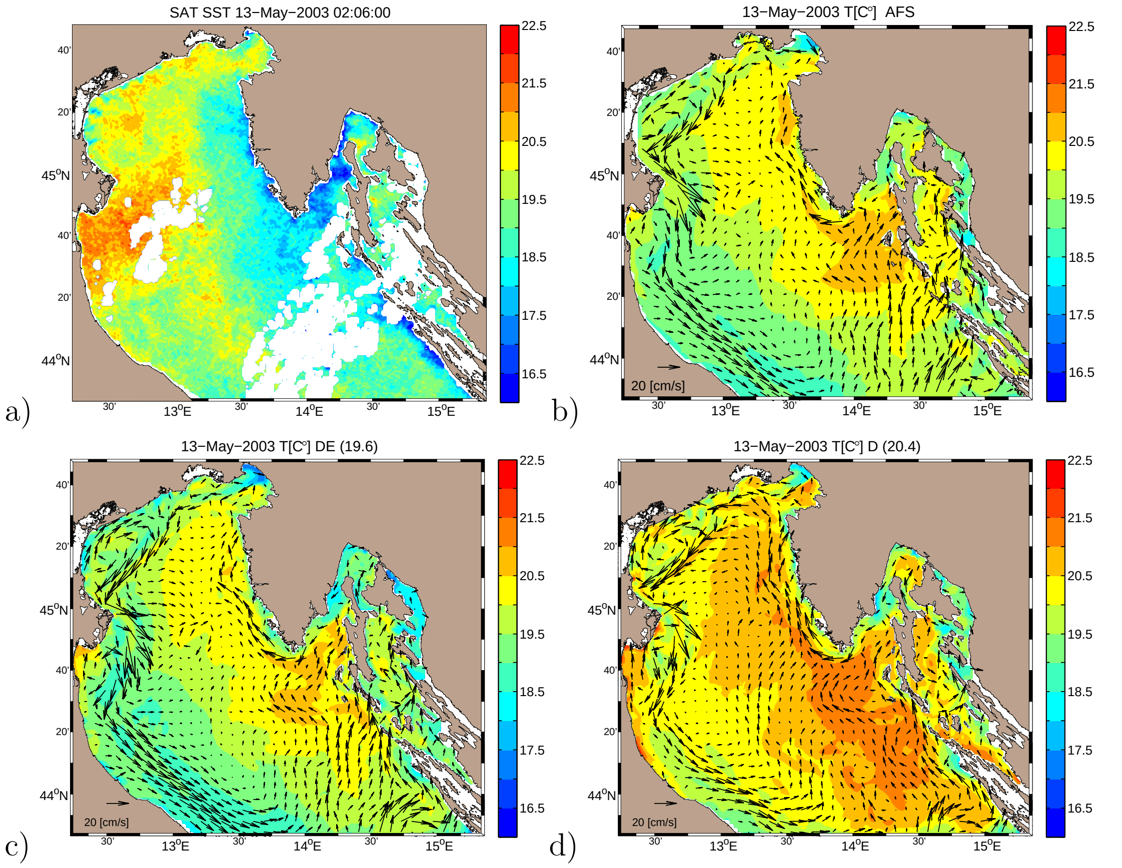

Figure 4.10: SST maps on May 13th: a) Satellite SST image; b) AFS daily mean SST field and currents. ASHELF SST and currents after one week of simulation from the Spring CREA experiment starting May 5th: c) forced by ECMWF (DE); d) forced by LAMI (D).

corrects the *DE* surface temperature bias in Rovinj but it rather warms up the bottom layer respect to AFS. Contemporary it reduces surface salinity bias up to the 50% in summer CREA.

Maps in figure 4.10 show ASHELF results from spring CREA on May 13th compared to a the satellite image at nighttime (a) and to SST and current velocity fields generated from AFS (b). After one week of simulation *DE* (c) reproduces almost the same temperature and velocity pattern of AFS but with a colder water belt all along the coastline. The only exception is Emilia Romagna coastal area just below the Po River delta, where an anti-cyclonic vortex, observed also in *Montanari et al.* (2006), confines warmer waters of river origin. This warming confirms the positive effect of Po river temperature implementation in ASHELF that determines lower temperature RMSE.

The heat flux correction term introduced at the Po River mouth is though not enough to reproduce the observed warm plume displayed in the satellite image (a). D (d) generates similar SST and currents patterns but with a general increase of SST that resembles observations only on the Italian side of the Northern Adriatic basin. Current field exhibits an intensification of the EAC off the Istria peninsula and a weakening of the WACC. A common circulation feature is the anti-cyclonic gyre settling north of the Po River delta, just in front the Venice Lagoon.

Salinity maps for August 18th (figure 4.11) put on evidence a different ASHELF salinity and current patterns after a week of simulation from the corresponding AFS one. The significant improvement of salinity result inside the Gulf of Trieste can be addressed first to the changes in the circulation caused by both ASHELF higher resolution topography and more accurate river data (*Malačič and Petelin*, 2009). AFS (a) and *DE*(b) both reproduce the ICCC consistently with numerical results from *Zavatarelli and Pinardi* (2003). In AFS the ICCC is part of an anti-cyclonic meander which ends at the entrance of the Gulf of Trieste where the current bifurcates partially entering the Gulf in its southern side and partially turning west along the italian coast. In *DE* (b) the anti-cyclonic meander ends southern respect AFS and the bifurcation of the current driving north does not enter the Gulf, but it drives south fresh waters that belong to Tagliamento river and the Marano/Grado lagoons. ASHELF salinity results further improve when LAMI forcing is applied (c), since it better resolves the spatial variability of north-easerly wind that blew on August 16th and 17th, in particular the Trieste and the Senj Jets (*Dorman et al.*, 2007), influencing the circulation in the north-east area. Figure 4.11c shows how the Trieste Jet pushes and keeps the fresh water towards the northern coastal strip, strengthening the coastal current. The ICCC looks weaker since the anti-cyclonic gyre shrank and weakens. An anti-cyclone delineates again in front of Venice Lagoon still confining fresh water towards the lagoon. The WACC is more intense and moves towards the Emilia Romagna coastal area in front of the Reno River mouth where it deviates back offshore following the bathymetric slope.
Next we present the results of BA initialization for CREA experiments in which ASHELF has been forced by LAMI (fig. 4.12 and 4.13)

4.6.1 Spring CREA Experiment

In Emilia Romagna (fig. 4.12a) B slightly improves temperature bringing the area average profile closer to observations between 5 and 12 m, while salinity profile exhibits a surface value reduction on the order of 0.5 psu, even if observed salinity is still far away fresher. Salinity surface bias is 4 psu. In

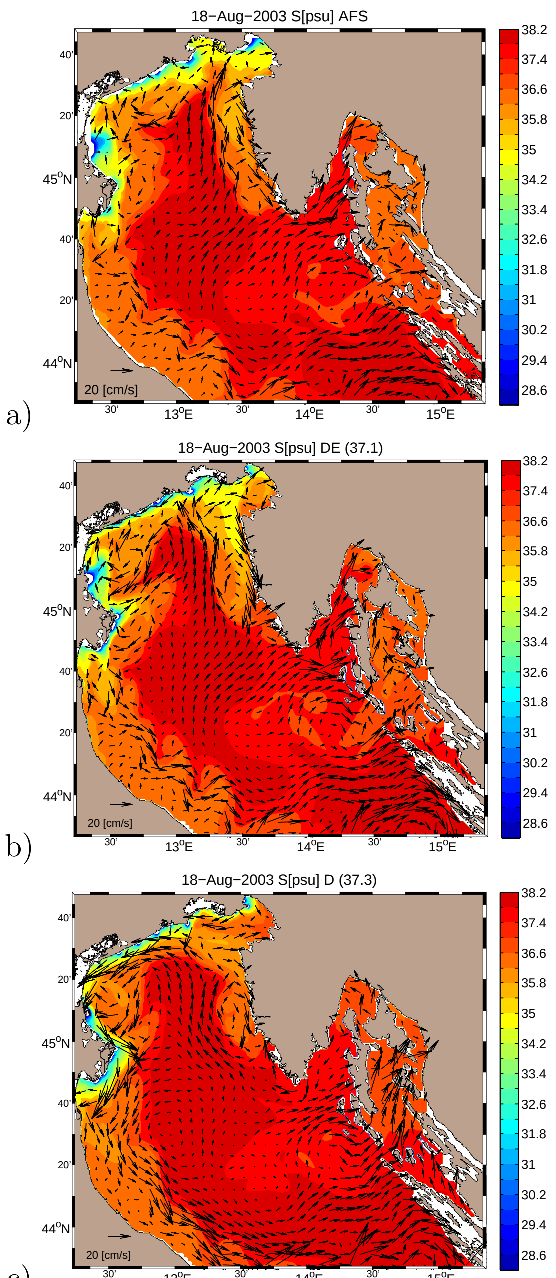

Figure 4.11: Model results after one week of simulation from the Summer CREA experiment starting August 11th. a) AFS salinity daily mean field and currents; b) ASHELF salinity daily mean field and currents forced by ECMWF (DE); c)ASHELF salinity field and currents forced by LAMI.

this area our blending procedure could not bring the AFS temperature and salinity values close to observations below 5 m because of the scarce number of samples reaching this depth and this partially affected our predictive skill below the thermocline. While temperature reproduces the spring surface warming, salinity misrepresents the freshwater signal. Looking at model outputs during the simulation time period we noticed that waters fresher than 30 psu vanished after three days of simulations. This suggests at first that our approximation of rivers salinity equal to 15 psu is not appropriate to predict Emilia Romagna coastal waters.

In Rovinj coastal area (fig. 4.12b) B temperature profile overlaps the observed one up to 15 meters depth, while below it reduces of $0.4C^{\circ}$ the AFS and D biases. B salinity profile establishes a significant enhancement in all water column. The small enhancement of both salinity and temperature in the bottom layer suggests again the ineffective correction capability of our technique due to the insufficient number of observations together with a bottom water advection effect.

The enlargement of correlation length scales as function of depth in OA procedure could have had a positive effect but the resulting scales would have been not realistic. Moreover, enlarging information from few observed points to the overall area would have not been statistically significant.

The third CREA exercize (SU), in which ASHELF spins up one week before blending its temperature and salinity fields with coastal observations did not improve the B predictive skills.

4.6.2 Summer CREA Experiment

Temperature predictive skill has not been affected from B initialization in Emilia Romagna coastal strip (fig.4.13a), while salinity that in D case worsened, got back closer to the observed profile, still presenting a surface small positive bias.

Inside the Gulf of Trieste (fig. 4.13b) B determines a big improvement since it allows to correct the totally lack of stratification of AFS IC, which ASHELF in this case can partially sustain during the week of simulation. The mean temperature RMSE decreased of a 40%. B salinity further ameliorate D outcome with a misfit reduction of 0.8 psu. Salinity RMSE decreased of a 65% respect to AFS and of the 40% respect to D.

B in Rovinj area (fig.4.13c) can reproduce to a certain extent the strong thermal stratification, rather sustaining warmer waters above the thermocline, located at 15 m depth, and colder waters below. Temperature RMSE reduced of about a 30%. B salinity misfit diminished uniformly of 0.2 psu

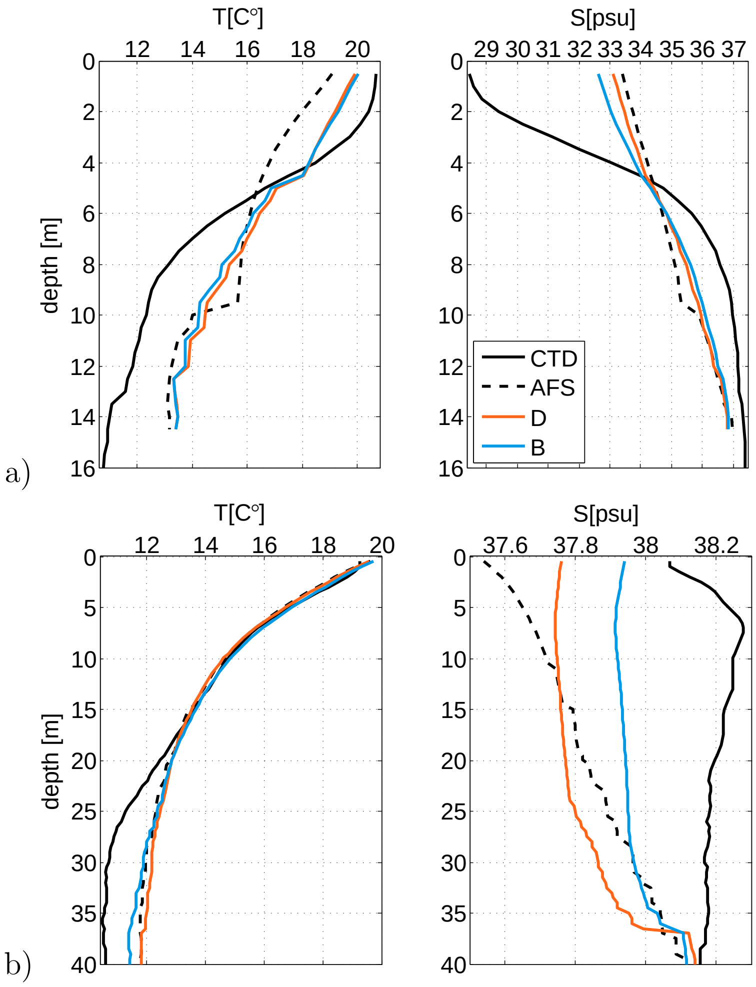

Figure 4.12: Model results from the Spring CREA experiment starting May 5th. a) Emilia Romagna on May 12th; b) Rovinj coastal area on May 13th.

respect to D, with a general RSME decrease of the 50% respect to AFS. Summer CREA SU exercise results have been included in figure 4.13 since small improvement have been noticed from RMSE values in table 4.4. Inside the Gulf of Trieste and in the Rovinj area salinity profile got closer to the observed one in the upper 15 m of the water column, confirming the outcome of the spin up experiment, that the new river data in these areas ameliorates our predictive capabilities.

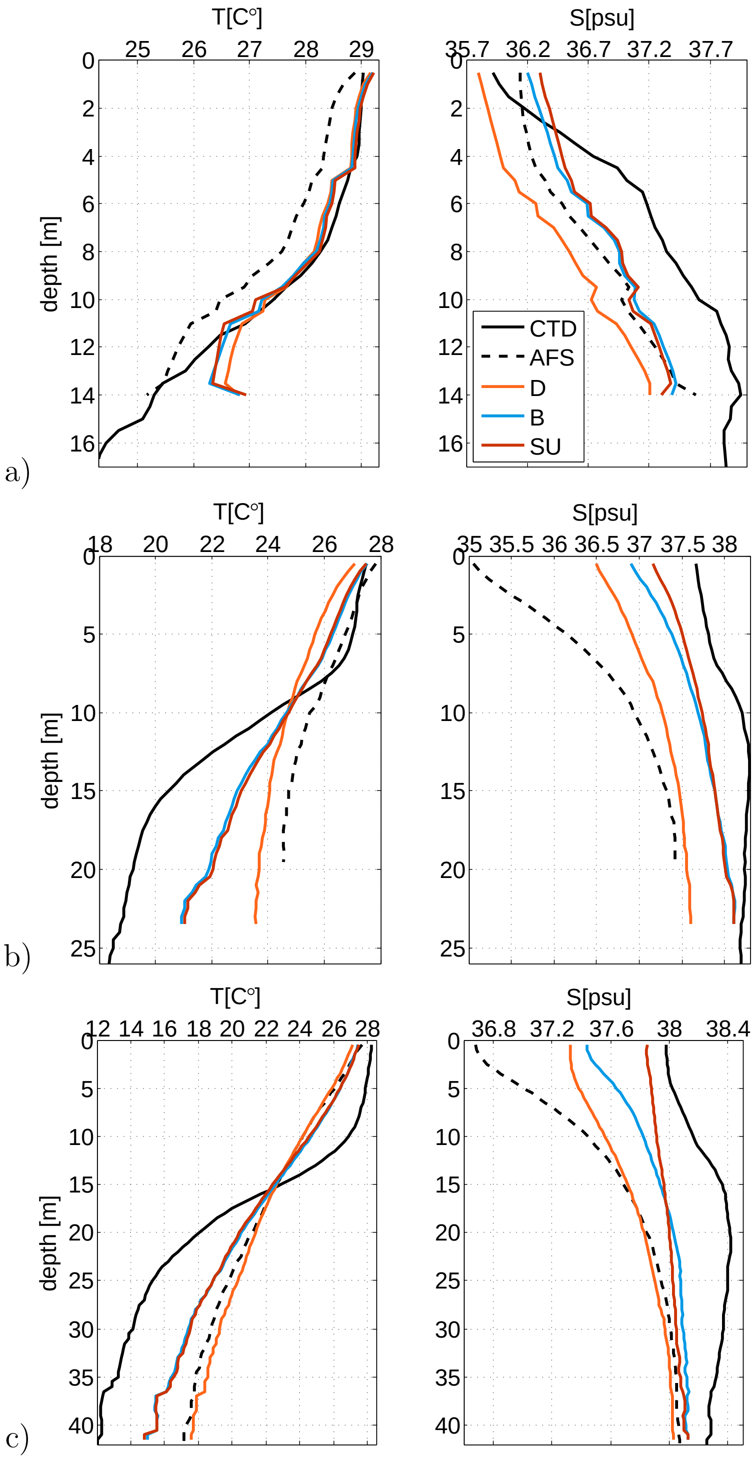

Figure 4.13: Model results after one week of simulation from the Summer CREA experiment starting August 11th. a) Emilia Romagna; b) Gulf of Trieste; c) Rovinj.

4.7 Summary and Conclusions

CREA exercises in the Northern Adriatic sea demonstrated that a coastal OOPS based on an operational forecasting system and coastal observational networks of opportunity can increase out predictive skills in the relative coastal areas. Unfortunately the lack of more extended observational data sets did not allow the system verification in other parts of the domain.
The interpolation/extrapolation procedure, which takes into account the mean water column structure and the ambient stratification, successfully allowed to reproduce or slightly improve AFS temperature and salinity results. This proves, at the same time, that ASHELF nesting within AFS has been correctly implemented. The spin up experiment reinforces these outcome. The experiment has been designed to start from 21 successive days in two different periods of the year characterized from completely different ambient and dynamical situations. The initialization procedure was always effective. The comparison of many ASHELF realizations with observations on the target days, supports the effectiveness of the nesting technique in downscaling AFS circulation features and producing coherent results. It further indicated a salinity error reduction after a 7 days period of spin up. Salinity is in fact a conservative tracer and its forcing acts on long time scales determining a clear positive trend when higher quality river or precipitation data are introduced. Temperature result is not much influenced by the spin up time, except for the Emilia Romagna spring case, where the inclusion of a Po river temperature signal in the surface heat flux computation could partially correct the initial cold bias within the surface layer after 7 days of spin up.
River temperature effect came out to be a necessary requirement to successfully simulate the Northern Adriatic during spring time, in particular the Emilia Romagna region, highly influenced from the Po River. Po River warm plume observed from satellite images misses in our simulations, meaning that, our first attempt to reproduce it, was not fully effective.
High resolution atmospheric forcing (LAMI) improved ASHELF predictive skills, better resolving the spatial variability of the wind, specially Bora wind. Our quantitative results have been also confirmed from the analysis of temperature, salinity and currents maps. We could in fact detect circulation features, like the ICCC, consistent with the known characteristics of the Northern Adriatic.
Blending initialization technique, based on *Mariano and Brown* (1992) OA scheme, was effective in correcting AFS fields with coastal observations. The higher quality of blended IC allowed to predict temperature and salinity after a week reducing AFS error to a significant extent. The average spin up time of 7 days suggested from energetic considerations, fits perfectly our CREA

experimental design, tailored on a weekly sampling frequency. In fact, a preliminary spin up time before model-data fusion (SU experiment), positively affected only salinity in the Gulf of Trieste and in Rovinj coastal area during summertime, when meso-scale dominates the circulation pattern.

Emilia Romagna is the area where CREA succeeded less. The reason might be the very high space/time variability that characterizes this very shallow area subject to the direct influence of Po River and of the WACC. Here we face "uncertainty cascade" (*Ferreira-Coelho and Rixen*, 2008) problem where numerical model uncertainty due to unresolved processes (tides, waves) or sub-grid scale noise, sum up with atmospheric forcing uncertainty and the lack of boundary observations, like daily minor rivers outflow and temperature. Another issue is the effectiveness of the sampling scheme which is not optimal for CREA, since it should include stations far off shore that would allow to better resolve the bottom layer and the transition zone between the WACC pathway and the shoreline. This area is characterized from strong gradients parallel or perpendicular to the shoreline in function of the dynamical regime. Adaptive sampling methodology might be particularly helpful since it permits to optimize the monitoring efforts, maximizing ASHELF results and rendering the monitoring activity more sustainable.

This work wanted to demonstrate the feasibility of a CREA system based on an operational regional forecasting system and coastal monitoring networks of opportunity. As a first attempt we used temperature and salinity from ADRICOSM observational system to assess our predictive capabilities and to show that weekly coastal monitoring activities, like the one carried out operationally from ARPA Emilia Romagna, are desirable to implement a CREA system able to support coastal environment management activities and needs. Future development will consider the assimilation of current velocity observations and biochemicals, like nutrients, to rapidly assess the coastal environment in the future with the necessary multi-disciplinary approach.

Chapter 5

Conclusions

A new Coastal Rapid Environmental Assessment (CREA) strategy has been developed and successfully applied to the Northern Adriatic Sea. CREA strategy exploited the recent advent of operational oceanography to establish a CREA system based on an operational regional forecasting system and opportunity observations from coastal monitoring networks. The methodology wishes to initialize a coastal high resolution model (ASHELF), nested within an coarser resolution operational forecasting system (in our case AFS), blending the large scale AFS operational analyses with the available coastal observations to generate the best initial conditions and produce short range forecast in the near coastal area of the Northern Adriatic Sea.
Our main objective has been to set up a methodology to reduce forecast uncertainty in the coastal area using opportunity observations. Accurate nowcasts and forecasts are designed to support coastal operational and management activity effectively.
CREA system implementation followed three main phases covered in the three main chapters of the thesis.

The first *Descriptive phase* was meant to study the hydrodynamic properties of Emilia Romagna (EMR) coastal area through statistical analysis of the unique historical data set collected by the local environmental protection agency (ARPA EMR), during its weekly operational monitoring activity in the coastal strip. EMR operational monitoring system is one of the coastal networks of opportunity that we exploited in CREA system development.
Monthly climatology of basic hydrodynamic parameters like temperature and salinity have been mapped to characterize their spatial distribution and seasonal variability. A quality control procedure based on monthly climatology has been set up to check measurements in real time and improve future data archiving. Seasonal variability of the water column indicates a persistent am-

bient stratification, at monthly time scales, sustained by the direct influence of the Po River and amplified by the onset of the seasonal thermocline during spring and summer. Making the hypothesis of buoyancy-inertia balance, we estimated monthly geostrophic currents and consequently elaborated a schematic of the climatological circulation. This approximation ends up to be valid particularly during periods of low vertical mixing, thus weak wind regime (spring-summer).
EMR is part of Adriatic shelf region of fresh water influence (ROFI). ROFI characteristics fit our classification of the EMR coastal area into three zones. Zone A, in the northernmost part of EMR coastal strip, presents the highest time/space variability due the direct influence of Po river. Zone A is characterized prevalently by anti-cyclonic circulation. The frequent isolation of this embayment area, lee of the Po River delta, from the dynamics interesting the rest of the coast, is perhaps the most interesting aspect of our analysis and it permits to explain its enhanced environmental criticality.
Zone C, in the southernmost EMR coastal strip, shows predominantly temperature and salinity gradients perpendicular to the coast that sustain the coastal current (WACC) heading south along the italian shoreline.
The central zone B exhibits transition characteristics between zone A and C where the current is on average directed towards the coast and it may favor downwelling phenomena.

The second *Dynamical phase* regarded the implementation of ASHELF model in the Northern Adriatic embedded into an operational modeling system consisting of the MFS in the outer domain and the AFS in the intermediate domain. Two preparatory simulations have been performed in spring and summer 2003, results of a model calibration process, to test ASHELF set up, the nesting procedure and the rapid initialization procedure which interpolate/extrapolates AFS large scale daily fields into ASHELF grid. ASHELF and AFS models, that are forced by the same atmospheric data from ECMWF, have been validated by an extensive pool of satellite and in situ observations with the final result of a successful implementation of ASHELF model and the nesting technique. ASHELF increased resolution was not sufficient to improve model results versus AFS, that represents our reference level. ASHELF and AFS present on average same temperature and salinity predictive skills and we may ascribe it to the occurrence of phase type errors that are more probable when new high resolution circulation features are introduced by the enhanced resolution. ASHELF shows respect to AFS a major realism in the near coastal area thanks to the introduction of a high resolution topography and new rivers data.

In the third *Predictive phase* we presented two weekly CREA experiments for spring and summer 2003 when the three coastal zones of opportunity were synchronously monitored. During this phase we also evaluated the impact of high resolution atmospheric forcing (LAMI) on the ASHELF forecast skill. The blending initialization technique adopted, based on Objective Analysis technique (*Mariano and Brown*, 1992), was effective in correcting AFS first guess fields with coastal observations and allowed to predict temperature and salinity reducing AFS error, considered our reference skill, to a significant extent. A seven days spin up time, suggested from energetic considerations, fits perfectly our CREA experimental design tailored on a weekly sampling frequency. Conversely a preliminary spin up, before model-data fusion did not increase substantially our predictive capabilities. CREA succeeded less in EMR coastal area due its high space/time variability induced by the direct influence of Po River, the Western Adriatic Coastal Current (WACC) and winds. ASHELF uncertainty, due to unresolved processes, and a sampling scheme, not optimal for CREA, might be the main reasons.

5.1 Future Developments

This work is a preliminary step towards the operational implementation of a CREA system that can sustain local environmental protection agencies in the management of the coastal zone and a rapid response to environmental emergencies.

The further development of CREA must consider different aspects. First the observing network should be optimized in order to reduce the error in the initial condition of the forecast. OSSE (Observational System Simulation Experiments) methodology can be applied to answer this question. The implementation of new operational coastal monitoring systems is desirable in the prospective of a sustainable coastal zone management demand. The emerging methodology of adaptive sampling (*Lermusiaux*, 2007) is also useful in predicting the type and location of observations that are expected to be most useful, based on a given estimation objective and the available resources.

The modeling system can be ameliorated introducing new processes necessary to model the coastal environment, like tides and waves. The collection of new river data on daily basis is advisable since they are fundamental to enhance our predictive capabilities in near coastal areas.

Adaptive modeling approach can be pursued too during the tuning and caibration of the numerical model. *Lermusiaux* (2007) suggests a definition of model functionals and parameters that quantitatively learn from observa-

tions and evolve with data as they are collected. Model properties that need to be improved are identified through model-data misfit. A model property is thus said to be adaptive if its formulation, classically assumed constant, is estimated or variable as function of data values.
Moreover adaptive schemes based on ensemble of simulations which use different models, model structures or parameters may be applied to get better predictive skills. Multi model hyper-ensamble forecasts (*Rixen et al.*, 2008) exploit the power of an optimal local combination of available information including ocean, atmospheric and wave models to obtain superior forecasting skills when compared to individual models because they allow for local correction and/or bias removal.
The presented CREA approach may finally extend from temperature and salinity to other parameters, like currents velocity, and bio-geo-chemicals to fully assess the coastal environment with a multidisciplinary intent.

Appendix A

Northern Adriatic River Data

River discharge data considered in ASHELF has been extracted from different climatological data sets. Most of the Italian rivers data comes from *Raicich* (1994), except for Isonzo that together with Dragonia and Mirna, have been taken from *Malačič and Petelin* (2009). Croatian river data are from *Pasaric* (2004). Table A.1 lists the fresh water source points defined in ASHELF model and their relative outflow in m^3/sec. *Raicich* (1994) data set comprehends many outflow rates grouped according to the location of hydrologic basins like some Italian northern coast rivers originating from the Alps or some eastern coast rivers rising from the Apennines. River discharge in the coastal area between Marecchia and Tronto (not included) minus Foglia has been divided between Marecchia and the main hydrographic basins in the Marche Region (Tesino, Aso, Ete Vivo, Tenna, Chienti, Potenza, Musone, Esino, Misa, Cesano, Metauro) to define Marecchia flow rate. The discharge estimated into the plain between Po and Marecchia has been divided between rivers Uso, Rubicone, Bevano, Po di Volano. Canal Bianco outflow rate has not been changed but its name has been changed in Po di Levante because this is the name of the last part of the river. None fresh water source has been positioned in the plain between Adige and Po and between Adige and Brenta except these last two rivers. Bacchiglione and Agno-*Guà* flow into the Brenta river before reaching the sea so their runoff has not been considered. Plain between Piave and Brenta corresponds to the hydrographic basin ending into the Venice Lagoon, so the monthly flow has been divided between the three main lagoon outlets: Porto di Chioggia, Porto di Malamocco, Porto di Lido. In the plain between Tagliamento and Piave the outflow has been divided between two main rivers beyond Livenza and Sile: Canale Nicessolo, and Canale dei Lovi. Plain between Isonzo and Tagliamento is characterized by resurgent rivers flowing into the Marano and Grado Lagoons and the most important are Stella, Zellina, Aussa. The estimated outflow of the plain plus

the outflow of Stella river has been divided between the main lagoon outlets: Porto di Lignano, Zellina, Porto Buso, Canale di Morgo, La Fusa, Bocca di Primero.
None detailed information on eastern coast rivers is available in *Raicich* (1994) since climatologies in greater part of Eastern Adriatic were based on indirect estimates with evenly distributed inflow along the coast. Croatian rivers (Rasa, Rjecina, Dubracina) data comes from *Pasaric* (2004) monthly climatologies estimated from data covering the period 1947-2000.

River	Jan	Feb	Mar	Apr	May	Jun	Jul	Aug	Sep	Oct	Nov	Dec
Foglia	10.8	18.0	12.5	9.3	7.	6 2.9	0.8	0.33	2.0	3.1	10.0	12.8
Marecchia	12.3	19.2	16.3	14.4	12.1	5.8	2.5	1.7	2.8	4.3	9.5	13.9
Uso	8.0	10.5	11.0	8.0	5.5	2.2	1.3	1.0	1.5	4.3	9.3	9.5
Rubicone	8.0	10.5	11.0	8.0	5.5	2.2	1.3	1.0	1.5	4.3	9.3	9.5
Savio	17.0	25.3	21.3	15.7	11.7	5.3	1.7	1.3	3.0	6.7	15.7	20.0
Bevano	8.0	10.5	11.0	8.0	5.5	2.2	1.3	1.0	1.5	4.3	9.3	9.5
Fiumi Uniti	17.0	25.3	21.3	15.7	11.7	5.3	1.7	1.3	3.0	6.7	15.7	20.0
Lamone	17.0	25.3	21.3	15.7	11.7	5.3	1.7	1.3	3.0	6.7	15.7	20.0
Reno	66	86	90	65	44	23	10	8	12	35	75	78
Po di Volano	8.0	10.5	11.0	8.0	5.5	2.2	1.3	1.0	1.5	4.3	9.3	9.5
Po	1597	1285	1283	1298	2179	1753	1113	697	1443	2102	2436	1906
Po di Levante	22.0	20.0	13.0	15.0	17.0	21.0	16.0	18.0	29.0	33.0	29.0	27.0
Adige	147.0	135.0	148.0	185.0	243.0	346.0	261.0	215.0	239.0	214.0	224.0	182.0
Brenta	73.0	61.0	78.0	137.0	104.0	105.0	64.0	44.0	81.0	104.0	145.0	122.0
Porto di Chioggia	10.7	9.7	16.0	22.3	16.3	21.0	17.0	10.7	17.3	20.0	27.0	19.3
Porto di Malamocco	10.7	9.7	16.0	22.3	16.3	21.0	17.0	10.7	17.3	20.0	27.0	19.3
Porto di Lido	10.7	9.7	16.0	22.3	16.3	21.0	17.0	10.7	17.3	20.0	27.0	19.3
Sile	52.0	48.0	48.0	47.0	50.0	56.0	55.0	54.0	56.0	56.0	57.0	56.0
Piave	5.0	0.0	25.0	53.0	70.0	90.0	61.0	41.0	59.0	71.0	117.0	60.0
Livenza	103.0	86.0	84.0	91.0	77.0	80.0	74.0	63.0	81.0	87.0	117.0	117.0
Canale Nicessolo	14.0	13.0	21.0	29.5	21.5	27.0	22.0	14.0	23.0	26.5	35.5	25.5
Canale dei Lovi	14.0	13.0	21.0	29.5	21.5	27.0	22.0	14.0	23.0	26.5	35.5	25.5
Tagliamento	42.0	20.0	60.0	93.0	92.0	105.0	91.0	93.0	122.0	149.0	180.0	116.0
Porto Lignano	9.6	8.1	9.5	11.5	9.5	10.3	9.6	10.0	10.8	11.2	12.0	11.3
Zellina	9.6	8.1	9.5	11.5	9.5	10.3	9.6	10.0	10.8	11.2	12.0	11.3
Porto Buso	9.6	8.1	9.5	11.5	9.5	10.3	9.6	10.0	10.8	11.2	12.0	11.3
Canale di Morgo	9.6	8.1	9.5	11.5	9.5	10.3	9.6	10.0	10.8	11.2	12.0	11.3
La Fosa	9.6	8.1	9.5	11.5	9.5	10.3	9.6	10.0	10.8	11.2	12.0	11.3
Bocca di Primero	9.6	8.1	9.5	11.5	9.5	10.3	9.6	10.0	10.8	11.2	12.0	11.3
Isonzo	101.0	92.0	105.0	137.0	129.0	118.0	80.0	63.0	91.0	127.0	160.0	121.0
Dragonia	1.5	1.5	1.4	1.5	1.3	0.5	0.2	0.1	0.2	1.5	1.8	1.6
Mirna	10.6	9.7	8.7	9.4	6.1	4.9	1.9	2.1	4.2	7.7	11.4	10.4
Rasa	2.4	2.3	1.8	1.8	1.1	0.6	0.33	0.33	0.8	1.4	2.5	2.1
Rjecina	7.2	7.0	6.3	8.5	6.9	3.2	2.1	1.0	5.1	8.6	12.4	12.8
Dubracina	6.1	4.3	3.4	3.1	3.0	2.3	1.5	1.3	2.5	4.7	6.1	6.8

Table A.1: ASHELF Rivers and monthly climatological outflow in m^3/sec.

Appendix B

Satellite SST Data Validation

Satellite sea surface temperature (SST) data at high horizontal resolution have been employed for ASHELF model validation. We exploited the AVHRR data set from NOAA 12, 13, 14, 15, 16 and 17 satellites, collected in the framework of DOLCEVITA Project (Dynamics of Localized Currents and Eddy Variability in the Adriatic, http://thayer.dartmouth.edu/adriatic/) and then elaborated by OGS (Istituto Nazionale di Oceanorafia e di Geofisica Sperimetale in Trieste, Italy). *Notarstefano et al.* (2006) computed SST mapped on a 1.2 km horizontal resolution grid.
SST data have been previously validated for the year 2003 with ADRICOSM in situ CTD observations in the Gulf of Trieste and the Emilia Romagna coastal area, to have an insight of SST data accuracy into the domain under investigation. Data with cloud masking have been considered. Only maps that cover more than the 50% of the available CDT points within the monitoring network have been selected to obtain more trustable skill scores.
First we calculated RMSE between CTD data and all the available daily images, to study RMSE general distribution (fig.B.1a and fig.B.2a). In both figures B.1a and B.2a can be noticed multiple RMSE values per day. Then we divided all the calculated RMSE within three hours bins considering the SST data record time, to better understand if there were any trend on daily basis with respect to the average CTD sampling time, indicated in figures B.1b and B.2b by a black triangle on the abscissa. In both areas, as expected, the minimum RMSE value occur for SST images collected close to the CTD sampling time. In plots B.1c and B.2c, only RMSE values for images collected within plus/or minus 2 hours from the average CTD monitoring time are displayed.
Inside the Gulf of Trieste, the RMSE oscillates between $0.2 - 1.2C\circ$ interval, with annual average of $0.59C\circ$. The highest values occur in May/June. In Emilia Romagna coastal area the RMSE oscillation is wider, with minimum

values of about $0.2C\circ$ and maximum values of about $2C\circ$. The annual RMSE average is of $0.76C\circ$.
Highest SST RMSE values of Emilia Romagna area can be ascribed to the strong Po river water influence in this area that might generate intense temperature gradients, as stated in chapter 2. These gradients can interfere with the cloud masking algorithm thus compromising its result.

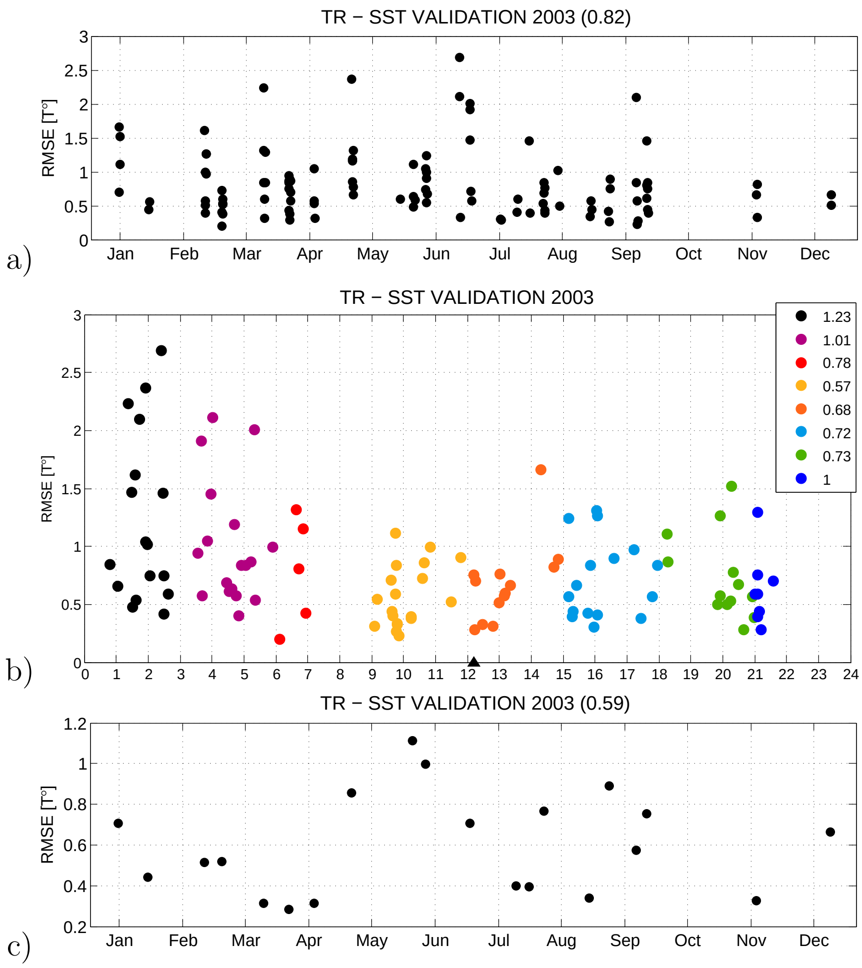

Figure B.1: High resolution satellite SST validation with coastal CTD in the Gulf of Trieste for the year 2003: a) RMSE time series calculated at the CTD monitoring days, considering all the available daily SST images. b) Data from (a) have been divided as function of sampling day time within 3 hours intervals. RMSE have been calculated separately for each time interval. The black triangle on the abscissa indicates the annual average CTD sampling time. c) RMSE time series from SST-CTD cross-validation, considering only SST images closer to the CTD sampling time.

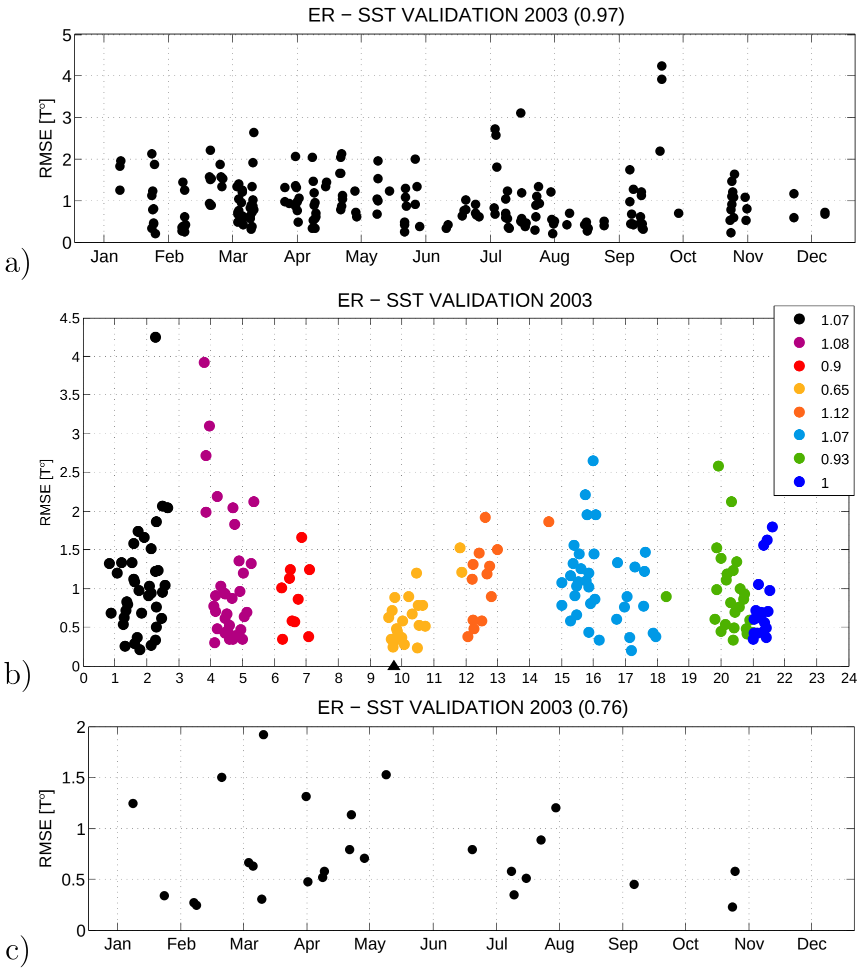

Figure B.2: High resolution satellite SST validation with coastal CTD in the Emilia Romagna coastal area. (see fig.B.2 for details)

Bibliography

Artegiani, A., D. Bregant, E. Paschini, N. Pinardi, F. Raicic, and A. Russo (1997a), The Adriatic Sea general circulation. Part I: Air Sea interactions and water mass structure, *Journal of Physical Oceanography*, *27*, 1492–1514.

Artegiani, A., D. Bregant, E. P. N. Pinardi, F. Raicic, and A. Russo (1997b), The Adriatic Sea general circulation. Part II: Baroclinic circulation structure, *Journal Physical Oceanography*, *27*, 1515–1532.

Artioli, Y., G. Bendoricchio, and L. Palmeri (2005), Defining and modelling the coastal zone affected by the po river (italy), *Ecological Modelling*, *184*(1), 55 – 68, doi:DOI: 10.1016/j.ecolmodel.2004.11.008, a special issue in memory of Guiseppe Bendoricchio.

Bergamasco, A., M. Gacic, R. Boscolo, and G. Umgiesser (1996), Winter oceanographic conditions and water mass balance in the northern Adriatic (february 1993), *Journal of Marine Systems*, *7*, 67–94.

Blumberg, A., and G. Mellor (1987), A description of a three-dimensional coastal ocean circulation model, in *Three-Dimensional Coastal Ocean Circulation Models*, edited by N.S.Heaps, American Geophyical Union, Washington DC.

Boyer, T. P., C. Stephens, J. I. Antonov, M. E. Conkright, R. A. Locarnini, T. D. O'Brien, and H. E. Garcia (2002), Salinity, in *NOAA Atlas NESDIS 50*, *World Ocean Atlas 2001*, vol. 2, edited by S. Levitus, U.S. Government Printing Office, Washington D.C., 176 pp.

Bretherton, F., R. Davis, and C.B.Fandry (1976), A tecnique for objective analysis and design of oceanographic experiments applied to mode-73, *Deep Sea Research*, *30*, 985–1002.

Carter, E., and A. Robinson (1987), Analysis model for the estimation of oceanic fields, *Journal of Atmospheric and Oceanic Technology*, *4*, 49–74.

Castellari, S., N. Pinardi, and K. Leaman (1998), A model study of air-sea interactions in the Mediterranean Sea, *Journal of Marine Systems*, *18*, 89–114.

Castellari, S., N. Pinardi, and A. Coluccelli (2006), The ADRICOSM Pilot Project : A coastal and river Basin prediction system for the Adriatic Sea, *Acta Adriatica*, *47*, 5–18.

Celio, M., V. *Malačič*, A. Bussani, B. *Čermelj*, C. Cominci, and B. Petelin (2006), The coastal scale observing system component of ADRICOSM: Gulf of trieste network, *Acta Adriatica*, *47*, 65–79.

Dorman, C. E., et al. (2007), February 2003 marine atmospheric conditions and the bora over the northern Adriatic, *Journal of Geophysical Research*, *111*, C03S03.

Estournel, C., F. Auclair, M. Lux, C. Nguyen, , and P. Marsaleix (2009), Scale orientedembedded modeling of the North-Western Mediterranean in the frame of mfstep, *Ocean Science*, *5*, 7390.

Estubier, A., and M.Levy (2000), Quel schma numrique pour le transport d'organismes biologiques par la circulation ocanique, *Tech. rep.*, Ple de modlisation, Institut Pierre-Simon Laplace.

Ferreira-Coelho, E., and M. Rixen (2008), Maritime rapid environmental assessment new trends in operational oceanography, *Journal of Marine Systems*, *69*(1-2), doi:DOI: 10.1016/j.jmarsys.2007.02.002.

Flather, R. (1976), A tidal model of the northwest continental shelf, *Memories de la Socyete Royales des Science de Liege*, *6(10)*, 141–164.

Gaberšek, S., R. Sorgente, S. Natale, A. Ribotti, A. Olita, M. Astraldi, and M. Borghini (2007), The Sicily Channel Regional Model forecasting system: initial boundary conditions sensitivity and case study evaluation, *Ocean Science*, *33*.

Giani, M., A. Rinaldi, D. Degobbis, and R. Vollenweider (2005), Mucilages in the adriatic and tyrrhenian seas, *Science of The Total Environment*, *353*(1-3), 1 – 2, doi:DOI: 10.1016/j.scitotenv.2005.09.007, mucilages in the Adriatic and Tyrrhenian Seas.

Guarnieri, A., P. Oddo, G. Bortoluzzi, M. Pastore, N. Pinardi, and M. Ravaioli (2009), The Adriatic Basin Forecasting System new model and system development. coastal to Global Operational Oceanography: Achievements and Challenges., in *Proceeding of 5th EuroGOOS Conference*, edited by H. Dahlin, N. Fleming, and S. Petersson, Exeter UK.

Hill, A. (1998), Buoyancy effects in coastal and shelf seas, in *The Global Coastal Ocean: Processes and Methods*, edited by K. H. Brink and A. Robinson, The Sea, chap. 2, John Wiley and Sons, Inc.

Jeffries, M., and C. Lee (2007), A climatology of the northern Adriatic Sea's response to bora and river forcing, *Journal of Geophysical Research*, *112*.

Kourafalou, V. (1999), Process studies on the Po River Plume, North Adriatic Sea, *Journal of Geophysical Research*, *104* (C12).

Kourafalou, V., and K. Tsiaras (2007), A nested circulation model for the North Aegean Sea, *Ocean Science*, *3*, 1–16.

Legates, D., and C. Willmott (1990), Mean Seasonal and spatial variability in gauge-corrected, global precipitation, *International Journal of Climatology*, *10*, 111–127.

Lermusiaux, P. F. J. (2007), Adaptive modeling, adaptive data assimilation and adaptive sampling, *Physica D*, *230*, 172–196.

Limić, N., and M. Orlić (1986), Objective Analysis of geostrophic currents in the Adriatic Sea, *Geofizika*, *3*.

Lyons, D. M., N.Supić, and N. Smodlaka (2007), Geostrophic circulation patterns in the northeastern Adriatic Sea and the effects of air-sea coupling: May-september 2003, *Journal of Geophysical Research*, *112*, C03S08.

Malačič, V., and B. Petelin (2009), Climatic circulation in the gulf of trieste (northern Adriatic), *Journal of Geophysical Research*, *114*.

Mariano, A., and O. Brown (1992), Efficient Objective Analysis of dinamically heterogeneous and nonstationary fields via the parameter matrix, *Deep Sea Research*, *39(7/8)*, 1255–1271.

Mellor, G., and T. Yamada (1982), Development of a turbulence closure model for geophysical fluid problems, *Reviews of Geophysics and Space Physics*, *20*, 851–875.

Montanari, G., A. Rinaldi, N. Pinardi, S. Simoncelli, and L. Giacomelli (2006), I quaderni di arpa, in *The currents of Emilia-Romagna coastal strip during the period 1995-2002*, Agenzia Regionale Prevenzione e Ambiente dell'Emilia-Romagna (ARPA).

Natale, S., R. Sorgente, S. G. andA. Ribotti, and A. Olita (2006), Central Mediterranean Sea forecast: effects of high-resolution atmospheric forcings, *Ocean Science Discussion*, *3*, 637669.

Nittis, K., N. Pinardi, and A. Lascaratos (1993), Characteristics of the summer 1987 flow field in the Ionian Sea, *Journal of Geophysical Research*, *98*, 171–184.

Notarstefano, G., E. Mauri, and P. Poulain (2006), Near surface structure and surface diurnal warming in the Adriatic Sea using satellite and drifter data, *Remote Sensing of Environment*, *101*, 194–211.

Oddo, P., and N. Pinardi (2008), Lateral open boundary conditions for nested limited area models: A scale selective approach, *Ocean Modeling*, pp. 134–156.

Oddo, P., N. Pinardi, and M. Zavatarelli (2005), A numerical study of the interannual variability of the Adriatic Sea (2000-2002), *Science of the Total Environment*, pp. 39–56.

Oddo, P., N. Pinardi, M. Zavatarelli, and A. Coluccelli (2006), The Adriatic basin Forecasting System, *Acta Adriatica*.

Oddo, P., M. Adani, N. Pinardi, C. Fratianni, M. Tonani, and D. Pettenuzzo (2009), A nested Atlantic-Mediterranean Sea general circulation model for operational forecasting, *Ocean Science*, pp. 461–473.

Orlanski, I. (1976), A simple boundary condition for unbounded hyperbolic flows, *Journal of Computational Physics*, *21*, 251–269.

Pasaric, M. (2004), Annual cycle of river discharge along the Adriatic coast of Croatia, in *37th Congress Proceedings*, vol. 37, CIESM.

Paschini, E., A. Artegiani, and N. Pinardi (1993), The mesoscale eddy field of the middle adriatic sea during fall 1988, *Deep Sea Research Part I: Oceanographic Research Papers*, *40*(7), 1365 – 1377, doi:DOI: 10.1016/0967-0637(93)90117-L.

Pinardi, N., I. Allen, E. Demirov, G. K. P. De Mey, A. Lascaratos, P.-Y. L. Traon, C. Maillard, G. Manzella, and C. Tziavos (2003), The Mediterranean ocean Forecasting System: first phase of implementation (1998-2001), *Annales Geophysicae*, *21*, 413–436.

Poulain, P. (2001), Adriatic Sea surface circulation as derived from drifter data between 1990 and 1999, *J. Mar. Sys.*, *29*, 3–32.

Poulain, P., E. Mauri, and L. Ursella (2004), Unusual upwelling event and current reversal off the Italian Adriatic coast in summer 2003, *Geophysical Research Letters*, *31*.

Raicich, F. (1994), Note on the flow rates of the Adriatic rivers, *Tech. rep.*, Consiglio Nazionale delle Ricerche, Istituto Sperimentale Talassografico.

Rixen, M., E. Ferreira-Coelho, and R. Signell (2008), Surface drift prediction in the Adriatic Sea using hyper-ensemble statistics on atmosphetic, ocean and wave models: Uncertainties and probability distribution areas, *Journal of Marine Systems*, *69*, 86–98.

Robinson, A. (1999), Forecasting and simulating coastal ocean processes and variabilities with the harvard ocean prediction system, in *Coastal Ocean Prediction*, edited by C. Mooers, no. 56 in Coastal and Estuarine Studies Series, pp. 77–100, American Geophysical Union.

Robinson, A. (2002), Rapid assessment of the coastal ocean environment, in *Ocean Forecasting*, edited by N. Pinardi and J. Woods, chap. 11, Springer Verlag.

Robinson, A., A. Hecht, N. Pinardi, J. Bishop, W. Leslie, Z. Rosentroubt, A. Mariano, and S. Brenner (1987), Small synoptic/mesoscale eddies and energetic variability of the eastern Levantine basin, *Nature*, *327*, 131–134.

Signell, R. (2003), Cruise report from adria03 23 April - 15 may 2003, adriatic sea, *Tech. Rep. CD-61*, SACLANTCEN, NATO Saclant Undersea Research Centre, La Spezia, Italy.

Signell, R., S. Carniel, L. Cavaleri, J. Chiggiato, J. Doyle, J. Pullen, and M. Sclavo (2005), Assessment of wind quality for oceanographic modeling in semi-enclosed Basins, *Journal of Marine Systems*, *53*, 217–233.

Smagorinsky, J. (1993), Some historical remarks on the use of non-linear viscosities, in *Large eddy simulations of complex engineering and geophysical flows*, pp. 3–36, Cambridge University Press.

Stephens, C., J. I. Antonov, T. P. Boyer, M. E. Conkright, R. A. Locarnini, T. D. O'Brien, and H. E. Garcia (2002), Temperature, in *NOAA Atlas NESDIS 49*, *World Ocean Atlas 2001*, vol. 1, edited by S. Levitus, U.S. Government Printing Office, Washington D.C., 167 pp.

Supić, N., M. Orlić, and D. Degobbis (2000), Istrian coastal countercurrent and its year-to-year variability, *Estuarine, Coastal and Shelf Science*, pp. 385–397.

Supic, N., and M. Orlic (1999), Seasonal and interannual variability of the northern adriatic surface fluxes, *Journal of Marine Systems*, *20*(1-4), 205 – 229, doi:DOI: 10.1016/S0924-7963(98)00083-9.

Tonani, M., N. Pinardi, S. Dobricic, I. Pujol, and C. Fratianni (2008), A high resolution free-surface model of the mediterranean Sea, *Ocean Science*, pp. 1–14.

Zavatarelli, M., and N. Pinardi (2003), The Adriatic Sea modeling system: A nested approach, *Annales Geophysicae*, pp. 345–364.

Zavatarelli, M., N. Pinardi, V. H. Kourafalou, and A. Maggiore (2002), Diagnostic and prognostic model studies of the Adriatic Sea general circulation: Seasonal variability, *Journal of Geophysical Research*, *107*(C1).